

The tale of two aminophosphines: exploiting the Ramirez
mechanism to access difluoroenolate chemistry from
trifluoromethyl ketones

By

Alvaro I. Briceno-Strocchia

A Thesis submitted in conformity with the requirements for the degree of Master of Science

Department of Toronto

The tale of two aminophosphines: exploiting the Ramirez mechanism to access difluoroenolate chemistry from trifluoromethyl ketones

Alvaro I. Briceno-Strocchia

Master of Science

Department of chemistry
University of Toronto

2019

Abstract

Selective aliphatic C-F bond cleavage of trifluoromethyl ketones mediated by tris(dialkylamino)phosphines are explored to access difluoroenolate chemistry. Two aminophosphines derivatives are investigated: P(NMeCH₂CH₂)₃N (me-VB) and P(NEt₂)₃. The me-VB/B(C₆H₅)₃ FLP reacts with 2,2,2-trifluoroacetophenone to generate difluoroalkenyl phosphatrane (DFEP). The azaphosphatrane structure disallowed access to difluoroenolate chemistry under mild conditions. Difluoroenolate chemistry was accessed when reacting me-VB with 2,2,2-trifluoroacetophenone in the absence of B(C₆H₅)₃ to generate the aldol-homoadduct product. Switching the aminophosphine to P(NEt₂)₃ enabled the formation of difluoroalkenyl phosphonium (DFEPn3) when reacting with 2,2,2-trifluoroacetophenone in the presence of B(C₆H₅)₃. The acyclic phosphonium character of DFEPn3 enabled facile access to difluoroenolate chemistry using fluoride or hydroxide as the nucleophile. The first example of converting 2,2,2-trifluoroacetophenone to 2,2-difluoroacetophenone at room temperature using main-group compounds is reported.

Acknowledgements

I would like to thank Professor Doug Stephan for the amazing opportunity to work in his lab for my Master of Science Degree. His charismatic, approachable, friendly energy captivated me as a prospective student. His creativity and drive to discover interesting transformations propelled me to work hard and stay motivated. The countless conversations in the lunch room will always be held dearly in my heart, for they provided a respite and calm atmosphere, enabling me to work my best. I thank you immensely for taking me on as a student. The compassion and understanding you provided was a key ingredient for my success, so I thank you deeply.

My experience in the Stephan group was intense, with long hours and plenty of frustration, but my fellow Stephanites made every day a joy in the lab. The friendships I have built over the last year and a half will last for my lifetime. Every single Stephanite contributed to the completion of my degree. Mid-afternoon coffee breaks, conversations in the group room, and after hour shenanigans provided a phenomenal work space to grow and feel safe. You people are the absolute best.

And finally, last but most certainly not least, I would like to acknowledge my mom and dad. It is inconceivable to summarize what your contribution to the completion of this degree was in 100 pages. So I will say this: gracias por todo. Without you, this would have been impossible. Thank you for the endless love, support and care you have given me. You are the real MVPs, and I will be indebted to you forever.

Table of contents:

1	Introduction to Trifluoromethyl Ketone Derivatization and Frustrated Lewis Pairs	1
1.1	Trifluoromethyl ketones and their application for difluoromethylene-containing organofluorines	1
1.2	Frustrated Lewis Pair activation of H ₂ and other small molecules	4
1.3	Application of FLP to intercept reaction intermediates.....	8
1.4	Frustrated Lewis Pair selective functionalization of organofluorine compounds through C-F bond activation	10
1.5	Scope of the thesis	11
2	The “Ramirez Intermediate” trapped by FLPs: Access to potential difluoroenolate synthons from TFMK	13
2.1	Using me-VB/B(C ₆ H ₅) ₃ FLP to capture DFEP: mechanism, reactivity towards nucleophiles, and difluoroenolate chemistry	16
2.2	Using P(NEt ₂) ₃ /B(C ₆ H ₅) ₃ FLP to capture DFEPn3: facile access to difluoroenolate chemistry.....	28
2.3	Stability of [DFEPn3][OTf] under ambient conditions: reactions in aqueous medium .	30
2.4	Conclusion	33
3	References.....	35
4	Supporting Information	40
4.1	General Considerations.....	40

4.2	Synthetic Procedure	40
4.3	Auxiliary Reactions	47
4.4	Nucleophilic reactions on [DFEPn3][OTf].....	59
4.5	NMR Spectra:	68
4.6	Computational Protocol	96
4.7	X-Ray Crystallography:	109

Table of Figures:

Figure 1: Molecular structure of DFEP. Counteranion and protons omitted for clarity. C, black; N, blue; O, red; F, pink.	17
Figure 2: Computational mechanism for the formation of [DFEP][FB(C ₆ H ₅) ₃]	18
Figure 3: Resolved partial structure of FEP (E-isomer). Counteranion and protons omitted for clarity. C, black; N, blue; O, red; F, pink.....	21
Figure 4: Molecular structure of EP. Counteranion and protons omitted for clarity. C, black; N, blue; O, red; F, pink.	23

Table of Schemes:

Scheme 1: Applications of Trifluoromethyl ketones as drug intermediates and serine protease inhibitor ⁴	2
Scheme 2 General reaction pathways for selective C-F bond functionalization to generate DFMKs from TFMKs. Common difluoroenolate synthon accessed using two divergent methods. Uneyama method: 2 equiv Mg, 4 equiv TMSCl, THF, 0 °C. Ogoshi method: 1.5 equiv, B ₂ pin ₂ , 1.5 equiv NaOtBu, 1 mol% CuCl/Phen, THF, 30 °C	3
Scheme 4: Observed exceptions to the classical view of Lewis acid-Lewis base interactions	4
Scheme 5: First example of FLP reversibly activating H ₂	5
Scheme 6: Initial perception of FLPs. Necessary steric “frustration” to disallow quenching of constituents’ reactivity.	6
Scheme 7: Mechanism for FLP activation of H ₂ . Important secondary interactions enables preorganization of FLP components. Non-linear transition state for H ₂ activation. Phosphonium/hydridoborate salt species formed.	6
Scheme 8: Reaction of P(tBu) ₃ with CO ₂ in the context of FLPs. No observed reactivity without LA present. Scheme generally applicable to other small molecule activation by FLP	7
Scheme 9: me-VB/B(C ₆ F ₅) ₃ FLP capture of me-VB-Ph(NCO) reaction intermediate.	9
Scheme 10: P(tBu) ₃ /B(C ₆ F ₅) ₃ FLP-mediated defluorination of simple fluoroalkanes	10
Scheme 11: Selective defluorination of PhCF ₃ to form PhCF ₂ H. This scheme is generally applied for the synthesis of PhCFH ₂ and PhCH ₃ from PhCF ₂ H and PhCFH ₂ , respectively.	11
Scheme 12: Proposed Ramirez mechanism for generation of difluorotris(dimethylamino)phosphorane. Opportunity for FLP strategy highlighted in red.	14

Scheme 13: me-VB/B(C ₆ H ₅) ₃ FLP enabling selective oxidation of azaphosphatrane using an F ₂ surrogate.....	14
Scheme 14: Formation of [DFEP][FB(C ₆ H ₅) ₃].....	16
Scheme 15: Formation of [FEP][OTf] isomers by selective hydrodefluorination of [DFEP][OTf]	20
Scheme 16: Formation of [EP][OTf] by selective defluorination of [FEP][OTf]	22
Scheme 17: Paquin et al. method for nucleophilic substitution of silylated β,β-difluorostyrenes. ⁵⁴	24
Scheme 18: Reaction between me-VB and 2,2,2-trifluoroacetophenone in DCM.....	25
Scheme 19: Formation of [PhC(O)CF ₂ COCF ₃ Ph][FP[NMeCH ₂ CH ₂] ₃ N] salt.....	26
Scheme 20: Formation of 2,2,4,4,4-pentafluoro-3-tert-butyldimethylsilyloxy-1,3 diphenylbutan-1-one	27
Scheme 21: Formation of [DFEPn ₃][FB(C ₆ H ₅) ₃].....	28
Scheme 22: Reaction between [DFEPn ₃][OTf and [TBA][F ₂ SiPh ₃].....	29
Scheme 23: Reaction of [DFEPn ₃][OTf and [NEt ₃ *3HF] to form 2,2-difluoroacetophenone....	30
Scheme 24: Reaction of [DFEPn ₃][OTf] and KOH in 1:1 mixture H ₂ O:THF.....	31

Table of Figures S:

Figure S1: Semi-quantitative $^{31}\text{P}\{\text{H}\}$ NMR spectrum analysis on the hydrodefluorination selectivity.	49
Figure S2: $^{19}\text{F}\{\text{H}\}$ NMR (377 MHz, CH_2Cl_2) stacked spectrum depicting half hour intervals starting from minute two after addition of 2,2,2-trifluoroacetophenone to 1 (top spectrum). CH_2FCI (triplet at -169 ppm, $^2J_{\text{F-H}}= 47$ ppm), CHF_2Cl (doublet at -163 ppm $^2J_{\text{F-F}}= 79$ Hz) suggest fluoride activation of DCM. HF_2^- (doublet at -152 ppm, $^2J_{\text{F-H}}= 121$ Hz) suggests fluoride release. These chemical shifts and coupling constants were observed in Ramsden and coworkers paper on XeF_2 reactivity in different organic solvents. ⁶²	50
Figure S3: ^{31}P NMR (162 MHz, CH_2Cl_2) stacked spectrum depicting half hour intervals starting from minute two after addition of 2,2,2-trifluoroacetophenone to 1 (top). Peak at -29 ppm suggests DFEP product (alongside presence of corresponding difluorovinyl peaks in ^{19}F NMR). Fluoroazaphosphatrane evidently grows in as the reaction progresses (doublet at -43 ppm, 726 Hz).....	51
Figure S4 : ^{19}F NMR (377 MHz, CH_2Cl_2) spectrum of 1 M solution of TBAF added dropwise at -78 °C to a stirring solution of DFEP[FB(C ₆ H ₅) ₃] in DCM. Peaks at -69, -98 and -112 ppm indicate fluoroazaphosphatrane, and unreactive DFEP, respectively. Intermediate observed at -101 ppm was generated but not isolated.	53
Figure S5: ^{31}P NMR (162 MHz, CH_2Cl_2) spectrum of 1 M solution of TBAF added dropwise at -78 °C to a stirring solution of DFEP[FB(C ₆ H ₅) ₃] in DCM. Fluoroazaphosphatrane is clearly present, with two peaks very similar to DFEP (-27 ppm), alongside phosphine oxide byproduct.	54

Figure S6: ^{19}F NMR (377 MHz, THF) spectra for equimolar mixture of 2,2,2-trifluoroacetophenone and 1 in THF (crude mixture). No observed DFEP after 5 minutes of addition. Set of doublets at -98 and -105 ppm same as in DCM condition. Coupling constant consistent with two geminal fluorides. ⁶³	56
Figure S7: ^{31}P NMR (162 MHz, THF) spectra for equimolar mixture of 2,2,2-trifluoroacetophenone and 1 in THF. Excess 1 at 120.6 ppm and fluoroazaphosphorane doublet at -43 ppm (crude mixture).	57
Figure S8: ^{19}F NMR (377 MHz, THF) spectra for solution of two equivalents of 2,2,2-trifluoroacetophenone to me-VB (crude mixture).	58
Figure S9: ^{31}P NMR (162 MHz, THF) spectra for solution of two equivalents of 2,2,2-trifluoroacetophenone to me-VB	
Figure S10: ^{19}F NMR (377 MHz, THF) spectra for addition of $[\text{nBu}_4][\text{F}_2\text{SiPh}_3]$ to DFEPn3[OTf]. Doublet at -58 ppm represents $\text{F}_2\text{P}(\text{NEt}_2)_3$ and singlet at -168 ppm represents FSiPh_3 . Small product peaks observed not characterized.....	60
Figure S11: ^{31}P NMR (162 MHz, THF) spectra for addition of $[\text{nBu}_4][\text{F}_2\text{SiPh}_3]$ to DFEPn3[OTf]. Triplet at -56 ppm represents $\text{F}_2\text{P}(\text{NEt}_2)_3$	61
Figure S12: ^{19}F NMR (377 MHz, THF) spectra for addition of 0.8 equivalent of $\text{NEt}_3 \cdot 3\text{HF}$ to a solution of $[\text{DFEPn}_3][\text{OTf}]$. Doublet at -58 ppm represents $\text{F}_2\text{P}(\text{NEt}_2)_3$ and doublet at -25 ppm represents 2,2-difluoroacetophenone. Small peaks at -92 ppm and -105 ppm represent unreacted DFEPn3.....	62
Figure S13: ^1H NMR (400 MHz, CDCl_3) spectra for addition of 0.8 equivalent of $[\text{NEt}_3][3\text{HF}]$. This spectrum is from a semi-purified sample where the crude mixture was dropped in pentane to remove starting material.	63

Figure S14: ^{31}P NMR (162 MHz, THF) spectra for addition of 0.8 equivalent of $\text{NEt}_3 \cdot 3\text{HF}$ to a solution of $[\text{DFEPn3}][\text{OTf}]$. Triplet represents $\text{F}_2\text{P}(\text{NEt}_2)_3$	64
Figure S15: ^{19}F NMR (377 MHz, in CDCl_3) spectra for addition of 1 equivalent of KOH in 1:1 THF to H_2O . Doublet at -76 ppm suggests the formation of $(\text{Net}_2)_2\text{P}(\text{O})\text{F}$	65
Figure S16: ^{31}P NMR (162 MHz, in CDCl_3) spectra for addition of 1 equivalent of KOH in 1:1 THF to H_2O . Doublet at -76 ppm suggests the formation of $(\text{Net}_2)_2\text{P}(\text{O})\text{F}$	66
Figure S17: ^{19}F NMR (377 MHz, in 1:1 95 % EtOH: THF) spectrum for the addition of $[\text{DFEPn3}][\text{OTf}]$ to NaOEt in 1:1 95 % EtOH: THF mixture. Pair of doublet of doublets at -83.02 represents the ethanol addition product across DFEPn3 alkene. Doublet at -94 ppm and -111 ppm represent the E- and Z- addition-substitution products of ethoxide at the C-F bond. Residual DFEPn3 peaks at -94 ppm and -107 ppm.	67
Figure S18 ^{31}P NMR (162 MHz, in 1:1 95 % EtOH: THF) spectrum for the addition of $[\text{DFEPn3}][\text{OTf}]$ to NaOEt in 1:1 95 % EtOH: THF mixture. Doublet at 38 ppm and 37 ppm represent the Z- and E- isomer. Doublet of doublets at 37 ppm represents residual DFEPn3. Singlet at 36 ppm represents the ethanol addition product.	68
Figure S19: ^1H NMR (500 MHz, CDCl_3) spectrum of $\text{DFEP}[\text{FB}(\text{C}_6\text{H}_5)_3]$	69
Figure S20 : ^{13}C NMR (100 MHz, CDCl_3) spectrum of $\text{DFEP}[\text{FB}(\text{C}_6\text{H}_5)_3]$	70
Figure S21: ^{19}F NMR (377 MHz, CDCl_3) spectrum of $\text{DFEP}[\text{FB}(\text{C}_6\text{H}_5)_3]$	71
Figure S22: $^{31}\text{P}\{^1\text{H}\}$ NMR (162 MHz, CDCl_3) spectrum of $\text{DFEP}[\text{FB}(\text{C}_6\text{H}_5)_3]$. Peak at -10.9 ppm corresponds to $\text{HP}[(\text{MeNCH}_2\text{CH}_2)_3\text{N}]^+$,.....	72
Figure S23: ^{11}B NMR (128 MHz, CDCl_3) spectrum of $\text{DFEP}[\text{FB}(\text{C}_6\text{H}_5)_3]$	73
Figure S24: $^{19}\text{F}\{^1\text{H}\}$ NMR (377 MHz, CDCl_3) spectrum of $\text{DFEP}[\text{OTf}]$	74
Figure S25: $^{31}\text{P}\{^1\text{H}\}$ NMR (162 MHz, CDCl_3) spectrum of $\text{DFEP}[\text{OTf}]$	75

Figure S26: ^1H NMR (400 MHz, CDCl_3) spectrum of FEP[OTf].....	76
Figure S27: ^{13}C NMR (100 MHz, CDCl_3) spectrum of FEP[OTf].....	77
Figure S28: ^{19}F NMR (377 MHz, CDCl_3) spectrum of FEP[OTf].....	78
Figure S29: ^{31}P NMR (162 MHz, CDCl_3) spectrum of FEP[OTf].	79
Figure S30: ^1H NMR (500 MHz, CDCl_3) spectrum of EP[OTf].	80
Figure S31: ^{13}C NMR (500 MHz, CDCl_3) spectrum of EP[OTf].....	81
Figure S32: ^{19}F NMR (377 MHz, CDCl_3) spectrum of EP[OTf].....	82
Figure S33: $^{31}\text{P}\{^1\text{H}\}$ NMR (162 MHz, CDCl_3) spectrum of EP[OTf].	83
Figure S34: ^1H NMR (500 MHz, CDCl_3) of $[\text{DFEPn3}][\text{FB}(\text{C}_6\text{H}_5)_3]$	84
Figure S35: ^{13}C NMR (100 MHz, CDCl_3) spectrum of $\text{DFEPn3}[\text{FB}(\text{C}_6\text{H}_5)_3]$	85
Figure S36: ^{19}F NMR (377 MHz, CDCl_3) spectrum of $\text{DFEPn3}[\text{FB}(\text{C}_6\text{H}_5)_3]$	86
Figure S37: $^{31}\text{P}\{^1\text{H}\}$ NMR (162 MHz, CDCl_3) spectrum of $\text{DFEPn3}[\text{FB}(\text{C}_6\text{H}_5)_3]$	87
Figure S38: ^{11}B NMR (128 MHz, CDCl_3) spectrum of $\text{DFEPn3}[\text{FB}(\text{C}_6\text{H}_5)_3]$	88
Figure S39: ^1H NMR (500 MHz, CD_2Cl_2) spectrum of $[\text{PhC}(\text{O}-$ $\text{BPh}_3)\text{CH}_2][\text{HP}(\text{MeNCH}_2\text{CH}_2)_3\text{N}]$	89
Figure S40: ^{13}C NMR (100 MHz, CD_2Cl_2) spectrum of $[\text{PhC}(\text{O}-$ $\text{BPh}_3)\text{CH}_2][\text{HP}(\text{MeNCH}_2\text{CH}_2)_3\text{N}]$	90
Figure S41: ^{19}F NMR (377 MHz, CD_2Cl_2) spectrum of $[\text{PhC}(\text{O}-$ $\text{BPh}_3)\text{CH}_2][\text{HP}(\text{MeNCH}_2\text{CH}_2)_3\text{N}]$	91
Figure S42: ^{31}P NMR (162 MHz, CDCl_3) spectrum of $[\text{PhC}(\text{O}-$ $\text{BPh}_3)\text{CH}_2][\text{HP}(\text{MeNCH}_2\text{CH}_2)_3\text{N}]$	92

Figure S43: ^{11}B NMR (128 MHz, CD_2Cl_2) spectrum of $[\text{PhC}(\text{O}-\text{BPh}_3)\text{CH}_2][\text{HP}(\text{MeNCH}_2\text{CH}_2)_3\text{N}]$	93
Figure S44: ^1H NMR (500 MHz, CDCl_3) spectrum of 2,2,4,4,4-pentafluoro-3-silyl ether 1,3-diphenylbutan-1-one.	94
Figure S45: ^{13}C NMR (100 MHz, CDCl_3) spectrum of 2,2,4,4,4-pentafluoro-3-silyl ether 1,3-diphenylbutan-1-one.	95
Figure S46: $^{19}\text{F}\{\text{H}\}$ NMR (377 MHz, CDCl_3) spectrum for 2,2,4,4,4-pentafluoro-3-silyl ether 1,3-diphenylbutan-1-one.	96
Figure S47: Thermodynamic and kinetic prediction using DFT for generation of DFEP[FBPh ₃]. Energy's for stationary points, italicized, in kcal/mol.	99
Figure S48: Approximated structures (SMD(DCM)/PBE0-GD3BJ/def2-TZVPP//SMD(DCM)/PBE0-GD3BJ/def2-SVPP) used for calculation thermodynamic profile for DFEP[FBPH ₃] formation.	101

List of abbreviations

{1H} Proton-decoupled spectrum (NMR)	
Å	Ångström
br	Broad singlet (NMR)
°C	Celsius Degree
C-F	Carbon-fluorine bond
CF ₃	Trifluoromethyl group
-C-C _F -R	Generic group containing internal difluoromethylene group
d	Doublet (NMR)
DCM	Dichloromethane
dd	Doublet of Doublets (NMR)
DFEP	Difluoroalkenyl phosphatrane
DFMKs	Difluoromethyl ketones
dG [‡]	Transition state energy relative to starting stationary state
eq.	Equivalents
FEP	Fluoroalkenyl phosphatrane
FLP	Frustrated Lewis Pairs
EP	Alkenyl phosphatrane
Hz	Hertz
IPr	1,3-bis(2',6'-diisopropyl-phenyl)imidazole-2-ylidene
J	Coupling constant (NMR)

kcal	kilocalories
LA	Lewis acid
LB	Lewis base
LUMO	Lowest unoccupied molecular orbital
m	Multiplet (NMR)
MHz	Megahertz
mL	Millilitre
mmol	Millimole
mol	Mole
M	Molar
Me	Methyl
Me-VB	2,8,9-trimethyl-2,5,8,9-tetraaza-1-phospha-bicyclo[3.3.3]undecane
Mes	Mesityl
nBu	butyl
NMR	Nuclear magnetic resonance
o	ortho
OTf	Triflate
p	para
Ph	Phenyl
Pin	2,3-dimethyl-2,3-butane-diolate
ppm	Parts per million (NMR)
R	Generic aliphatic or aromatic group

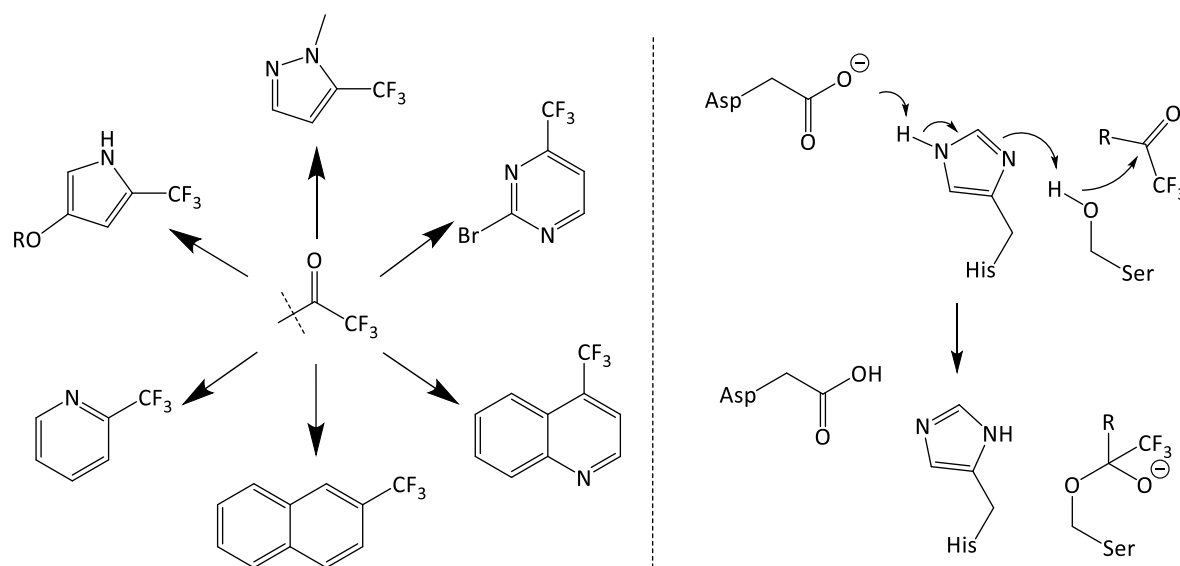
s	Singlet (NMR)
SMD	Solvent Model based on Density
t	Triplet (NMR)
TBA	Tetrabutylammonium
tBu	<i>tert</i> -butyl
TFA	2,2,2-trifluoroacetophenone
TFMKs	Trifluoromethyl ketones
THF	Tetrahydrofuran
TMS	Trimethyl silyl
TMDA	Tetramethyldiamine
VT-NMR	Variable Temperature NMR experiments
Δ	Heat
δ	Chemical shift (ppm)
σ	Sigma orbital
σ^*	Sigma antibonding orbital
z	Charge

1 Introduction to Trifluoromethyl Ketone Derivatization and Frustrated Lewis Pairs

1.1 Trifluoromethyl ketones and their application for difluoromethylene-containing organofluorines

Organofluorine chemistry has become an integral part of society. Approximately 40 % and 25 % of agricultural and pharmaceutical compounds contain a fluorine atom, respectively.¹ The strength and polarity of the C-F bond alters the bioavailability, metabolic processing, chemical and thermal stability among other factors² which render organofluorine compounds desirable target molecules to be accessible in variety through convenient protocols to test for biological applications. The advancement of chemical technology to incorporate fluorine and fluorine-containing groups into organic molecules has supported the increased demand for synthetic tools to access complex organofluorine compound. The most common fluorine-containing functional group found in organofluorine compounds are trifluoromethyl groups (-CF₃)³ because of their

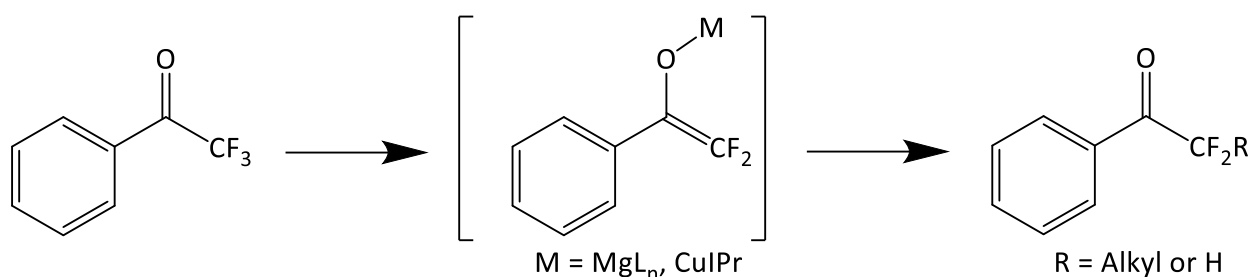
metabolic stability, bioisosterism,⁴ and strong ¹⁹F nuclear magnetic imaging (MRI) resonance for ex vivo and in vivo biological studies.⁵



Scheme 1: Applications of Trifluoromethyl ketones as drug intermediates and serine protease inhibitor⁴

Trifluoromethyl ketones (TFMKs) have the general formula $R-C(O)CF_3$ where the terminal methyl group contains three strong C-F bonds. The cumulative inductive effects of the C-F bonds increase the electrophilic character at the carbonyl carbon compared to protic ketones. The inductive effect of the trifluoromethyl group further stabilizes tetrahedral adducts making trifluoromethyl ketones potent nucleophilic acceptors at the carbonyl position. As a result, trifluoromethyl ketones have found application as mechanistic probes and as enzyme-inhibitors (Scheme 1).⁴ The development for TFMK synthesis has enabled wider access to diverse TFMK intermediates for complex $-CF_3$ containing heterocycles, medicinal compounds and fluorinated analogues of natural products.⁶ TFMKs also provide a rich pool of starting materials for difluoromethyl ketones (DFMKs) via selective C-F functionalization. DFMKs include compounds with difluoromethyl group ($-CF_2H$) or difluoromethylene group ($-CF_2-R$). Difluoromethyl groups are important bioisosteres similar to the $-CF_3$ group with hydrogen-bond

donor properties due to the acidic proton.⁷ Difluoromethylene groups demonstrate unique conformational preference at the $-C-C_F-R$ bond angle inducing profound effects on bioactivity.⁸ DFMKs have been used for the synthesis of difluoromethylene-containing drugs such as Lubiprostone.⁹ Synthesis of DFMKs from TFMKs provides a facile route to an important family of organofluorine compounds from readily accessible materials.



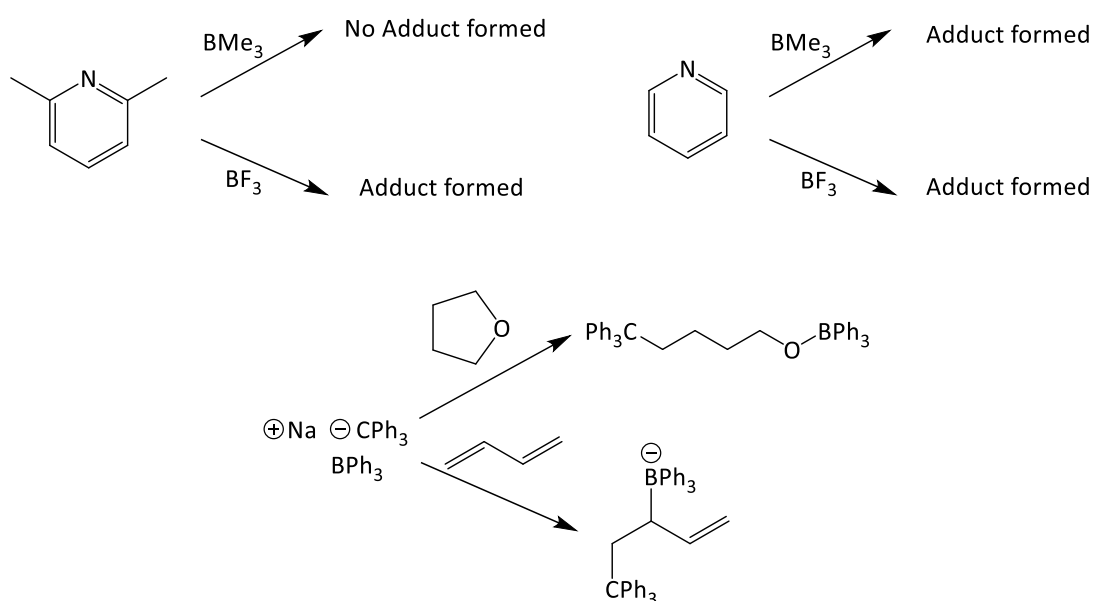
Scheme 2: General reaction pathways for selective C-F bond functionalization to generate DFMKs from TFMKs. Common difluoroenolate synthon accessed using two divergent methods. Uneyama method: 2 equiv Mg, 4 equiv TMSCl, THF, 0 °C. Ogoshi method: 1.5 equiv, B₂pin₂, 1.5 equiv NaOtBu, 1 mol% CuCl/Phen, THF, 30 °C

Two methodologies are currently available for the access of DFMKs from TFMKs. In 1999, Uneyama and coworkers developed a Mg(0)/TMSCl-mediated α -defluorination to generate difluoroenol silyl ether.¹⁰ Two electron reduction of the carbonyl π -bond by two equivalents of Mg(0) enables cleavage of the α -C-F bond to generate a Mg(II) species and a difluoroenolate which attacks the silyl chloride.¹¹ This methodology has been extensively used in the literature as a facile method to access difluoroenolate chemistry. The reactivity of the difluoroenol silyl ether necessitates the use of these compounds shortly after synthesis. The second method was recently published by Ogoshi¹² using the electron-rich (IPr)CuBpin system developed by Sadigui¹³ to access catalytic β -elimination of the Cu-TFMK C-F bond generating a transition-metal enolate species which performed cross-aldol reactions with aldehyde. Cross-aldol products were

accessible despite competition with the starting TFMK. The Ogoshi methodology presents the first catalytic TFMK transformation to DFMK derivatives.

1.2 Frustrated Lewis Pair activation of H₂ and other small molecules

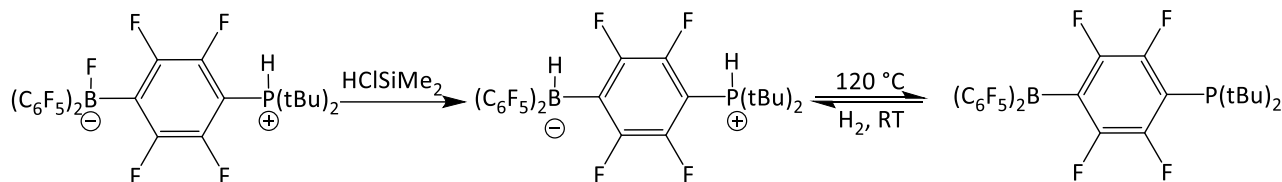
The interaction between Lewis base and Lewis acid through the donation of a lone pair to accepting orbitals was established by Gilbert N. Lewis through the observation of stable Lewis acid-base adducts.¹⁴ Exceptions were identified when bulky substituents were used. Brown and



Scheme 3: Observed exceptions to the classical view of Lewis acid-Lewis base interactions

coworkers reported the adduct formation between 2,6-lutidine and BF₃ but no adduct was observed with BMe₃; pyridine formed adducts with both borane derivatives (Scheme 3 top).¹⁵ Wittig reported the THF ring opening from THF-BPh₃ after addition of [Na][CPh₃] instead of simple THF displacement from the borane and Tochtermann reported the 1,2-addition across 1,3-butadiene using the same Lewis acid/base system (Scheme 3 bottom).¹⁶ The tendency to inhibit adduct formation and take advantage of unquenched Lewis acid and basic sites to access

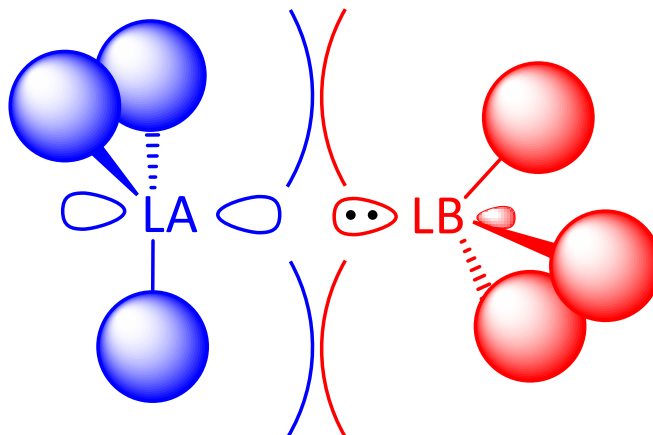
chemistry by choosing a sterically encumbered Lewis pair was evident but unexplored until recently.



Scheme 4: First example of FLP reversibly activating H₂

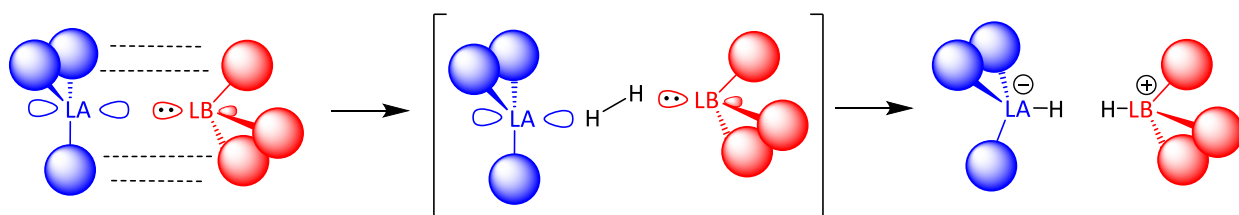
In 2006, the Stephan group prepared a phosphonium/hydridoborate species

[Mes₂PH(C₆F₄)BH(C₆F₅)₂] which liberated H₂ upon thermolysis under reduced pressure to generate the corresponding neutral phosphine/borane species [Mes₂P(C₆F₄)B(C₆F₅)₂].¹⁷ The sterically congested geometry around the phosphine and borane sites inhibited the adduct formation through intermolecular Lewis acid and base interaction. The unquenched phosphine/borane species enabled the activation and splitting of H₂ to regenerate the parent phosphonium/borate zwitterion. The reversible interconversion between [Mes₂P(C₆F₄)B(C₆F₅)₂] and [Mes₂PH(C₆F₄)BH(C₆F₅)₂] through activation and release of H₂ broke the 100 year old dogma¹⁸ by representing the first non-transition metal systems reversibly activating H₂.



Scheme 5: Initial perception of FLPs. Necessary steric “frustration” to disallow quenching of constituents’ reactivity.

The initial expansion of phosphine/borane pairs to determine which enacted H_2 activation to generate the corresponding phosphonium/borate salt resulted in two generalizations:¹⁹ 1) activation of H_2 was only observed when a sterically frustrated Lewis pair (FLP) was used and 2) the overall strength of the FLP must be compensatory to enable splitting of H_2 . Erker and coworkers shortly after published an intramolecular P/B FLP linked by an ethylene bridge capable of splitting H_2 , further expanding the accessibility of intramolecular FLP systems through hydroboration of vinylphosphanes using Piers’ Borane ($\text{HB}(\text{C}_6\text{F}_5)_2$).²⁰ These three seminal papers marked the birth of the FLP field of chemistry.



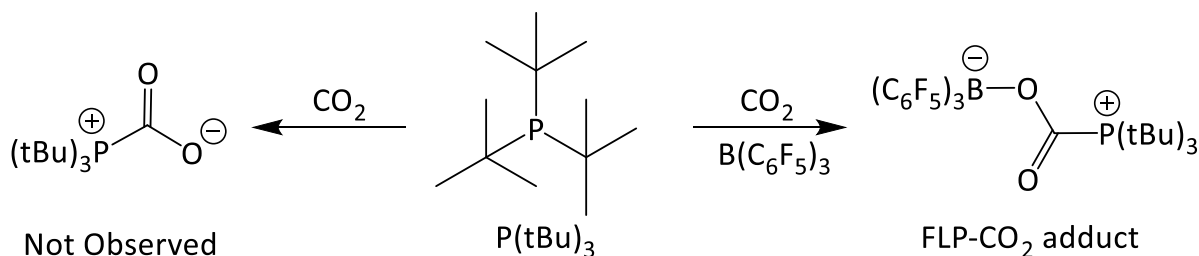
Scheme 6: Mechanism for FLP activation of H_2 . Important secondary interactions enables preorganization of FLP components.

Non-linear transition state for H_2 activation. Phosphonium/hydridoborate salt species formed.

The mechanism for H_2 activation by FLP systems was investigated through computational methods, starting a rich relationship between mechanistic FLP understanding and computational

investigation. Papai and coworkers' computational investigation on to the FLP mechanism for H₂ activation suggested the importance of secondary non-covalent van der Waals interactions between the bulky substituents of the FLP (PtBu₃/B(C₆F₅)₃).²¹ This investigation was expanded by Grimme and coworkers who concluded that the activation of H₂ by the FLP was rate limiting to the preparation of the "preorganized" FLP complex – colloquially referred to as the encounter complex (Scheme 7). Furthermore, the FLP was conceptualized not as a molecular entity but as an electric field.²² Grimme's investigation correlated with the experimental observation of steric hindrance alongside cumulative FLP strength for H₂ activation. A quenched Lewis acid/base pair would effectively constitute an electric field of zero rendering H₂ splitting inhibited.

The reversible activation of H₂ by FLP systems enabled hydrogenation chemistry of unsaturated systems with main-group compounds. Hydrogenation of imines²³ represented the first example with the expansion to enamines²⁴ and silyl enol ethers²⁵ shortly after. Hydrogenation mediated by FLPs expanded to include carbonyls,²⁶ alkenes,²⁷ and alkynes²⁸ among other substrates sparking a renaissance of metal-free hydrogenation protocols.²⁹



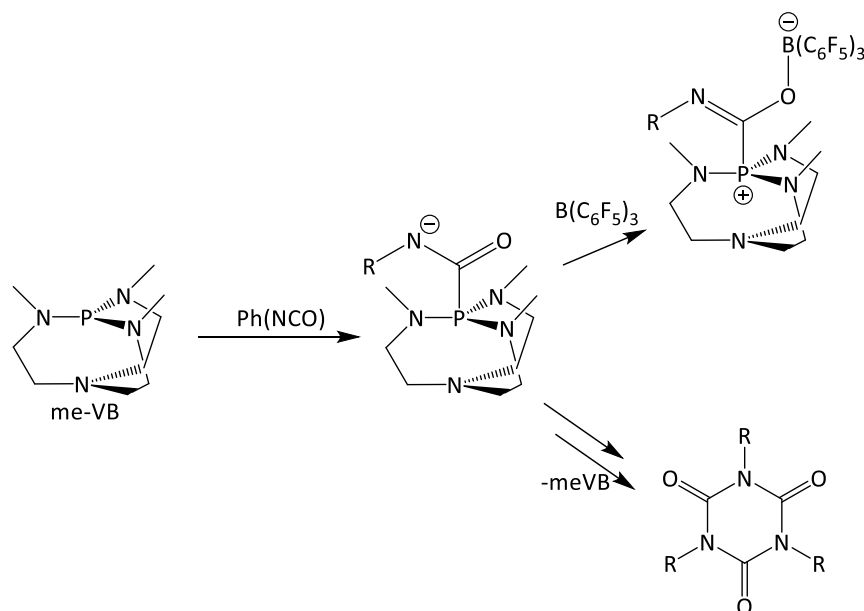
Scheme 7: Reaction of P(tBu)₃ with CO₂ in the context of FLPs. No observed reactivity without LA present. Scheme generally applicable to other small molecule activation by FLP

The chemistry of FLPs is not limited to hydrogenation catalysis. FLP activation of small molecules has expanded to include CO₂,³⁰ SO₂, N₂O,³¹ CO,³² alkenes,³³ and alkynes.³⁴ The chemistry of FLP/CO₂ is of particular note because the FLP-CO₂ adducts enable access to value

added compounds from the ubiquitous C₁-feedstock.³⁵ The capture of CO₂ by inter- and intramolecular FLP's was initially observed using PtBu₃/B(C₆F₅)₃ and Mes₂P(CH₂)B(C₆F₅)₂, respectively.³⁰ The ability of PtBu₃/ B(C₆F₅)₃ to capture CO₂ is of particular significance because the Dielmann group³⁶ determined there was no interaction between the free-base PtBu₃ and CO₂. Despite the lack of experimental evidence for PtBu₃- CO₂ interaction, Ensing and coworkers' computational investigation concluded the stepwise interaction between PtBu₃/B(C₆F₅)₃ FLP and CO₂ proceeds through initial P-C interaction³⁷ Similar to FLP reactivity with H₂, the FLP-CO₂ adduct represents the ability for FLP systems to access chemistry inaccessible to the individual components (Scheme 8). Numerous publications showcasing the reduction of CO₂ mediated by FLP capture have been published demonstrating the efficacy of the FLP protocol to access value added products using the C₁- source.³⁸ The recent breakthrough of Hu and Wu³⁹ to enable the first example of metal-free hydrogenation of CO₂ using a Lewis pair a mere 10 years after the first FLP capture of CO₂ perfectly illustrates the rapid innovation of FLP chemistry.

1.3 Application of FLP to intercept reaction intermediates

The FLP-adducts formed from FLPs reacting with small molecule could be conceptualized as trapped reaction intermediates. There is no case where H₂ interacts with either main-group Lewis acids (LA) or Lewis bases (LB), but CO₂ can interact with strong bases only.³⁶ The central electrophilic carbon of CO₂ gets attacked by the strong nucleophilic LB to generate a carboxylate intermediate. The FLP adduct can be interpreted as the LA capped LB-CO₂ species.⁴⁰



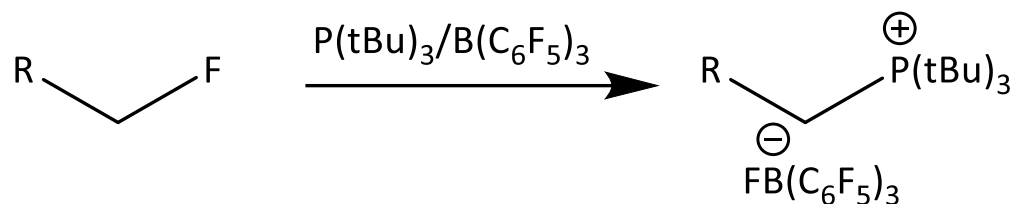
Scheme 8: me-VB/B(C₆F₅)₃ FLP capture of me-VB-Ph(NCO) reaction intermediate.

Johnstone and coworkers⁴¹ demonstrated the efficacy of FLPs to capture reaction intermediates when implementing me-VB/B(C₆F₅)₃ as the FLP system. Verkade's superbase (me-VB) is known to cyclotrimerize isocyanates to form isocyanurates through initial attack at the electrophilic carbon to generate the amide-zwitterionic species (Scheme 8). The me-VB/B(C₆F₅)₃ FLP was observed to perform 1,2-addition across the C-O double bond of PhNCO. Presumably due to the strong oxyphilicity of the borane, the trapped resonance structure was the alkoxyborate. Distinct from the FLP/H₂ reaction, the FLP components can interact with the substrate by themselves to enact their respective reactions. Finding an FLP where the reactivity of the components is not quenched by adduct formation is the premise of FLP chemistry, and could enable access to reaction intermediates previously too elusive for isolation.

The me-VB/B(C₆F₅)₃ FLP described above shifted the paradigm of FLP chemistry even further. Me-VB forms a stable zwitterionic adduct with B(C₆F₅)₃ determined by no exchange observed between me-VB/B(C₆F₅)₃ adduct and free B(C₆F₅)₃ using ¹⁹F NMR spectroscopy.⁴¹ Systems

where the LA/LB pair showing dynamic equilibria are capable of accessing FLP reactivity had been established.⁴² In the case of stable adducts, the Grimme interpretation of the FLP as a field potential does not seem straight forward on the basis of free vs. adduct FLP. Indeed, there was no observed exchange in the NMR scale, but computational investigation suggested the ability to access the encounter complex by elongation of the P-B bond rendering substrate activation at ambient temperature possible. Therefore, the requirement for steric frustration to preclude the quenching of LA/LB reactivity has become looser introducing the necessity to explore “classical” Lewis adducts for FLP reactivity. Computational efforts seem sufficient to determine the barrier for dissociation.

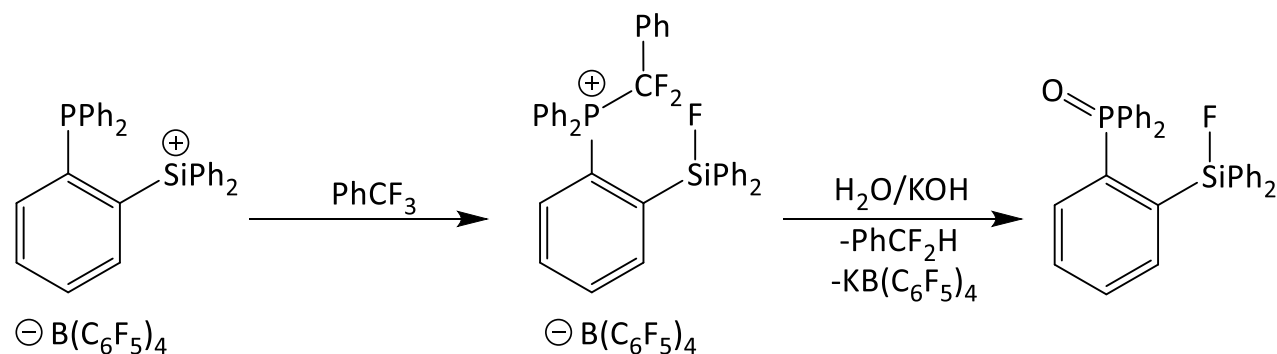
1.4 Frustrated Lewis Pair selective functionalization of organofluorine compounds through C-F bond activation



Scheme 9: P(tBu)₃/B(C₆F₅)₃ FLP-mediated defluorination of simple fluoroalkanes

FLPs have found applications in the activation of C-F bonds. Stoichiometric defluorination reactions of simple fluoroalkanes (F-CH₂-R, R=alkyl chain) using the PtBu₃/B(C₆F₅)₃ FLP generated the [R-CH₂-PtBu₃][FB(C₆F₅)₃] salts (Scheme 9).⁴³ The borane activates the C-F bond towards nucleophilic displacement by the phosphine through interaction at the fluorine atom. The fact that polyfluorinated systems did not undergo the above transformation can be rationalized by the increased delocalization of the electron density throughout the whole molecule reducing the polarizability of individual C-F bonds. Selective defluorination and

subsequent functionalization of simple fluoroalkanes is an important start towards C-F bond functionalization mediated by FLPs.



Scheme 10: Selective defluorination of PhCF_3 to form PhCF_2H . This scheme is generally applied for the synthesis of PhCFH_2 and PhCH_3 from PhCF_2H and PhCFH_2 , respectively.

Selective defluorination of an aryl- CF_3 group was enabled when an intramolecular Si^+/P FLP was used generating the difluorobenzyl-substituted phosphonium and fluorosilane (scheme 10).⁴⁴ The generation of the Si-F bond from the silylium cation provides an exceptional driving force to defluorinate and generates the difluorobenzyl-phosphonium. Basic aqueous hydrolysis enabled the cleavage of the $\text{P-CF}_2\text{-Ar}$ fragment to generate the phosphine oxide and $\text{HF}_2\text{C-Ar}$. The same protocol when using $\text{HF}_2\text{C-Ar}$ or $\text{H}_2\text{FC-Ar}$ resulted in the formation of $\text{H}_2\text{FC-Ar}$ or $\text{H}_3\text{C-Ar}$, respectively, representing the first main-group mediated conversion of CF_3 to CF_2H to CFH_2 .⁴⁵

1.5 Scope of the thesis

The objective of this thesis aims to establish FLPs as a promising methodology for controlled access to difluoroenolate chemistry from trifluoromethyl ketones. $\text{P(NMeCH}_2\text{CH}_2)_3\text{N}$ (me-VB) and $\text{P(NEt}_2)_3$ in the presence of $\text{B(C}_6\text{H}_5)_3$ generated difluoroalkenyl P(V) species from selective aliphatic C-F bond cleavage of 2,2,2-trifluoroacetophenone. These difluoroalkenyl P(V) species

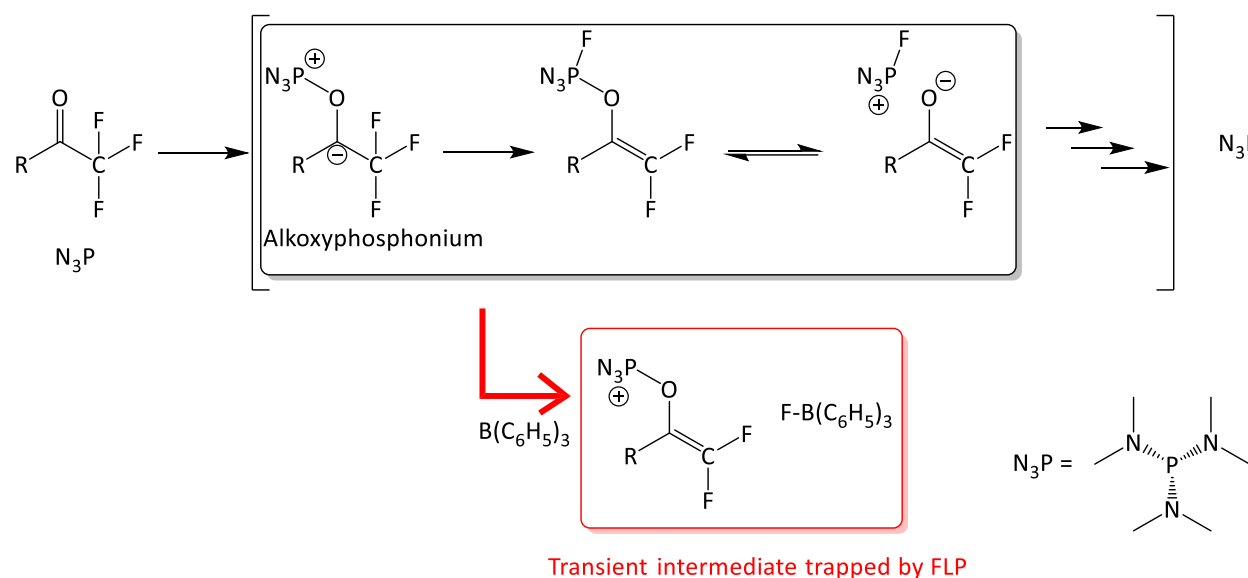
were proposed reaction intermediates which resemble difluoroenolate synthons. The me-VB system generated difluoroalkenyl phosphatrane (DFEP) whose mechanism of formation was computationally probed. The azaphosphatrane structure of DFEP enabled selective O-P bond cleavage with free fluoride, so me-VB with 2,2,2-trifluoroacetophenone in the absence of Lewis acid resulted in the formation of aldol-homoadduct product. Using $P(\text{NEt}_2)_3/\text{B}(\text{C}_6\text{H}_5)_3$ FLP generated difluoroalkenyl phosphonium (DFEPn3) by reacting with 2,2,2-trifluoroacetophenone. The acyclic DFEPn3 structure enabled facile access to difluoroenolate chemistry. Formation of 2,2-difluoroacetophenone was reported. The chemistry of DFEPn3 with nucleophiles is presented to provide the functional limitations and potential for further derivatization to generate complex fluorinating synthons. Crystallographic data was refined by Dr. Timothy C. Johnstone and Dr. James LaFortune.

2 The “Ramirez Intermediate” trapped by FLPs: Access to potential difluoroenolate synthons from TFMK

Main-group activation of aliphatic C-F bonds using Lewis acids is a common method for aliphatic C-F functionalization.⁴⁶ The FLP-mediated defluorination using $\text{P}(\text{tBu})_3/\text{B}(\text{C}_6\text{F}_5)_3$ was modified to catalyze hydrodefluorination of simple alkanes with $\text{B}(\text{C}_6\text{F}_5)_3$ as the catalyst and hydrosilanes as the hydride source.⁴³ Main-group Lewis base-mediated aliphatic C-F bond functionalization are also known but much fewer systems have been developed.^{46b} $\text{S}_{\text{N}}2'$ nucleophilic attack on aliphatic C-F bonds adjacent to π -systems is presently the only mechanism for main-group Lewis base activation of aliphatic C-F bonds.^{46b} The π -system lowers the C-F LUMO energy accelerating nucleophilic attack. Trifluoromethyl ketones are candidates for the $\text{S}_{\text{N}}2'$ mechanism for C-F bond activation. In fact, the low-valent metal $\text{Mg}(0)/\text{TMSCl}$ system developed by Uneyama and the catalytic Cu/B system developed by Ogoshi, presented in section 1.1, undergo C-F bond cleavage by reducing the carbonyl bond.¹¹⁻¹² Presently, there is no main-group Lewis base system for selective C-F bond activation of trifluoromethyl ketones.

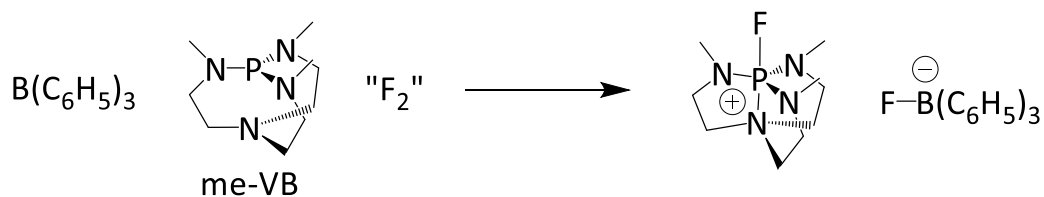
In 1966, Ramirez⁴⁷ published a rebuttal to Mark's synthesis of a stable difluoromethylenephosphorane from tris(dimethylamino)phosphine reacting with 2,2,2-trifluoroacetophenone (TFA).⁴⁸ Ramirez concluded the major compound synthesized was difluorotris(dimethylamino)phosphorane. The proposed mechanism (Scheme 12) involved the

transient generation of an alkoxyphosphonium zwitterionic species which enables C-F bond cleavage. The resulting equivalent of fluoride forms fluoroalkoxyphosphorane which



Scheme 11: Proposed Ramirez mechanism for generation of difluorotris(dimethylamino)phosphorane. Opportunity for FLP strategy highlighted in red.

decomposes to generate difluorophosphorane. Preventing the formation of the fluoroalkoxyphosphorane with a Lewis acid trapping the released equivalent of fluoride was envisioned to result in a rare example of selective aliphatic C-F bond cleavage of TFMK by phosphines. The resulting product closely resembles a difluoroenolate synthon thereby potentially granting access to difluoroenolate chemistry using main-group compounds.



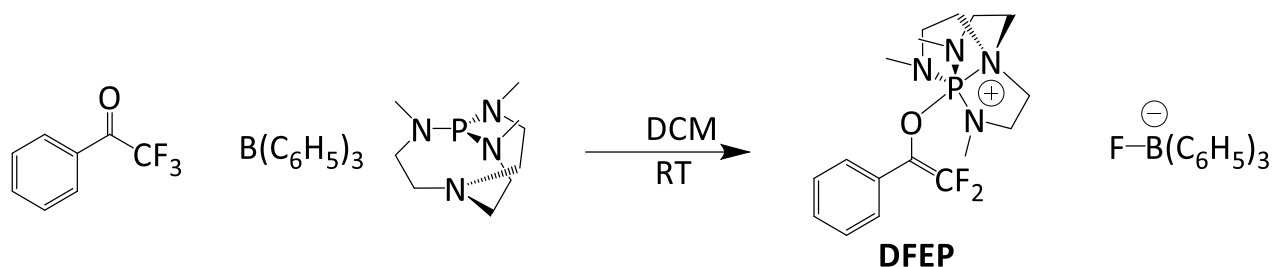
Scheme 12: *me-VB*/*B(C₆H₅)₃* FLP enabling selective oxidation of azaphosphatrane using an *F₂* surrogate

Our group developed an FLP system using proazaphosphatane (me-VB) and triphenylborane ($\text{B}(\text{C}_6\text{H}_5)_3$) to successfully isolate the first fluoroazaphosphatane salt $[\text{FP}(\text{NMeCH}_2\text{CH}_2)_3\text{N}][\text{FB}(\text{C}_6\text{H}_5)_3]$ using an F_2 surrogate.⁴⁹ The Lewis acid was capable of preventing fluoride-mediated decomposition of the fluoroazaphosphatane species. Therefore, the me-VB/ $\text{B}(\text{C}_6\text{H}_5)_3$ FLP was a promising system to generate the alkoxyphosphonium species in the presence of a fluoride trap to inhibit fluoride-mediated decomposition.

Herein, we report the successful implementation of FLPs using tris(dialkylamino)phosphines to capture the difluoroalkenyl P(V) species by preventing fluoride decomposition. Two derivatives, DFEP and DFEPn₃, were synthesized using Verkade's Superbase (me-VB) and tris(diethylamino)phosphine, respectively. Selective hydrodefluorination reactions of DFEP were identified. Divergent conditions to access difluoroenolate chemistry for the two P(V) derivatives were identified based on the P(V) structure. The caged DFEP species disallowed facile access to

the difluoroenolate chemistry, whereas the phosphonium derivative DFEPn3 readily enabled synthesis of α,α -difluoroacetophenone.

2.1 Using me-VB/B(C₆H₅)₃ FLP to capture DFEP: mechanism, reactivity towards nucleophiles, and difluoroenolate chemistry



Scheme 13: Formation of [DFEP][FB(C₆H₅)₃]

Addition of an equimolar solution of me-VB/B(C₆H₅)₃ to 2,2,2-trifluoroacetophenone (TFA) in DCM generates an ¹⁹F NMR spectrum which shows two doublet signals at -97 ppm (²J_{F-F} = 70 Hz) and -111 ppm (²J_{F-F} = 70 Hz). A broad fluoride signal at -197 ppm and a doublet in the ¹¹B NMR spectrum at 4 ppm (¹J_{B-F} = 76 Hz) suggests the formation of the fluoroborate (FB(C₆H₅)₃). The ³¹P NMR spectrum shows a single peak at -27 ppm, consistent with a strong transannular interaction suggesting a 5-coordinate azaphosphatrane.⁵⁰ The NMR spectroscopic data is consistent with the formation of a difluoroalkenyl phosphatrane (DFEP) with FB(C₆H₅)₃ as the counteranion. The [DFEP][FB(C₆H₅)₃] salt is readily isolated in 87 % yield as a white solid by adding pentane to a concentrated DCM solution, decanting the supernatant and washing the solid with pentane. Suitable crystals of [DFEP][FB(C₆H₅)₃] for single crystal X-ray diffraction were grown by layering pentane onto a concentrated DCM solution.

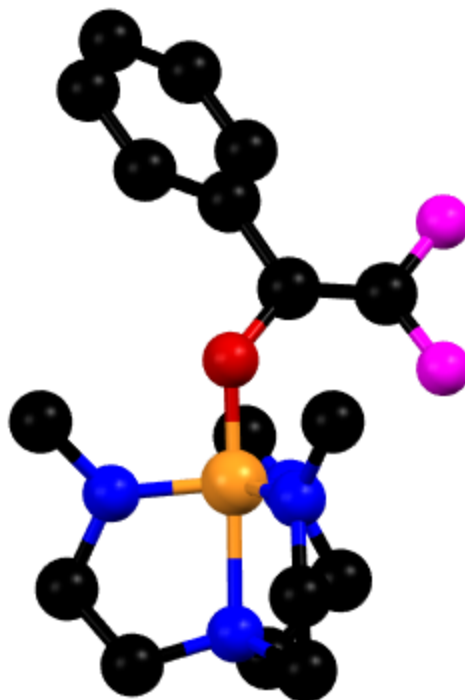


Figure 1: Molecular structure of DFEP. Counteranion and protons omitted for clarity. C, black; N, blue; O, red; F, pink.

The short transannular interaction ($2.033(2) \text{ \AA}$) between bridgehead P-N results in a pseudo trigonal bipyramidal geometry at the P(V) centre ($\Sigma N_{\text{eq}}\text{-P-N}_{\text{eq}} = 358.7^\circ$). The pseudo-pyramidal bridgehead nitrogen (337.5°) oriented towards the P(V) O-P σ^* confirms the observed NMR spectral data suggesting a 5-coordinate azaphosphatrane species. The *gem*-difluoromethylene C-C bond distance ($1.307(6) \text{ \AA}$) was found to be considerably shorter than the aromatic ring C-C bond length ($1.379(4) \text{ \AA}$) and azaphosphatrane ethylene bridge ($1.466(6) \text{ \AA}$). Mass spectral data ($m/z=371.1802$) corroborate the formulated structure.

The formation of the [DFEP][FB(C₆H₅)₃] salt implied the successful implementation of the FLP strategy to inhibit the fluoride-mediated decomposition proposed by Ramirez. Computational investigation was performed to elucidate the working mechanism because Ramirez's initial report of aminophosphines attack at carbonyl oxygen of fluorinated ketones had not been

computationally investigated.⁵¹ The mechanistic investigation was computed by the author at the PBE1PBE/def2TZVPP//PBE1PBE/def2SVPP level employing Grimme's D3 dispersion with Becke-Johnson damping method (GD3BJ)⁵² and SMD solvent correction for the geometry optimization. The me-VB/B(C₆H₅)₃ FLP was treated as a "classical" FLP where the base and acid are completely dissociated to simplify the computational requirements. This simplification is valid because me-VB/B(C₆H₅)₃ association and dissociation is under dynamic equilibrium in solution.⁴⁹ Omitted visually for simplicity, all stationary point energies prior to IS3 included the energy values for B(C₆H₅)₃ (Figure 2).

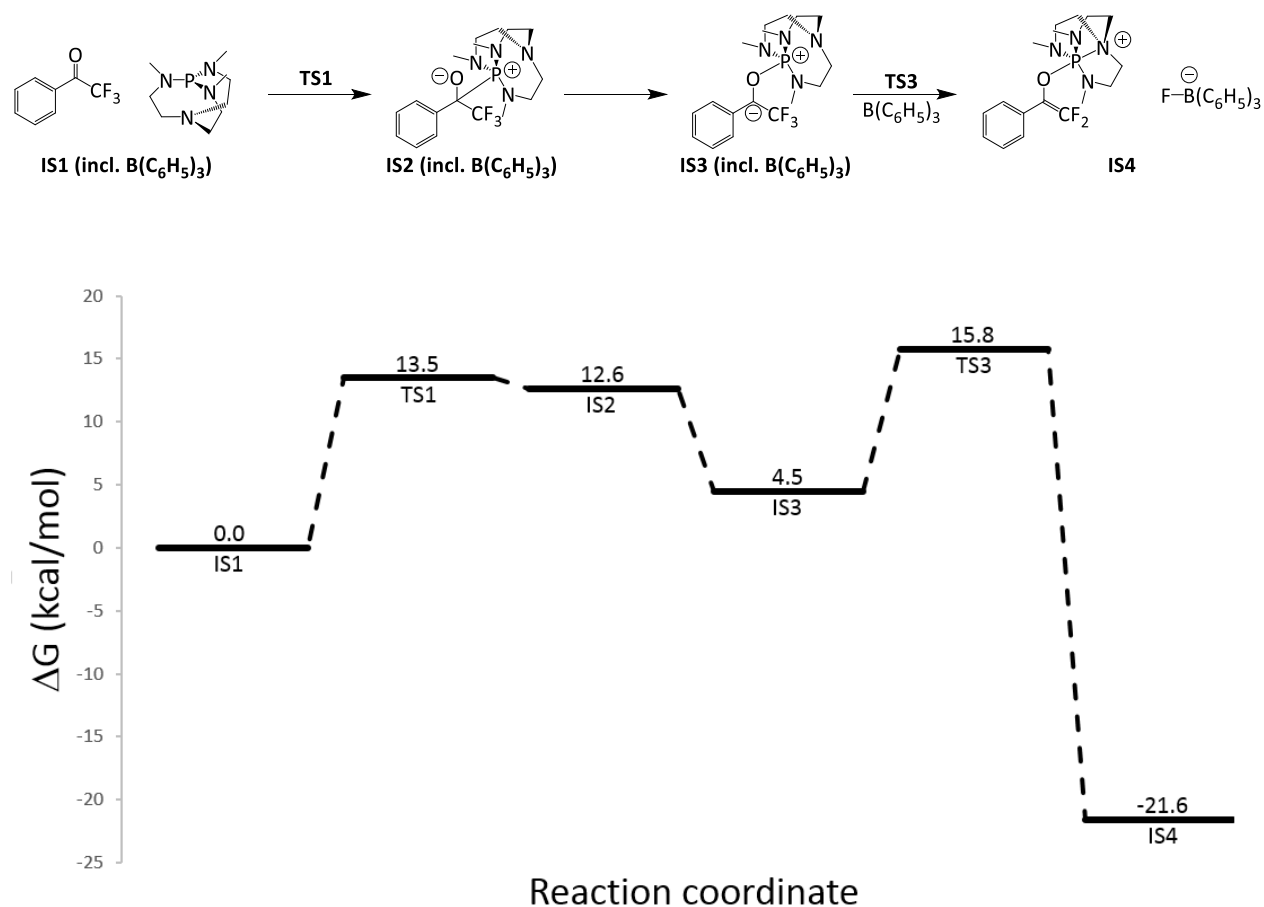
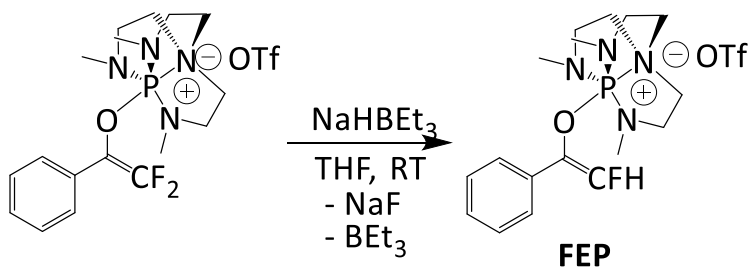


Figure 2: Computational mechanism for the formation of [DFEP][FB(C₆H₅)₃]

Figure 2 shows the reaction coordinate for the formation of [DFEP][FB(C₆H₅)₃] using a modified mechanistic proposal from the initial Ramirez mechanism (Scheme 12). The initial interaction between me-VB and 2,2,2-trifluoroacetophenone was calculated to involve the carbonyl carbon ($dG^\ddagger = 13.5$ kcal/mol). In contrast, Ramirez's proposed mechanism of initial interaction at the carbonyl oxygen resulted in a higher transition state barrier ($dG^\ddagger = 32.3$ kcal/mol). Attempts to identify a transition state for the isomerization of IS2 to form IS3 failed. Multiple publications debating the nature of phosphine interaction with activated carbonyl systems such as quinones⁵³ or α -diketo esters⁵⁴ have refuted Ramirez's interpretation suggesting initial interaction at the carbonyl oxygen. No transition state for the C-P to O-P isomerization has been published. C-F bond cleavage from IS3 to generate [DFEP][FB(C₆H₅)₃] was computed to be a thermodynamically favoured bimolecular process involving a low energy barrier ($dG^\ddagger = 11.4$ kcal/mol) from IS3. Overall, the rate-determining state for the reaction involves an energy barrier of 15.8 kcal/mol. The reaction was found to be exothermic with a Gibbs free energy of 21.6 kcal/mol. The kinetic and thermodynamic profile suggests a fast and spontaneous chemical process. Indeed, the reaction between FLP me-VB/B(C₆H₅)₃ and 2,2,2-trifluoroacetophenone is complete under 2 minutes.

The reactivity of DFEP was investigated using the [DFEP][OTf] salt to reduce the potential of fluoroborate decomposition and include an ¹⁹F internal standard. The [DFEP][OTf] salt was formed by adding one equivalent of TMSOTf to a DCM solution of [DFEP][FBC₆H₅)₃]. The [DFEP][OTf] salt was isolated with the same protocol as the parent salt in 89 % yield.



Scheme 14: Formation of [FEP][OTf] isomers by selective hydrodefluorination of [DFEP][OTf]

Selective hydrodefluorination of [DFEP][OTf] was observed using one or two equivalents of NaHBEt₃ (1M THF solution) to form the mono- or dihydrodefluorination products, respectively. Adding 1 equivalent of NaHBEt₃ to a [DFEP][OTf] solution in THF resulted in the consumption of the DFEP fluorine signals (-98 ppm and -111 ppm) and formation of two new ¹⁹F NMR peaks at -151 ppm (²J_{F-H}= 77 Hz) and -169 ppm (²J_{F-H}= 79 Hz). The ¹H NMR spectrum shows two doublets at 7.1 ppm (²J_{H-F}= 79 Hz) and 6.8 ppm (77 Hz). The ³¹P NMR spectrum showed the consumption of the DFEP signal (singlet at -27 ppm) and the appearance of two singlets at -31 ppm and -33 ppm, respectively, indicating two distinct azaphosphatranes species. The ¹⁹F, ¹H and ³¹P NMR spectra indicate the formation of the Z- and E- isomers⁵⁵ of fluoroalkenyl phosphatranes (FEP) species. Semi-quantitative ³¹P NMR experiment was conducted to corroborate the selectivity for the hydrodefluorination reaction (see section 3.3 for details). The boron spectrum showed a broad signal at 60 ppm suggestive of free borane present in solution. Precipitate was observed suggesting the formation of the NaF salt. The [FEP][OTf] isomers were isolated as white solids by adding pentane to a concentrated THF solution of the crude mixture, dissolving [FEP][OTf] in DCM, decanting the mixture and removing volatiles under *vacuo*. An isolated yield of 80 % was obtained. Single crystals of [FEP][OTf] isomers were grown through pentane

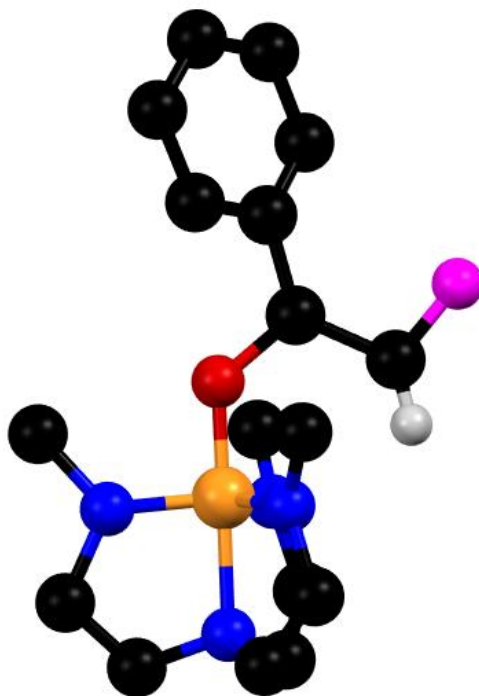
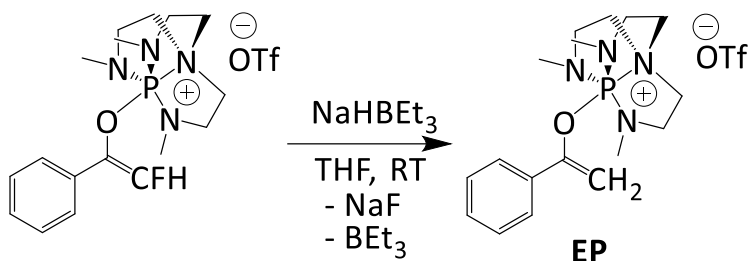


Figure 3: Resolved partial structure of FEP (E-isomer). Counteranion and protons omitted for clarity. C, black; N, blue; O, red; F, pink.

layering over a concentrated solution in DCM. Poor quality crystals only enabled the first half of the collection to represent the proposed structure of FEP. The fact that the diffraction data suggested an atom was present where the fluorine would be if the E-isomer was crystallized was the only useful data available. All the bond lengths are nonsensical. The mass spectral data corroborated the formation of the [FEP][OTf] isomers.



Scheme 15: Formation of [EP][OTf] by selective defluorination of [FEP][OTf]

Addition of a second equivalent of NaHBEt₃ to the crude mixture of [FEP][OTf] resulted in the disappearance of the ¹⁹F NMR signals corresponding to the FEP isomers (-151 ppm and -169 ppm). The ³¹P NMR spectrum corroborated the consumption of the FEP isomers by the disappearance of the two signals (-31 ppm and -33 ppm); a new species indicated by a singlet at -32 ppm suggested the formation of a new azaphosphatranium species. The ¹H NMR spectrum showed a set of doublets at 5.2 ppm (¹J_{H-H} = 2 Hz) and 4.8 ppm (¹J_{H-H} = 2 Hz). The ¹¹B NMR signal and precipitate formation suggested the generation of free borane and NaF salt. The NMR spectral data suggested the hydrodefluorination of FEP to form an alkenyl phosphatranium (EP). Mass spectral data corroborated the structure of [EP][OTf]. The product [EP][OTf] was collected as a white solid in 85 % yield through the same method as the [FEP][OTf] isomers. Single crystals were grown by layering pentane over a concentrated DCM solution. Single-crystal X-ray diffraction corroborated the structure of [EP][OTf].

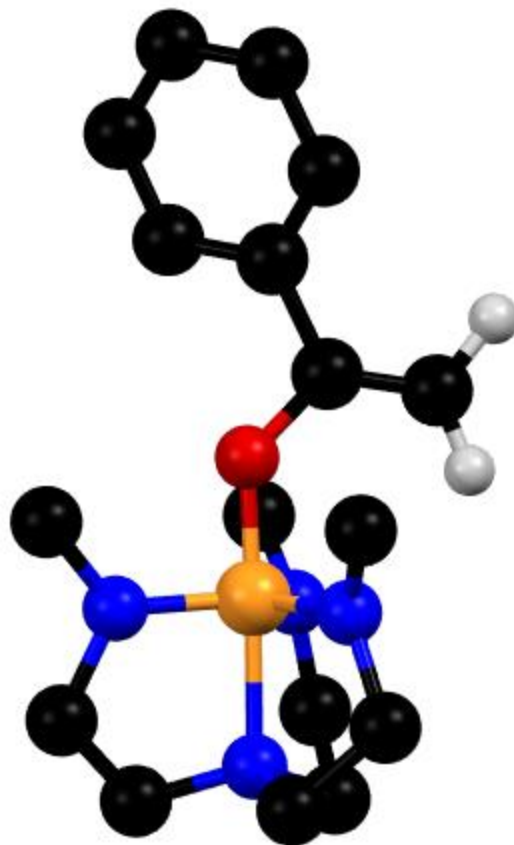
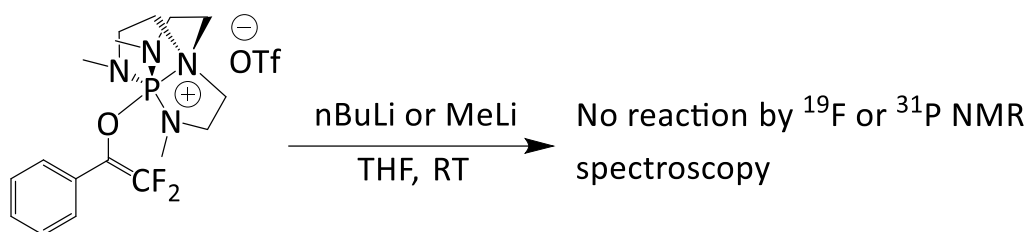


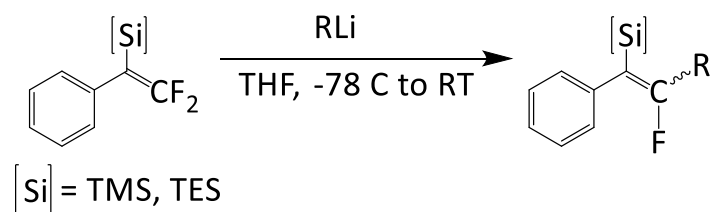
Figure 4: Molecular structure of EP. Counteranion and protons omitted for clarity. C, black; N, blue; O, red; F, pink.

The bridgehead P-N transannular distance for the XRD of EP was 1.982(3) Å which is considerably shorter than found in DFEP (2.033(2) Å). Decreasing the transannular distance results in the methyl groups “popping up” to eclipse the phosphatrane’s ethylene bridges.⁵⁶ The lower steric demand of the protons would decrease steric clash between the methyl groups as compared to the fluorines, possibly accounting for the observed difference in transannular distance. The sum of bond angles around P suggests a pseudo-trigonal bipyramidal geometry similar to DFEP. The bridgehead nitrogen had a smaller sum of bond angles of 335.3° compared to 337.7°, accounting for the shorter transannular distance.

Similar hydrodefluorination reactions of *gem*-difluoroalkene derivatives have become promising routes to access partially fluorinated building blocks useful for medicinal chemistry.⁵⁷ The simple protocol for the generation of DFEP and its defluorinated derivatives prompted our investigation towards the behaviour of DFEP towards nucleophiles.



To our surprise, addition of one equivalent of either MeLi or nBuLi to a solution of [DFEP][OTf] resulted in no observable change in the ^{19}F or ^{31}P NMR spectrum. This was true even when using a new bottle of organolithium reagent known to be in good condition. Including one equivalent of tetramethyldiamine (TMDA) to a solution of nBuLi did not enact chemistry from the organolithium reagent. Changing the nature of the organonucleophile to phenylmagnesium bromide still resulted in no change of the ^{19}F NMR or ^{31}P NMR spectrum. The lack of observable reactivity between the organolithium reagents and DFEP was surprising because similar conditions are used to perform addition-elimination reactions on

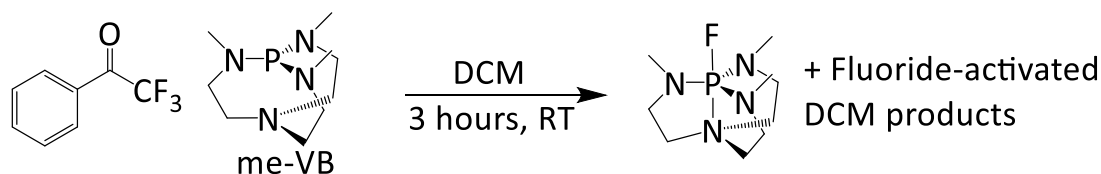


Scheme 16: Paquin et al. method for nucleophilic substitution of silylated β,β -difluorostyrenes.⁵⁸

silylated β,β -difluorostyrenes to generate silylated fluoroalkanes (scheme 16).⁵⁸ The lack of observable products indicative for the O-C bond breakage or O-P bond breakage was also

surprising. The effects of the azaphosphatrane moiety to protect the organic fragment from nucleophiles larger than hydride is exceptional. The methyl substituents pointing towards the difluoroenol moiety must impart substantial steric shielding.⁵⁶

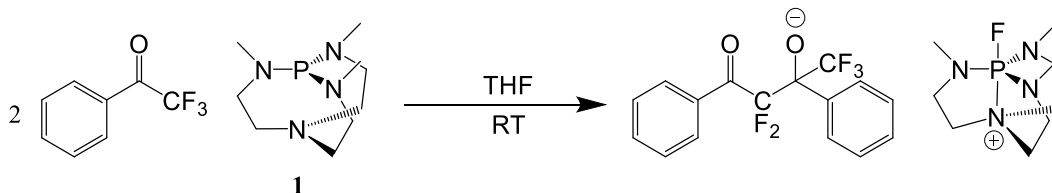
Other nucleophiles such as NaOH or fluoride surrogates ([TBA][F₂SiPh₃] and NEt₃·3HF) resulted in no reactivity according to NMR spectroscopy. However, addition of TBAF immediately changed the colourless solution to an orange colour. The ¹⁹F NMR spectrum demonstrated multiple new signals emerging, but the ³¹P NMR spectrum showed a doublet at -43 ppm (¹J_{P-F} = 724 Hz) and a singlet at 20 ppm corresponding to FP[NMeCH₂CH₂]₃N⁺ and OP(MeNCH₂CH₂)₃N, respectively. These two peaks suggest fluoride cleavage of O-P and O-C linkages of the DFEP species, respectively. The survival of the fluoroazaphosphatrane implicated fluoride-mediated decomposition of the fluoroazaphosphatrane was not occurring as observed in the Ramirez mechanism (scheme 12) because of the strong transannular interaction observed in the fluoroazaphosphatrane.⁴⁹ Therefore, investigation into the reaction involving me-VB with 2,2,2-trifluoroacetophenone in the absence of Lewis acid was conducted.



Scheme 17: Reaction between me-VB and 2,2,2-trifluoroacetophenone in DCM

Addition of 2,2,2-trifluoroacetophenone into a stirring solution of an equimolar me-VB mixture in DCM immediately resulted in an ¹⁹F NMR spectrum showing a triplet at -169 ppm (²J_{F-H} = 47 Hz), a doublet at -152 ppm (²J_{F-H} = 22 Hz), the DFEP peaks at -98 ppm and -111 ppm, and a doublet at -68 ppm (¹J_{F-P} = 726 Hz) corresponding to CFH₂Cl, HF₂⁻, DFEP, and

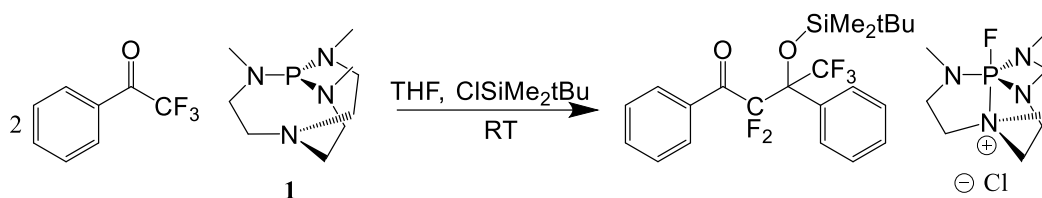
FP[NMeCH₂CH₂]₃N, respectively, among other transient species not identified. The ³¹P NMR spectrum showed a peak suggestive of DFEP (-29 ppm), and a doublet at -43 ppm (¹J_{P-F}= 726 Hz) corresponding to [FP[NMeCH₂CH₂]₃N]⁺. Two hours later, the dominant peaks in the ¹⁹F NMR spectrum corresponded to CFH₂Cl, CF₂HCl (-163 ppm, d, ²J_{F-H}= 79 Hz), and [FP[NMeCH₂CH₂]₃N]⁺, respectively. No observable peak suggesting a difluoroenolate species was present. The ³¹P NMR spectrum predominantly showed the FP[NMeCH₂CH₂]₃N⁺. Both ¹⁹F and ³¹P NMR spectra confirmed the survival of [FP[NMeCH₂CH₂]₃N]⁺ but the activation of the solvent implied the fluoride-mediated decomposition may still occur.



Scheme 18: Formation of [PhC(O)CF₂COCF₃Ph][FP[NMeCH₂CH₂]₃N] salt

Changing the solvent for THF provided a better indication to the fate of the difluoroenolate. An equimolar addition of me-VB to 2,2,2-trifluoroacetophenone in THF resulted in the formation of [FP[NMeCH₂CH₂]₃N]⁺ alongside a doublet of doublets at -73 ppm (⁴J_{F-F}= 14 Hz and 5 Hz), and a pair of doublet of quartets at -98 ppm (²J_{F-F}= 238 Hz and ⁴J_{F-F}= 5 Hz) and -106 ppm (²J_{F-F}= 238 Hz and ⁴J_{F-F}= 14 Hz), in the ¹⁹F NMR spectrum, suggesting the formation of 2,2,4,4,4-pentafluoro-3-hydroxy-1,3 diphenylbutan-1-one [PhC(O)CF₂COCF₃Ph]⁻ as the counteranion. Residual me-VB was observed in the ³¹P NMR spectrum. Doubling the equivalence of ketone to me-VB resulted in a cleaner product distribution with the predominant product as the

[PhC(O)CF₂COCF₃Ph][FP[NMeCH₂CH₂]₃N] salt (scheme19). *Tert*-Butyldimethylsilyl chloride was added to cap the alkoxide as



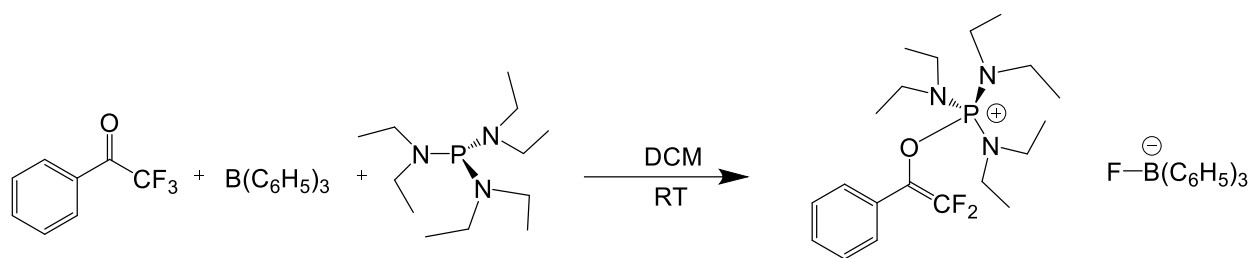
Scheme 19: Formation of 2,2,4,4,4-pentafluoro-3-tert-butyldimethylsilyloxy-1,3 diphenylbutan-1-one

2,2,4,4,4-pentafluoro-3-tert-butyldimethylsilyloxy-1,3 diphenylbutan-1-one. The silyl enol ether was collected with a 70 % isolated yield using flash chromatography over silica with 5 % EtOAc in hexane. This result represents an indirect observation of difluoroenolate chemistry accessed by main-group Lewis base-mediated selective defluorination of trifluoromethyl ketones.

The caged structure of the azaphosphatranes moiety in DFEP clearly provides substantial steric protection resulting in free fluoride or hydride to be the only nucleophiles which enacted chemistry. Furthermore, the transannular interaction of the azaphosphatranes renders nucleophilic attack at the O-P σ* inaccessible. Therefore, it was desirable to generate an acyclic derivative to facilitate subsequent transformations.

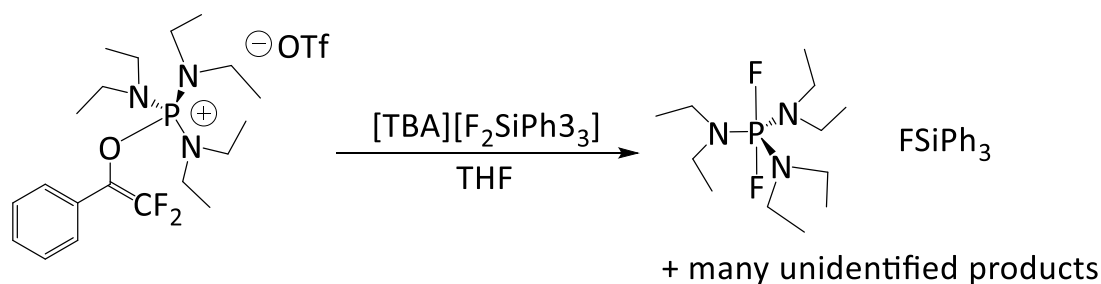
2.2 Using P(NEt₂)₃/B(C₆H₅)₃ FLP to capture DFEPn3: facile access to difluoroenolate chemistry

Acyclic tris(diethylamino)phosphine (PN3) was chosen due to ease of handling and reduced toxicity of the phosphine oxide relative to methyl derivative.



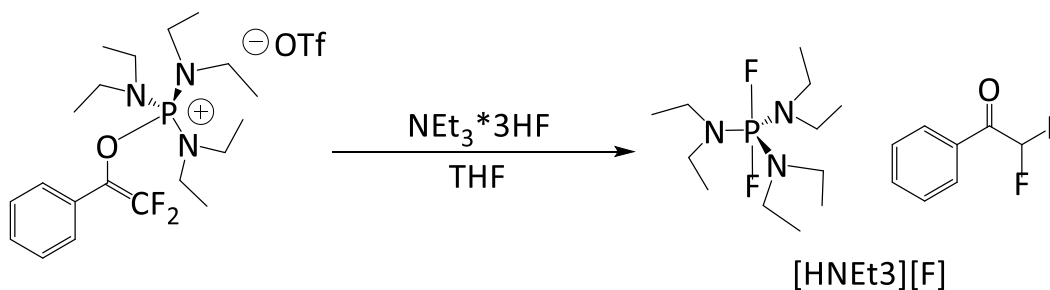
Scheme 20: Formation of [DFEPn3][FB(C₆H₅)₃]

An equimolar mixture of tris(diethylamino)phosphine (PN3) and triphenylborane in DCM results in no change to the chemical shifts relative to free-base or acid. Addition of 2,2,2-trifluoroacetophenone (TFA) to the FLP mixture resulted in the slow conversion (12 hours for completion) to a novel compound indicated by NMR spectroscopy. The ¹⁹F NMR spectrum showed the growth of a pair of doublet of doublets at -93 ppm (²J_{F-F}= 52 Hz, ⁴J_{F-P}= 6 Hz) and -105 ppm (²J_{F-F}= 52 Hz, ⁴J_{F-P}= 9 Hz) alongside a broad signal at -197 ppm. The ¹¹B NMR spectrum shows a doublet at 5 ppm (¹J_{B-F}= 76 Hz). The ³¹P NMR spectrum shows a doublet of doublets at 37 ppm (⁴J_{P-F}= 9, ⁴J_{P-F}= 6 Hz). The NMR spectral data suggested the formation of [DFEPn3][FB(C₆H₅)₃] salt. Mass spectral data (m/z= 402.2475) corroborated the proposed structure. The [DFEPn3][FB(C₆H₅)₃] was isolated from a concentrated DCM solution as a precipitate by adding pentane in 83 % yield. The [DFEPn3][OTf] salt was generated using the same protocol for [DFEP][OTf] in 87 % yield.



Scheme 21: Reaction between [DFEPn₃][OTf] and [TBA][F₂SiPh₃]

The formation of the DFEPn₃ was exciting because the acyclic P(V) phosphonium structure rendered the O-P σ^* orbital accessible for nucleophilic attack. The reactivity of [DFEPn₃][OTf] to fluoride anions was investigated by addition of an equimolar mixture of [TBA][F₂SiPh₃] and [DFEPn₃][OTf] in THF. The only identifiable peaks in the ¹⁹F NMR spectrum are a doublet at -58 ppm (¹J_{F-P} = 696 Hz) and a singlet at -168 ppm (FSiPh₃). The ³¹P NMR spectrum shows a triplet at -53 ppm (¹J_{P-Fax} = 696 Hz) suggestive of a five-coordinate phosphorous species. Together, the NMR spectral data suggests the fluoride cleavage of the O-P bond with a subsequent fluoride abstraction of the difluoroenolate moiety which leads to decomposition of the organic fragment and the formation of the difluorophosphorane (F₂PNEt₃) species. This result alongside the reactivity of me-VB with 2,2,2-trifluoroacetophenone corroborated the mechanism proposed by Ramirez. The DFEPn₃ intermediate is generated but susceptible to fluoride-decomposition resulting in fluorophosphonium and difluoroenolate species. The fluorophosphonium⁵⁹ is capable of interacting with the difluoroenolate through the F-P σ^* orbital to abstract another equivalent of fluoride and generate the difluorophosphorane. The PhC(O)CF carbene would also be generated. Efforts to capture this carbene species are underway.



Scheme 22: Reaction of [DFEPn3][OTf] and [NEt₃*3HF] to form 2,2-difluoroacetophenone

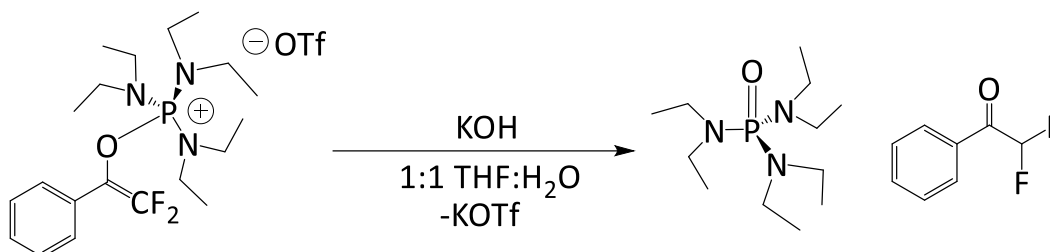
The possibility to trap the difluoroenolate moiety before subsequent fluoride abstraction by the fluorophosphonium seemed possible with an electrophile present. However, it was recognized that the fluoride abstraction by the fluorophosphonium would be a possible competitive pathway. Dropwise addition of [DFEPn3][OTf] to a stirring solution of dilute NEt₃*3HF in THF resulted in the ¹⁹F NMR spectrum showing the formation of F₂PNEt₃ (doublet at -57 ppm) and a new peak at -123 ppm (²J_{F-H} = 53 Hz) alongside a broad peak at -190 ppm. The fluorine peak at -123 ppm alongside a triplet at 6.3 ppm (²J_{H-F} = 53 Hz) in the ¹H NMR spectrum represents the formation of 2,2-difluoroacetophenone. The ³¹P NMR spectrum confirmed the formation of F₂PNEt₃. Isolation of the ketone was not performed due to time constraints.

The FLP-mediated conversion of 2,2,2-trifluoroacetophenone to 2,2-difluoroacetophenone represents the second methodology ever to enact this conversion and the first to accomplish it at room temperature.

2.3 Stability of [DFEPn3][OTf] under ambient conditions: reactions in aqueous medium

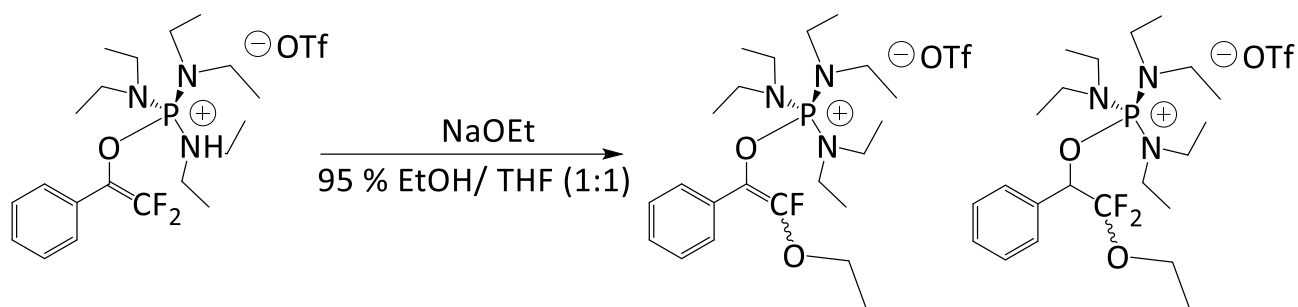
The stability of [DFEPn3][OTf] in the solid state was notable as no change in NMR spectral data was observed after two months in ambient atmosphere. This is in contrast to difluoro silyl ethers which require usage shortly after synthesis.¹⁰ The reactivity of the [DFEPn3][OTf] towards

fluoride indicated basic aqueous conditions could result in difluoroenolate chemistry through activation of the O-P bond representing a milder and safer condition to form 2,2-difluoroacetophenone.



Scheme 23: Reaction of [DFEPn3][OTf] and KOH in 1:1 mixture H₂O:THF

A mixture of 1:1 THF and H₂O was used to dissolve [DFEPn3][OTf]. No change in the ¹⁹F and ³¹P NMR spectrum was observed overnight at 60 °C. In contrast, difluoroenoxy silanes form 2,2-difluoroacetophenone under these conditions.⁶⁰ Adding one equivalent of KOH to the aqueous [DFEPn3][OTf] mixture resulted in no change at room temperature over a 24 hour period. However, at 60 °C overnight the ¹⁹F NMR spectrum shows the formation of three new peaks. The first was indicative of 2,2-difluoroacetophenone (-123 ppm, ²J_{F-H}= 53 Hz) and the second peak at -132 ppm (²J_{F-H}= 55 Hz) was interpreted to be the tetrahedral hydrate form of 2,2-difluoroacetophenone. The third was a doublet at -76 ppm (¹J_{P-F}= 950 Hz). The ³¹P NMR spectrum shows the formation of the phosphine oxide (OPNEt₃) alongside a doublet at 15 ppm (¹J_{P-F}= 950 Hz) suggesting the formation of (Et₂N)₂P(O)F.⁶¹ Isolation of 2,2-difluoroacetophenone was not performed due to time constraints.



Using fluoride as the nucleophile presented unambiguous evidence for electrophilic attack at the O-P bond to generate the difluoroenolate, but using KOH does not provide evidence towards O-P bond cleavage because O-C bond cleavage results in the same product distribution. Using ethoxide as the nucleophile was envisioned to provide distinct products whether O-P or O-C bond cleavage is observed. Addition of NaOEt in EtOH to a [DFEPn3][OTf] mixture in EtOH resulted in conversion of DFEPn3 into multiple product signals. The ^{19}F NMR spectrum shows a doublet at -112 ppm ($^4J_{\text{F-P}} = 10$ Hz), a doublet at -92.5 ppm ($^4J_{\text{F-P}} = 6$ Hz) and a pair of doublet of doublets at -83 ppm ($^2J_{\text{F-F}} = 143$ Hz, $^3J_{\text{F-H}} = 6$ Hz). The ^{31}P NMR spectrum shows clean conversion to three new peaks. A doublet at 38 ppm ($^4J_{\text{P-F}} = 10$ Hz), a doublet at 37 ppm ($^4J_{\text{P-F}} = 6$ Hz), and a singlet at 36 ppm. The NMR spectral data suggests the formation of the Z- and E-isomers from the addition-elimination reaction with ethoxide, and ethanol addition across the difluoroalkene double bond. The proposed addition-substitution of fluoride with ethoxide would represent a new methodology to access a potential oxyfluoroenolate synthons. Exploration to determine whether the fluoride-mediated O-P bond cleavage still occurs with the oxyfluoroenol phosphonium species is currently under investigation. Access to oxyfluoroketones has gained recent interest due to their chemical versatility.⁶²

2.4 Conclusion

The reaction between tris(dialkylamino)phosphine and 2,2,2-trifluoroacetophenone was explored in the context of Frustrated Lewis Pairs to trap a potential difluoroenolate synthon proposed by Ramirez. The *me*-VB/B(C₆H₅)₃ FLP reacts with 2,2,2-trifluoroacetophenone to generate difluoroalkenyl phosphatrane (DFEP) and fluoroborate (FB(C₆H₅)₃) through selective phosphine-mediated aliphatic C-F bond cleavage in the presence of a fluoride trap. The mechanism for the formation of [DFEP][FB(C₆H₅)₃] was computationally explored to involve initial interaction of the phosphine at the carbonyl carbon. Hydrodefluorination of DFEP by NaHBEt₃ to generate fluoroalkenyl phosphatrane (FEP) isomers and alkenyl phosphatrane (EP) was observed. Mild fluorinating agents such as NEt₃*3HF and [TBA][F₂SiPh₃] did not react with DFEP but highly reactive TBAF resulted in the cleavage of the O-P bond to generate a stable fluoroazaphosphatrane. The stability of the fluoroazaphosphatrane was applied to access difluoroenolate chemistry by reacting *me*-VB and 2,2,2-trifluoroacetophenone in the absence of B(C₆H₅)₃ to generate an aldol-homoadduct coupling product.

The stability of DFEP towards mild nucleophilic attack was rationalized to be imparted by the stabilized O-P σ* of the azaphosphatrane moiety. The use of an acyclic aminophosphine was explored. The P(NEt₂)₃/B(C₆H₅)₃ FLP reacted with 2,2,2-trifluoroacetophenone to generate difluoroalkenyl phosphonium (DFEPn₃) and fluoroborate. The acyclic structure of DFEPn₃ enabled facile fluoride-mediated cleavage of the O-P bond to access difluoroenolate chemistry. The first example of room temperature main-group compound-mediated conversion of 2,2,2-trifluoroacetophenone to 2,2-difluoroacetophenone was reported by reacting DFEPn₃ with NEt₃*3HF. Similar transformation to generate 2,2-difluoroacetophenone was accessible using KOH as the nucleophile, but the mechanism was ambiguous. An ethoxide nucleophile was

explored to better understand the electrophilic behaviour of DFEPn3. Addition-substitution reaction to exchange a fluoride with ethoxide was observed representing a facile access to a potential oxyfluoroenolate synthon.

3 References

1. Müller, K.; Faeh, C.; Diederich, F., Fluorine in Pharmaceuticals: Looking Beyond Intuition. *Science* **2007**, *317* (5846), 1881.
2. Wang, J.; Sanchez-Rosello, M.; Acena, J. L.; del Pozo, C.; Sorochinsky, A. E.; Fustero, S.; Soloshonok, V. A.; Liu, H., Fluorine in pharmaceutical industry: fluorine-containing drugs introduced to the market in the last decade (2001-2011). *Chemical reviews* **2014**, *114* (4), 2432-506.
3. Shen, Q.; Huang, Y.-G.; Liu, C.; Xiao, J.-C.; Chen, Q.-Y.; Guo, Y., Review of recent advances in CF bond activation of aliphatic fluorides. *Journal of Fluorine Chemistry* **2015**, *179*, 14-22.
4. Kelly, C. B.; Mercadante, M. A.; Leadbeater, N. E., Trifluoromethyl ketones: properties, preparation, and application. *Chem Commun (Camb)* **2013**, *49* (95), 11133-48.
5. K. Surya Prakash, G.; Wang, F., Fluorine: The New Kingpin of Drug Discovery. *Chimica oggi* **2012**, *30*, 30-36.
6. Meanwell, N. A., Fluorine and Fluorinated Motifs in the Design and Application of Bioisosteres for Drug Design. *Journal of medicinal chemistry* **2018**, *61* (14), 5822-5880.
7. Schweizer, E.; Hoffmann-Röder, A.; Schäfer, K.; A Olsen, J.; Fäh, C.; Seiler, P.; Obst-Sander, U.; Wagner, B.; Kansy, M.; Diederich, F., A Fluorine Scan at the Catalytic Center of Thrombin: C₂F, C₂OH, and C₂OMe Bioisosterism and Fluorine Effects on pK_a and log D Values. *ChemMedChem* **2006**, *1*, 611-21.
8. Wang, Y.; Callejo, R.; Slawin, A. M.; O'Hagan, D., The difluoromethylene (CF₂) group in aliphatic chains: Synthesis and conformational preference of palmitic acids and nonadecane containing CF₂ groups. *Beilstein journal of organic chemistry* **2014**, *10*, 18-25.
9. Orsi, D. L.; Altman, R. A., Exploiting the unusual effects of fluorine in methodology. *Chemical Communications* **2017**, *53* (53), 7168-7181.
10. Amii, H.; Kobayashi, T.; Hatamoto, Y.; Uneyama, K., Mg₀-promoted selective C–F bond cleavage of trifluoromethyl ketones: a convenient method for the synthesis of 2,2-difluoro enol silanes. *Chemical Communications* **1999**, (14), 1323-1324.
11. Uneyama, K.; Amii, H., A review of Mg metal-promoted C • F bond activation; a reliable synthetic approach to difluorinated organic compounds. *Journal of Fluorine Chemistry* **2002**, *114* (2), 127-131.
12. Doi, R.; Ohashi, M.; Ogoshi, S., Copper-Catalyzed Reaction of Trifluoromethylketones with Aldehydes via a Copper Difluoroenolate. *Angewandte Chemie International Edition* **2016**, *55* (1), 341-344.
13. Laitar, D. S.; Tsui, E. Y.; Sadighi, J. P., Catalytic Diboration of Aldehydes via Insertion into the Copper–Boron Bond. *Journal of the American Chemical Society* **2006**, *128* (34), 11036-11037.
14. Lowry, T. M., Valence and the structure of atoms and molecules. By Prof. G. N. Lewis. Pp. 172. American Chemical Monograph Series. New York: The Chemical Catalog Co., Inc., 1923. Price \$3. *Journal of the Society of Chemical Industry* **1924**, *43* (1), 17-17.
15. Brown, H. C.; Schlesinger, H. I.; Cardon, S. Z., Studies in Stereochemistry. I. Steric Strains as a Factor in the Relative Stability of Some Coördination Compounds of Boron. *Journal of the American Chemical Society* **1942**, *64* (2), 325-329.
16. Tochtermann, W., Struktur und Reaktionsweise organischer at-Komplexe. *Angewandte Chemie* **1966**, *78* (7), 355-375.
17. Welch, G. C.; Juan, R. R. S.; Masuda, J. D.; Stephan, D. W., Reversible, Metal-Free Hydrogen Activation. *Science* **2006**, *314* (5802), 1124-1126.

18. Stephan, D. W., The broadening reach of frustrated Lewis pair chemistry. *Science* **2016**, *354* (6317).
19. Welch, G. C.; Stephan, D. W., Facile Heterolytic Cleavage of Dihydrogen by Phosphines and Boranes. *Journal of the American Chemical Society* **2007**, *129* (7), 1880-1881.
20. Spies, P.; Erker, G.; Kehr, G.; Bergander, K.; Fröhlich, R.; Grimme, S.; Stephan, D. W., Rapid intramolecular heterolytic dihydrogen activation by a four-membered heterocyclic phosphane–borane adduct. *Chemical Communications* **2007**, (47), 5072-5074.
21. Rokob, T. A.; Hamza, A.; Stirling, A.; Soós, T.; Pápai, I., Turning Frustration into Bond Activation: A Theoretical Mechanistic Study on Heterolytic Hydrogen Splitting by Frustrated Lewis Pairs. *Angewandte Chemie International Edition* **2008**, *47* (13), 2435-2438.
22. Grimme, S.; Kruse, H.; Goerigk, L.; Erker, G., The Mechanism of Dihydrogen Activation by Frustrated Lewis Pairs Revisited. *Angewandte Chemie International Edition* **2010**, *49* (8), 1402-1405.
23. Chase, P. A.; Welch, G. C.; Jurca, T.; Stephan, D. W., Metal-Free Catalytic Hydrogenation. *Angewandte Chemie International Edition* **2007**, *46* (42), 8050-8053.
24. Spies, P.; Schwendemann, S.; Lange, S.; Kehr, G.; Fröhlich, R.; Erker, G., Metal-Free Catalytic Hydrogenation of Enamines, Imines, and Conjugated Phosphinoalkenylboranes. *Angewandte Chemie International Edition* **2008**, *47* (39), 7543-7546.
25. Wang, H.; Fröhlich, R.; Kehr, G.; Erker, G., Heterolytic dihydrogen activation with the 1,8-bis(diphenylphosphino)naphthalene/B(C₆F₅)₃ pair and its application for metal-free catalytic hydrogenation of silyl enol ethers. *Chemical Communications* **2008**, (45), 5966-5968.
26. Mahdi, T.; Stephan, D. W., Enabling Catalytic Ketone Hydrogenation by Frustrated Lewis Pairs. *Journal of the American Chemical Society* **2014**, *136* (45), 15809-15812.
27. Zhao, X.; Lough, A. J.; Stephan, D. W., Synthesis and Reactivity of Alkynyl-Linked Phosphonium Borates. *Chemistry – A European Journal* **2011**, *17* (24), 6731-6743.
28. Chernichenko, K.; Madarász, Á.; Pápai, I.; Nieger, M.; Leskelä, M.; Repo, T., A frustrated-Lewis-pair approach to catalytic reduction of alkynes to cis-alkenes. *Nature Chemistry* **2013**, *5*, 718.
29. (a) Stephan, D. W., “Frustrated Lewis pair” hydrogenations. *Organic & biomolecular chemistry* **2012**, *10* (30), 5740-5746; (b) Paradies, J., Metal-Free Hydrogenation of Unsaturated Hydrocarbons Employing Molecular Hydrogen. *Angewandte Chemie International Edition* **2014**, *53* (14), 3552-3557; (c) Lam, J.; Szkop, K. M.; Mosafari, E.; Stephan, D. W., FLP catalysis: main group hydrogenations of organic unsaturated substrates. *Chemical Society Reviews* **2019**.
30. (a) Mömming, C. M.; Otten, E.; Kehr, G.; Fröhlich, R.; Grimme, S.; Stephan, D. W.; Erker, G., Reversible Metal-Free Carbon Dioxide Binding by Frustrated Lewis Pairs. *Angewandte Chemie International Edition* **2009**, *48* (36), 6643-6646; (b) Mömming, C. M.; Otten, E.; Kehr, G.; Fröhlich, R.; Grimme, S.; Stephan, D. W.; Erker, G., Reversible, nicht metallunterstützte Bindung von Kohlendioxid durch frustrierte Lewis-Paare. *Angewandte Chemie* **2009**, *121* (36), 6770-6773.
31. Otten, E.; Neu, R. C.; Stephan, D. W., Complexation of Nitrous Oxide by Frustrated Lewis Pairs. *Journal of the American Chemical Society* **2009**, *131* (29), 9918-9919.
32. Sajid, M.; Elmer, L.-M.; Rosorius, C.; Daniliuc, C. G.; Grimme, S.; Kehr, G.; Erker, G., Facile Carbon Monoxide Reduction at Intramolecular Frustrated Phosphane/Borane Lewis Pair Templates. *Angewandte Chemie International Edition* **2013**, *52* (8), 2243-2246.
33. Zhao, X.; Stephan, D. W., Olefin–Borane “van der Waals Complexes”: Intermediates in Frustrated Lewis Pair Addition Reactions. *Journal of the American Chemical Society* **2011**, *133* (32), 12448-12450.
34. Dureen, M. A.; Stephan, D. W., Terminal Alkyne Activation by Frustrated and Classical Lewis Acid/Phosphine Pairs. *Journal of the American Chemical Society* **2009**, *131* (24), 8396-8397.
35. Fu, H. C.; You, F.; Li, H. R.; He, L. N., CO₂ Capture and in situ Catalytic Transformation. *Frontiers in chemistry* **2019**, *7*, 525.

36. Buss, F.; Mehlmann, P.; Muck-Lichtenfeld, C.; Bergander, K.; Dielmann, F., Reversible Carbon Dioxide Binding by Simple Lewis Base Adducts with Electron-Rich Phosphines. *J Am Chem Soc* **2016**, *138* (6), 1840-3.
37. Liu, L.; Lukose, B.; Ensing, B., A Free Energy Landscape of CO₂ Capture by Frustrated Lewis Pairs. *ACS Catalysis* **2018**, *8* (4), 3376-3381.
38. (a) Wang, X.; Xia, C.; Wu, L., Homogeneous carbon dioxide reduction with p-block element-containing reductants. *Green Chemistry* **2018**, *20* (24), 5415-5426; (b) Courtemanche, M.-A.; Légaré, M.-A.; Maron, L.; Fontaine, F.-G., Reducing CO₂ to Methanol Using Frustrated Lewis Pairs: On the Mechanism of Phosphine–Borane-Mediated Hydroboration of CO₂. *Journal of the American Chemical Society* **2014**, *136* (30), 10708-10717; (c) von Wolff, N.; Lefèvre, G.; Berthet, J. C.; Thuéry, P.; Cantat, T., Implications of CO₂ Activation by Frustrated Lewis Pairs in the Catalytic Hydroboration of CO₂: A View Using N/Si+ Frustrated Lewis Pairs. *ACS Catalysis* **2016**, *6* (7), 4526-4535; (d) Wang, T.; Stephan, D. W., Carbene-9-BBN Ring Expansions as a Route to Intramolecular Frustrated Lewis Pairs for CO₂ Reduction. *Chemistry – A European Journal* **2014**, *20* (11), 3036-3039.
39. Zhao, T.; Hu, X.; Wu, Y.; Zhang, Z., Hydrogenation of CO₂ to Formate with H₂: Transition Metal Free Catalyst Based on a Lewis Pair. *Angewandte Chemie International Edition* **2019**, *58* (3), 722-726.
40. Stephan, D. W.; Erker, G., Frustrated Lewis pair chemistry of carbon, nitrogen and sulfur oxides. *Chemical Science* **2014**, *5* (7), 2625-2641.
41. Johnstone, T. C.; Wee, G.; Stephan, D. W., Accessing Frustrated Lewis Pair Chemistry from a Spectroscopically Stable and Classical Lewis Acid-Base Adduct. *Angewandte Chemie* **2018**, *57* (20), 5881-5884.
42. Spies, P.; Kehr, G.; Bergander, K.; Wibbeling, B.; Fröhlich, R.; Erker, G., Metal-free dihydrogen activation chemistry: structural and dynamic features of intramolecular P/B pairs. *Dalton transactions* **2009**, (9), 1534-1541.
43. Caputo, C. B.; Stephan, D. W., Activation of Alkyl C–F Bonds by B(C₆F₅)₃: Stoichiometric and Catalytic Transformations. *Organometallics* **2012**, *31* (1), 27-30.
44. Mallov, I.; Ruddy, A. J.; Zhu, H.; Grimme, S.; Stephan, D. W., C–F Bond Activation by Silylium Cation/Phosphine Frustrated Lewis Pairs: Mono-Hydrodefluorination of PhCF₃, PhCF₂H and Ph₂CF₂. *Chemistry – A European Journal* **2017**, *23* (70), 17692-17696.
45. Bayne, J. M.; Stephan, D. W., C-F Bond Activation Mediated by Phosphorus Compounds. *Chemistry* **2019**, *25* (40), 9350-9357.
46. (a) Stahl, T.; Klare, H. F. T.; Oestreich, M., Main-Group Lewis Acids for C–F Bond Activation. *ACS Catalysis* **2013**, *3* (7), 1578-1587; (b) Amii, H.; Uneyama, K., C–F Bond Activation in Organic Synthesis. *Chemical reviews* **2009**, *109* (5), 2119-2183.
47. Ramirez, F., The reaction of triaminophosphines with perfluoroketones the so-called trisdimethylaminodifluoromethylenephosphorane. *Tetrahedron Letters* **1966**, *7* (30), 3651 - 3656.
48. Mark, V., Nucleophilic reactions of trivalent phosphorus compounds. Synthesis of stable difluoromethylenephosphorane analogs. *Tetrahedron Letters* **1964**, *5* (42), 3139 - 3144.
49. Johnstone, T. C.; Briceno-Strocchia, A. I.; Stephan, D. W., Frustrated Lewis Pair Oxidation Permits Synthesis of a Fluoroazaphosphatranes, [FP(MeNCH₂CH₂)₃N](⁺). *Inorganic chemistry* **2018**.
50. Tang, J. S.; Verkade, J. G., Synthesis and reactivity patterns of new proazaphosphatranes and quasi-azaphosphatranes ZP(MeNCH₂CH₂)₃N. *Journal of the American Chemical Society* **1993**, *115* (5), 1660-1664.
51. Ramirez, F.; Smith, C. P.; Pilot, J. F.; Gulati, A. S., Reaction of tertiary phosphines with hexafluoroacetone and with o-quinones. Attack by phosphorus on carbonyl oxygen and isolation of 2,2,2-trialkyl-2,2-dihydro-1,3,2-dioxaphospholanes. *The Journal of Organic Chemistry* **1968**, *33* (10), 3787-3794.

52. Grimme, S.; Ehrlich, S.; Goerigk, L., Effect of the damping function in dispersion corrected density functional theory. *Journal of Computational Chemistry* **2011**, *32* (7), 1456-1465.
53. Zhivetyeva, S. I.; Selivanova, G. A.; Goryunov, L. I.; Bagryanskaya, I. Y.; Shteingarts, V. D., Triphenylphosphanodefluorination of fluoranil and its derivatives. *Journal of Fluorine Chemistry* **2015**, *180*, 21-32.
54. Sabet-Sarvestani, H.; Eshghi, H.; Izadyar, M., Understanding the mechanism, thermodynamic and kinetic features of the Kukhtin-Ramirez reaction in carbamate synthesis from carbon dioxide. *RSC Advances* **2017**, *7* (3), 1701-1710.
55. Surya Prakash, G. K.; Hu, J.; Olah, G. A., Facile preparation of di- and monofluoromethyl ketones from trifluoromethyl ketones via fluorinated enol silyl ethers. *Journal of Fluorine Chemistry* **2001**, *112* (2), 355-360.
56. Windus, T. L.; Schmidt, M. W.; Gordon, M. S., Theoretical Investigation of Azaphosphatrane Bases. *Journal of the American Chemical Society* **1994**, *116* (25), 11449-11455.
57. Zhang, X.; Cao, S., Recent advances in the synthesis and CF functionalization of gem-difluoroalkenes. *Tetrahedron Letters* **2017**, *58* (5), 375-392.
58. Landelle, G.; Champagne, P. A.; Barbeau, X.; Paquin, J.-F., Stereocontrolled Approach to Bromofluoroalkenes and Their Use for the Synthesis of Tri- and Tetrasubstituted Fluoroalkenes. *Organic Letters* **2009**, *11* (3), 681-684.
59. Caputo, C. B.; Hounjet, L. J.; Dobrovetsky, R.; Stephan, D. W., Lewis Acidity of Organofluorophosphonium Salts: Hydrodefluorination by a Saturated Acceptor. *Science* **2013**, *341* (6152), 1374-1377.
60. Yu, J.-S.; Liu, Y.-L.; Tang, J.; Wang, X.; Zhou, J., Highly Efficient "On Water" Catalyst-Free Nucleophilic Addition Reactions Using Difluoroenoxy silanes: Dramatic Fluorine Effects. *Angewandte Chemie International Edition* **2014**, *53* (36), 9512-9516.
61. Sanhoury, M. A.; Ben Dhia, M. T.; Khaddar, M. R., Synthesis, characterization and solution behaviour of phosphoryl complexes of tin tetrafluoride. *Journal of Fluorine Chemistry* **2011**, *132* (11), 865-869.
62. Yuan, W.; Eriksson, L.; Szabó, K. J., Rhodium-Catalyzed Geminal Oxyfluorination and Oxytrifluoro-Methylation of Diazocarbonyl Compounds. *Angewandte Chemie International Edition* **2016**, *55* (29), 8410-8415.
63. Tang, J.-s.; Verkade, J. G., An improved synthesis of the strong base P(MeNCH₂CH₂)₃N. *Tetrahedron Letters* **1993**, *34* (18), 2903-2904.
64. Brown, H. C.; Racherla, U. S., Organoboranes. 44. A convenient, highly efficient synthesis of triorganylboranes via a modified organometallic route. *The Journal of Organic Chemistry* **1986**, *51* (4), 427-432.
65. Spyros, A.; Dais, P., ³¹P NMR spectroscopy in food analysis. *Progress in Nuclear Magnetic Resonance Spectroscopy* **2009**, *54* (3-4), 195-207.
66. ¹⁹F NMR and UV studies of xenon difluoride solution-vessel stability and its relevance to the fluorination of organic substrates. *Arkivoc* **2011**, *2011* (10), 221.
67. Peng, P.; Wu, J.-j.; Liang, J.-q.; Zhang, T.-y.; Huang, J.-w.; Wu, F.-h., Lithium triethylborohydride-promoted generation of α,α -difluoroenolates from 2-iodo-2,2-difluoroacetophenones: an unprecedented utilization of lithium triethylborohydride. *RSC Advances* **2017**, *7* (88), 56034-56037.
68. Frisch, M. J.; Trucks, G. W.; Schlegel, H. B.; Scuseria, G. E.; Robb, M. A.; Cheeseman, J. R.; Scalmani, G.; Barone, V.; Petersson, G. A.; Nakatsuji, H.; X. Li, M. C.; Marenich, A.; Bloino, J.; Janesko, B. G.; Gomperts, R.; Mennucci, B.; Hratchian, H. P.; Ortiz, J. V.; Izmaylov, A. F.; Sonnenberg, J. L.; Williams-Young, D.; Ding, F.; Lipparini, F.; Egidi, F.; Goings, J.; Peng, B.; Petrone, A.; Henderson, T.; Ranasinghe, D.; Zakrzewski, V. G.; Gao, J.; Rega, N.; Zheng, G.; Liang, W.; Hada, M.; Ehara, M.; Toyota, K.; Fukuda, R.; Hasegawa, J.; Ishida, M.; Nakajima, T.; Honda, Y.; Kitao, O.; Nakai, H.; Vreven, T.; Throssell, K.; J. A.

Montgomery, J.; Peralta, J. E.; Ogliaro, F.; Bearpark, M.; Heyd, J. J.; Brothers, E.; Kudin, K. N.; Staroverov, V. N.; Keith, T.; Kobayashi, R.; Normand, J.; Raghavachari, K.; Rendell, A.; Burant, J. C.; Iyengar, S. S.; Tomasi, J.; Cossi, M.; Millam, J. M.; Klene, M.; Adamo, C.; Cammi, R.; Ochterski, J. W.; Martin, R. L.; Morokuma, K.; Farkas, O.; Foresman, J. B.; Fox, D. J. *Gaussian 09, Revision E.01.*, Gaussian Inc., : Wallingford CT, 2016.

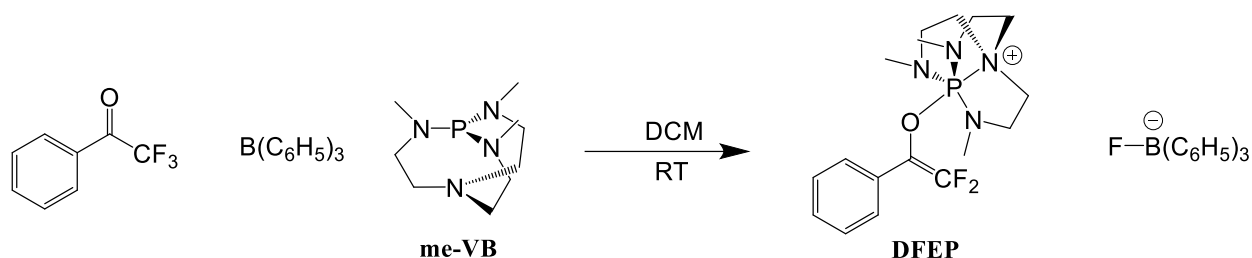
4 Supporting Information

4.1 General Considerations

All experimental manipulations were performed under dry and oxygen-free nitrogen atmosphere. Standard Schlenk techniques and VAC atmospheres glove box were used for all experiments unless otherwise specified. Glassware was oven-dried overnight and cooled under vacuum. Tetrahydrofuran (THF) was distilled off benzophenone/Na mixture, all other solvents (dichloromethane, pentanes) were used purchased from Sigma-Aldrich dried using a Grubbs-type innovative Technologies solvent purification system. All solvents were stored over 4 Å sieves. Deuterated solvents (CDCl_3) were purchased from Cambridge Isotopes Laboratories, Inc. and distilled from CaH_2 . 2,2,2-Trifluoroacetophenone was purchased from Tokyo Chemistry Industry America, 2,8,9-Trimethyl-2,5,8,9-tetraaza-1-phospha-bicyclo[3.3.3]undecane ($\text{P}(\text{MeNCH}_2\text{CH}_2)_3\text{N}$)⁶³ and triphenylborane were synthesized according to literature.⁶⁴ All heteronuclear (^{31}P , ^{19}F , ^{11}B) NMR data was collected using Bruker Avance III 400 MHz instrument and referenced to 85% H_3PO_4 (aqueous), CFCl_3 and $\text{BF}_3 \cdot \text{OEt}_2$, respectively. Mass spectrometry was collected by AIMS Mass Spectrometry Laboratory at the University of Toronto.

4.2 Synthetic Procedure

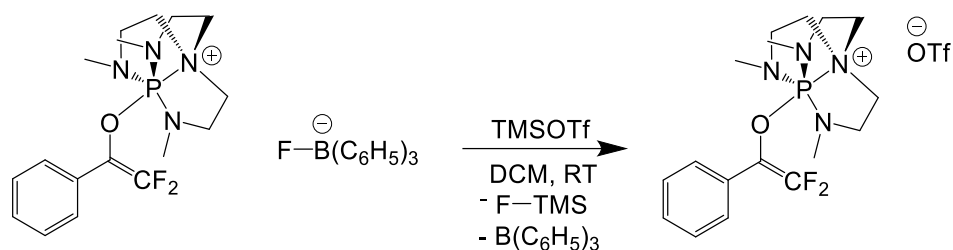
Synthesis of DFEP[FB(C_6H_5)₃]



To a solid mixture of me-VB (10 mg, 0.046 mmol, 1.0 equiv) and $B(C_6H_5)_3$ (22 mg, 0.046 mmol, 1.0 equiv), DCM (1.5 mL) was added to solubilize the FLP. Separately, 2,2,2-trifluoroacetophenone was dissolved as a DCM solution. The 2,2,2-trifluoroacetophenone DCM solution was added dropwise to a stirring solution of the FLP. The reaction was left to stir for 5 minutes. The product was isolated by precipitating a saturated DCM solution in pentane, filtering off supernatant, redissolving powder in DCM, and removing solvent under vacuum to form a white powder. ^{31}P , ^{19}F , ^{11}B , 1H , and ^{13}C NMR spectra were obtained.

^{19}F NMR (377 MHz, $CDCl_3$) δ -97.2 ppm (1F, d, $^2J_{F-F} = 70$ Hz), -111.1 (1F, d, $^2J_{F-F} = 70$ Hz), -196.5 (1F, broad). ^{31}P NMR (162 MHz, $CDCl_3$) δ -27.2 ppm (1P, s). ^{11}B NMR (128 MHz, $CDCl_3$) δ 4.0 ppm (1B, d, $^1J_{B-F} = 76$ Hz). 1H NMR (500 MHz, $CDCl_3$) δ 7.6 ppm (6H, dd, $^3J_{H-H} = 8$ Hz, 1 Hz), 7.4 (5H, m), 7.1 (6H, t, $^3J_{H-H} = 7$ Hz), 7.0 (3H, $^3J_{H-H} = 7$ Hz, $^4J = 1$ Hz), 2.83 (6H dt, $^3J_{H-P} = 13$ Hz, $^2J_{H-H} = 7$ Hz), 2.67 (9H, d, $^3J_{H-P} = 8$ Hz), 2.5 (6H, td, $^2J_{H-H} = 6$ Hz, $^4J_{H-P} = 3$ Hz). ^{13}C NMR (126 MHz, $CDCl_3$) δ 133 ppm (d, 1C, $^2J_{C-P} = 6$ Hz), 129.3 (s, 2C), 128.9 (s, 6C), 128.5 (s, 2C), 127.3 (dd, 1C, $^1J_{C-F} = 5$, $^1J_{C-F} = 3$ Hz), 126.8 (s, 1C), 126.4 (s, 6C), 123.4 (s, 3C), 46.1 (d, 3C, $^3J_{C-P} = 9$ Hz), 45.7 (d, 3C, $^2J_{C-P} = 10$ Hz), 38.4 (dd, 3C, $^2J_{C-P} = 4$, $^6J_{C-F} = 2$ Hz). Isolated yield: 87 %. HRMS (ESI+) calcd for: $C_{17}H_{26}F_2N_4OP^+$ 371.1807, found 371.1802.

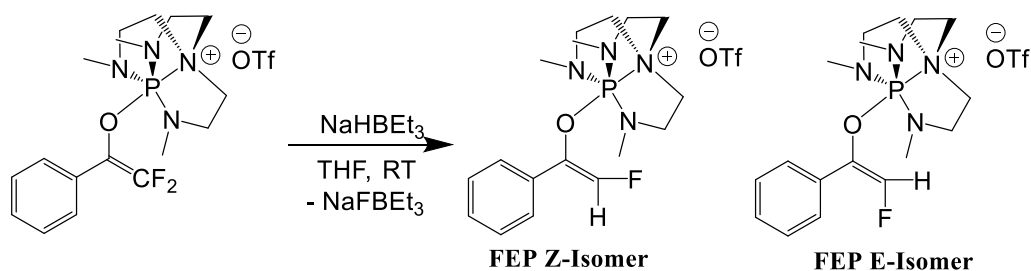
Synthesis of DFEP[OTf]



To a DCM (2 mL) solution of [DFEP][FB(C₆H₅)] (40 mg, 0.046 mmol 1 equiv), a DCM (2 mL) solution of TMSOTf (15 mg, 0.067 mmol, 1.5 equiv) was added dropwise. Solution was left to stir for 5 minutes then concentrated under vacuum and precipitated over pentane to isolate the desired product as a white powder. Filtered off supernatant and redissolved in DCM. White powder obtained by removing solvent under vacuum. ³¹P, ¹⁹F NMR spectra were obtained.

¹⁹F NMR (377 MHz, CDCl₃) δ -78.4 ppm (3F, s), -97.0 (1F, d, *J*_{F-F} = 70 Hz), -110.3 (1F, d, ²*J*_{F-F} = 70 Hz). ³¹P NMR (162 MHz, CDCl₃) δ -27.2 ppm (1P, s). Isolated yield: 89 %. HRMS (ESI+) calcd for: C₁₇H₂₆F₂N₄OP⁺ 371.1807, found 371.1802.

Synthesis of FEP[OTf]



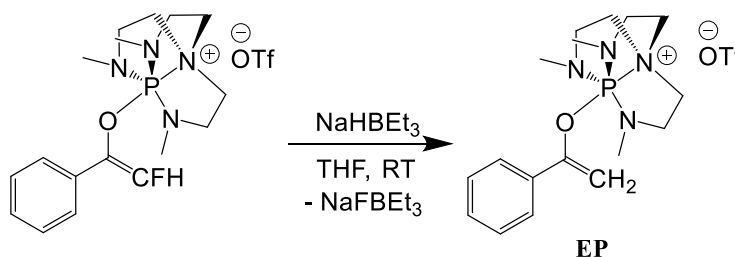
To a THF (2 mL) solution of [DFEP][OTf] (24 mg, 0.046 mmol, 1 equiv), a 0.01 M solution of NaHBET₃ (0.046 mmol, 1 equiv) was added dropwise under constant stirring over 5 minutes.

Desired product was isolated by precipitating in pentane, filtered off supernatant and redissolved

in DCM. White powder obtained by removing solvent under vacuum. ^{31}P , ^{19}F , ^{11}B , ^1H NMR spectra were obtained. The crude ^{11}B NMR spectrum was silent.

^{19}F NMR (377 MHz, CDCl_3) δ -78.2 ppm (3F, s) -151.32 ppm (1F, d, $J_{\text{H-F}} = 77$ Hz), -162.51 (1F, d, $J_{\text{H-F}} = 79$ Hz). ^{31}P NMR (162 MHz, CDCl_3) δ -31.59 ppm (1P, s), -33.13 (1P, s). ^1H NMR (400 MHz, CDCl_3) δ 7.6 ppm (2H (Z+E), m), 7.4 (8H, (Z+E)), 7.14 (1H (Z), d, $^2J_{\text{H-F}} = 79$ Hz), 6.8 (1H (E), d, $^2J_{\text{H-F}} = 77$ Hz), 3.3 (24H, m), 2.9 (6H, d (Z), $^3J_{\text{H-P}} = 12$ Hz), 2.9 (6H, d (E), $^4J_{\text{H-P}} = 11$ Hz). ^{13}C NMR (126 MHz, CDCl_3) δ 129.5 ppm (1C, s), 129.3 (1C, s), 129.1 (2C, s), 128.7 (2C, s), 127.1 (1C, d, $^1J_{\text{C-F}} = 7$ Hz), 126.0 (1C, d, $^2J_{\text{C-P}} = 3$ Hz), 47.0 (3C, d (3a), $^3J_{\text{C-P}} = 9$ Hz), 46.3 (3C, d (E), $^3J_{\text{C-P}} = 9$ Hz), 46.0 (3C, d (Z), $^3J_{\text{C-P}} = 9$ Hz), 45.7 (3C, d (E), $^2J_{\text{C-P}} = 10$ Hz). Isolated yield: 80% yield. HRMS (ESI+) calcd for: $\text{C}_{17}\text{H}_{27}\text{FN}_4\text{OP}^+$ 353.1901, found 353.1899.

Synthesis of EP[OTf]

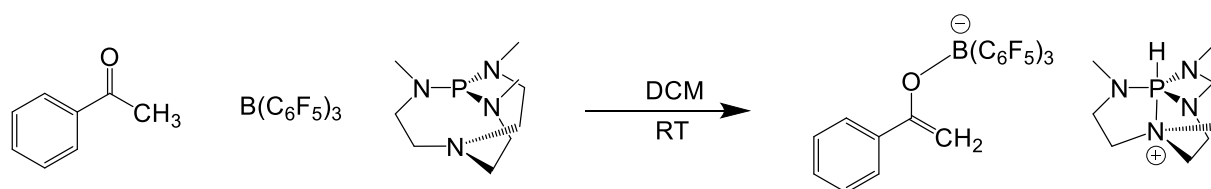


To a THF (2 mL) solution of DFEP[OTf] (24 mg, 0.046 mmol, 1 equiv), a 0.01 M THF solution of KHBEt_3 (0.046 mmol, 1 equiv) was added dropwise under constant stirring over 5 minutes.

Desired product was isolated by precipitating in pentane, filtered off supernatant and redissolved in DCM. White powder obtained by removing solvent under vacuum. ^{31}P , ^{19}F , ^1H NMR spectra were obtained.

^{19}F NMR (377 MHz, CDCl_3) δ -78.3 ppm (3F, s). ^{31}P NMR (162 MHz, CDCl_3) δ -33.6 ppm (1P, s). ^1H NMR (500 MHz, CDCl_3) δ 7.6 ppm (2H, m), 7.4 (3H, m), 5.2 (1H, $^2J_{\text{H-H}} = 2$), 4.8 (1H, $^2J_{\text{H-H}} = 2$), 3.3 (12H, m), 2.9 (9H, $^3J_{\text{H-P}} = 11$ Hz). ^{13}C NMR (100 MHz, CDCl_3) δ 153.3 ppm (1C, d, $^2J_{\text{C-P}} = 9$ Hz), 135.6 (1C, d, $^3J_{\text{C-P}} = 8$ Hz), 129.1 (1C, s), 128.7 (2C, s), 125.4 (2C, s), 95.3 (1C, s), 46.6 (3C, d, $^3J_{\text{C-P}} = 9$ Hz), 45.8 (3C, d, $^2J_{\text{C-P}} = 9$ Hz), 39.0 (3C, d, $^3J_{\text{C-P}} = 4$ Hz). Isolated yield: 85%. HRMS (ESI+) calcd for: $\text{C}_{17}\text{H}_{26}\text{F}_2\text{N}_4\text{OP}^+$ 371.1807, found 371.1802.

Synthesis of $[\text{PhC}(\text{O-B}(\text{C}_6\text{F}_5)_3)\text{CH}_2][\text{HP}(\text{MeNCH}_2\text{CH}_2)_3\text{N}]$:

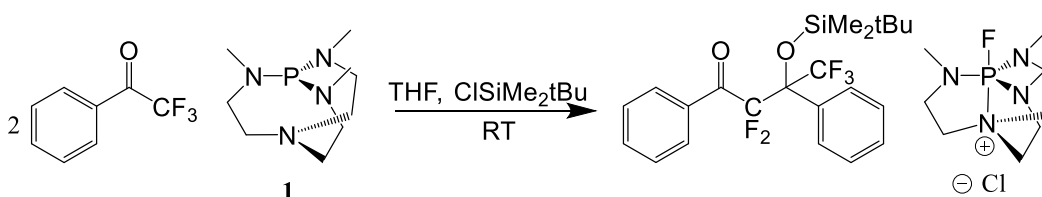


To a solid mixture of **1** (10 mg, 0.046 mmol, 1.0 equiv) and $\text{B}(\text{C}_6\text{F}_5)_3$ (23.7 mg, 0.046 mmol, 1.0 equiv), DCM (1.5 mL) was added. Separately, 2,2,2-trifluoroacetophenone was dissolved as a DCM solution. The 2,2,2-trifluoroacetophenone solution was added dropwise to the FLP mixture. The product was isolated by precipitating a saturated DCM solution in pentane, filtering off supernatant, redissolving powder in DCM, and removing solvent under vacuum to form a white powder. ^{31}P , ^{19}F , ^{11}B , ^1H , and ^{13}C NMR spectra were obtained.

^{19}F NMR (377 MHz, CDCl_3) δ -133.8 ppm (6F, d, $^3J_{\text{F-F}} = 24$ Hz), -163.1 (3F, m), -167.2 (6F, t, $^3J_{\text{F-F}} = 21$ Hz). ^{31}P NMR (162 MHz, CD_2Cl_2) δ -9.7 ppm (1P, d, $^1J_{\text{P-H}} = 498$ Hz). ^{11}B NMR (128 MHz, CDCl_3) δ -3.7 ppm (1B, s). ^1H NMR (500 MHz, CDCl_3) δ 7.7 ppm (2H, dm, $^3J_{\text{H-H}} = 8$ Hz), 7.2 (2H, tm, $^3J_{\text{H-H}} = 8$ Hz), 7.2 (1H, tm, $^3J_{\text{H-H}} = 7$ Hz), 5.2 (1H, d, $^1J_{\text{H-P}} = 494$ Hz), 2.9 (12H, m), 2.6 (9H, d, $^3J_{\text{H-P}} = 17$ Hz). ^{13}C NMR (100 MHz, CDCl_3) δ 159.0 (s), 148.5 (dm), 141.6 (s), 137.5

(tm), 128.0 (m), 127.5 (m), 126.0 (s), 83.2 (1C, s), 47.7 (3C, d, $^2J_{C-P} = 7$ Hz), 41.4 (3C, d, $^3J_{C-P} = 5$ Hz), 34.8 (3C, m). MS not available due to cleaning method forming boroformate adduct.

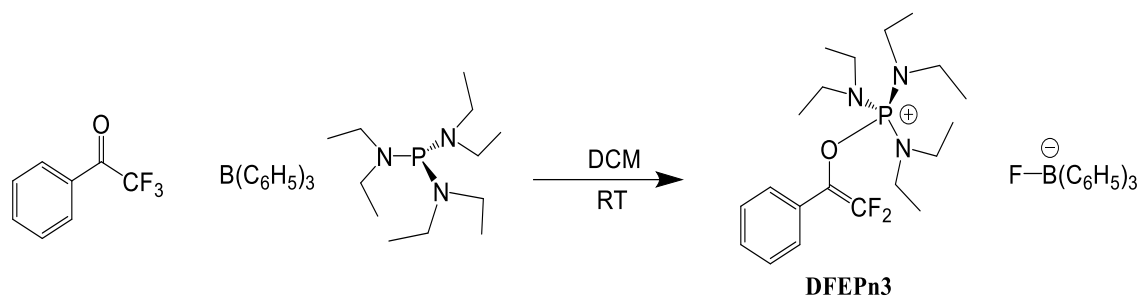
Synthesis of 2,2,4,4,4-pentafluoro-3-tert-butyldimethylsilyloxy-1,3 diphenylbutan-1-one:



A THF (1 mL) solution of 2,2,2-trifluoroacetophenone (8 mg, 0.046 mmol, 1 equiv) was added dropwise, rapidly, to a THF (1 mL) solution of 1 (5 mg, 0.023 mmol, 0.5 equiv). The reaction mixture was quickly quenched with a THF (0.5 mL) solution of ClSiMe₂tBu (12 mg, 0.070 mmol, 1.5 equiv). The chloride salt crashes out while the desired product remains in the supernatant. The 2,2,4,4,4-pentafluoro-3-silyl ether 1,3 diphenylbutan-1-one was isolated using a preparative TLC (5 % EtOAc in Hexane). ^{19}F , ^1H , and ^{13}C NMR spectra were collected.

Data for isolated neutral compound ((FP(NMeCH₂CH₂)N⁺ already reported⁴⁹): ^{19}F NMR (377 MHz, CDCl₃) δ -69.06 ppm (3F, dd, $^4J_{F-F} = 12$ Hz, 13 Hz), -104.2 (1F, dq, $^2J_{F-F} = 277$ Hz, $^4J_{F-F} = 12$ Hz), -104.5 (1F, $^2J_{F-F} = 277$ Hz, $^4J_{F-F} = 13$ Hz). ^1H NMR (500 MHz, CDCl₃) δ 7.8 ppm (2H, m), 7.6 (2H, m), 7.5 (1H, m), 7.3 (5H, m), 0.9 (9H, s), 0.12 (3H, s), 0.07 (3H, s). ^{13}C NMR (100 MHz, CDCl₃) δ 133.0 ppm, 130.3, 129.5, 128.5, 128.0, 127.6, 26.2, 19.5. Isolated yield: 70 %. HRMS (DART) calcd for: C₂₂H₂₇O₃Si[H₂O] 462.16496, found 462.1883.

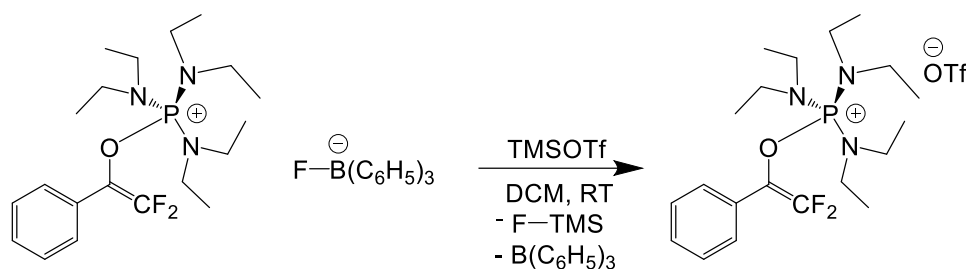
Synthesis of DFEPn3[FB(C₆H₅)₃]:



Hexaethyltriaminophosphine (11 mg, 0.046 mmol, 1.0 equiv) and $B(C_6H_5)_3$ (22 mg, 0.047 mmol, 1.0 equiv) were weighed separately and then mixed in DCM (1.5 mL). Separately, 2,2,2-trifluoroacetophenone was dissolved as a DCM solution and added dropwise to the FLP mixture. The product was isolated by precipitating a saturated DCM solution in pentane, filtering off supernatant, redissolving powder in DCM, and removing solvent under vacuum to form a white powder. ^{31}P , ^{19}F , ^{11}B , 1H , and ^{13}C NMR spectra were obtained.

^{19}F NMR (377 MHz, $CDCl_3$) δ -92.6 ppm (1F, dd, $^2J_{F-F} = 52$ Hz, $^4J_{F-P} = 6$ Hz), -105.1 (1F, d, $^2J_{F-F} = 52$ Hz, $^4J_{F-P} = 9$), -196.5 (1F, broad). ^{31}P NMR (162 MHz, $CDCl_3$) δ 37.4 ppm (1P, dd, $^4J_{P-F} = 9$, $^4J_{P-F} = 6$ Hz). ^{11}B { ^{19}F } NMR (128 MHz, $CDCl_3$) δ 4.0 ppm (1B, s). 1H NMR (500 MHz, $CDCl_3$) 7.5 ppm (6H, m), 7.5 (2H, d, $^3J_{H-H} = 2$ Hz), 7.5 (1H, d, $^3J_{H-H} = 2$ Hz), 7.3 (2H, m), 7.1 (6H, m), 6.9 (3H, m), 2.9 (12H, dq, $^3J_{H-P} = 11$ Hz, $^3J_{H-H} = 7$ Hz), 1.0 (18H, t, $^3J_{H-H} = 7$ Hz). ^{13}C NMR (100 MHz, $CDCl_3$) δ 133.1 (6C, s), 131.0 (1C, s), 129.5 (2C, s), 127.5 (6C, t, $^3J_{C-F} = 3$ Hz), 127.1 (1C, dt, $^2J_{C-P} = 5$ Hz, $^2J_{C-F} = 1$), 126.0 (6C, s), 122.9 (3C, s), 40.5 (6C, d, $^2J_{C-P} = 5$ Hz), 13.1 (6C, d, $^3J_{C-P} = 3$ Hz). Isolated yield: 83 %. HRMS (ESI+) calcd for: $C_{20}H_{35}F_2N_3OP^+$ 402.24803, found 402.2475.

Synthesis of DFEPn3[FB(C₆H₅)₃]:



To a DCM (2 mL) solution of [DFEPn3][FB(C₆H₅)] (0.046 mmol 1 equiv), a DCM (2 mL) solution of TMSOTf (15 mg, 0.067 mmol, 1.5 equiv) was added dropwise. Solution was left to stir for 5 minutes then concentrated under vacuum and precipitated over pentane to isolate the desired product as a white powder. Filtered off supernatant and redissolved in DCM. White powder obtained by removing solvent under vacuum. ³¹P, ¹⁹F NMR spectra were obtained.

¹⁹F NMR (377 MHz, CDCl₃) δ -78.4 ppm (3F, s), -92.6 (1F, dd, ²J_{F-F} = 52 Hz, ⁴J_{F-P} = 6 Hz), -105.1 (1F, d, ²J_{F-F} = 52 Hz, ⁴J_{F-P} = 9), -196.5 (1F, broad). ³¹P NMR (162 MHz, CDCl₃) δ 37.4 ppm (1P, dd, ⁴J_{P-F} = 9, ⁴J_{P-F} 6 Hz).

4.3 Auxiliary Reactions

Reactions with other phosphines:

POEt₃, PEt₃, PPh₃, PtBu₃ and PCy₃, were used as the Lewis base and B(C₆H₅)₃ as the Lewis acid to react with 2,2,2-trifluoroacetophenone. No change in the ¹⁹F NMR spectra was detected after 24 hours at room temperature. The temperature was elevated to 60 °C for an additional 8 hours and no reactivity was observed. PPh₃ formed an insoluble adduct with BPh₃.

Semi-quantitative ³¹P NMR experiment to quantify formation of FEP:

Analysis on the selectivity of the hydrodefluorination to form [FEP][OTf] from DFEP][OTF] was explored using ^{31}P NMR spectroscopy. The phosphorous group in both DFEP and FEP are very similar reducing the necessity for the determination of the long spin-lattice relaxation times T_1 . To increase the accuracy of the ^{31}P NMR spectral integration capillaries with $\text{P}(\text{C}_6\text{H}_5)_3$ (0.05 M) and $\text{Cr}(\text{acac})_3$ (0.005 M) in CDCl_3 were used.⁶⁵ The initial [DFEP][OTf] solution in THF (1 mL, 0.046 M) was prepared and added to a 5 mm NMR tube preloaded with the capillary tube. The solvent line meniscus was careful indicated to determine the volume used. After the NMR spectrum was obtained approximately 200 μL of the solvent was carefully evaporated. Using a micro syringe NaHBET_3 (46 μL , 1 M THF solution) was slowly added to the NMR solution. Additional solvent was added to reach the same volume as the initial NMR sample to appropriately compare the relatively integration between the initial and final NMR spectrum. Figure 1 (below) shows two important results: 1) the relative concentration of $\text{HP}(\text{NMeCH}_2\text{CH}_2)_3\text{N}^+$ remained constant suggesting the absence of P-O cleavage by hydride as side reaction and 2) the amount of FEP product relative to DFEP starting amount was close to 1:1.

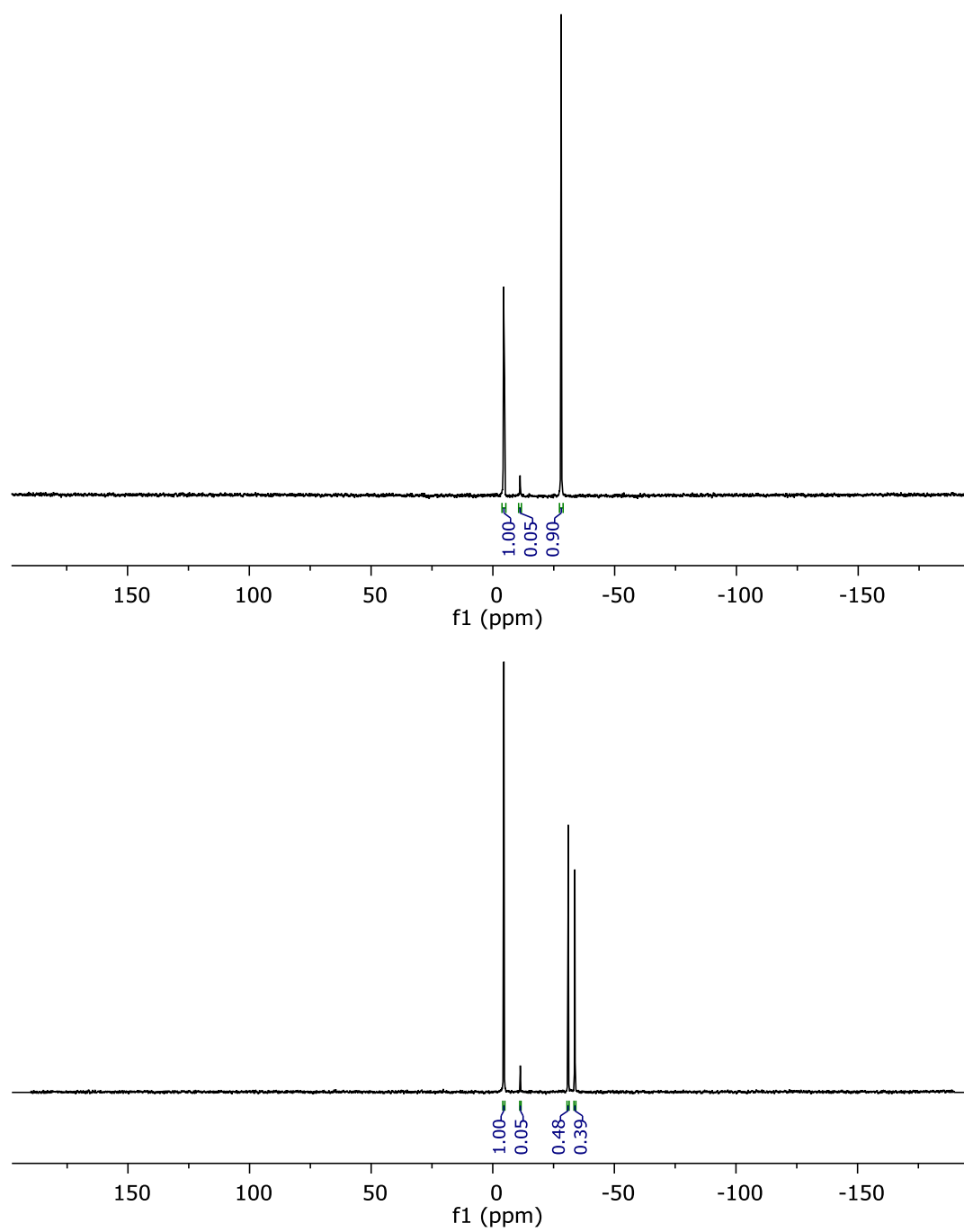
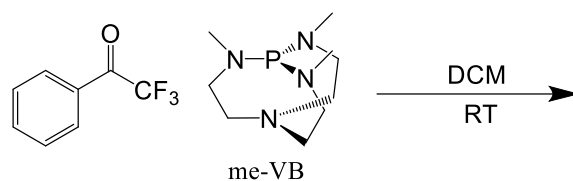


Figure S 1: Semi-quantitative $^{31}\text{P}\{\text{H}\}$ NMR spectrum analysis on the hydrodefluorination selectivity.

Initial spectrum (top) of $[\text{DFEP}][\text{OTf}]$ in THF and crude mixture after addition of 1 equivalent of NaHBEt_3 (bottom).

Reactivity between 2,2,2-trifluoroacetophenone and me-VB in DCM in DCM:



Mixture of equimolar amounts of 2,2,2-trifluoroacetophenone and **1** in DCM led to complex mixture which activates DCM resulting in formation of CFH_2Cl , DFEP, and fluoroazaphosphatane⁴⁹ among other transient products.

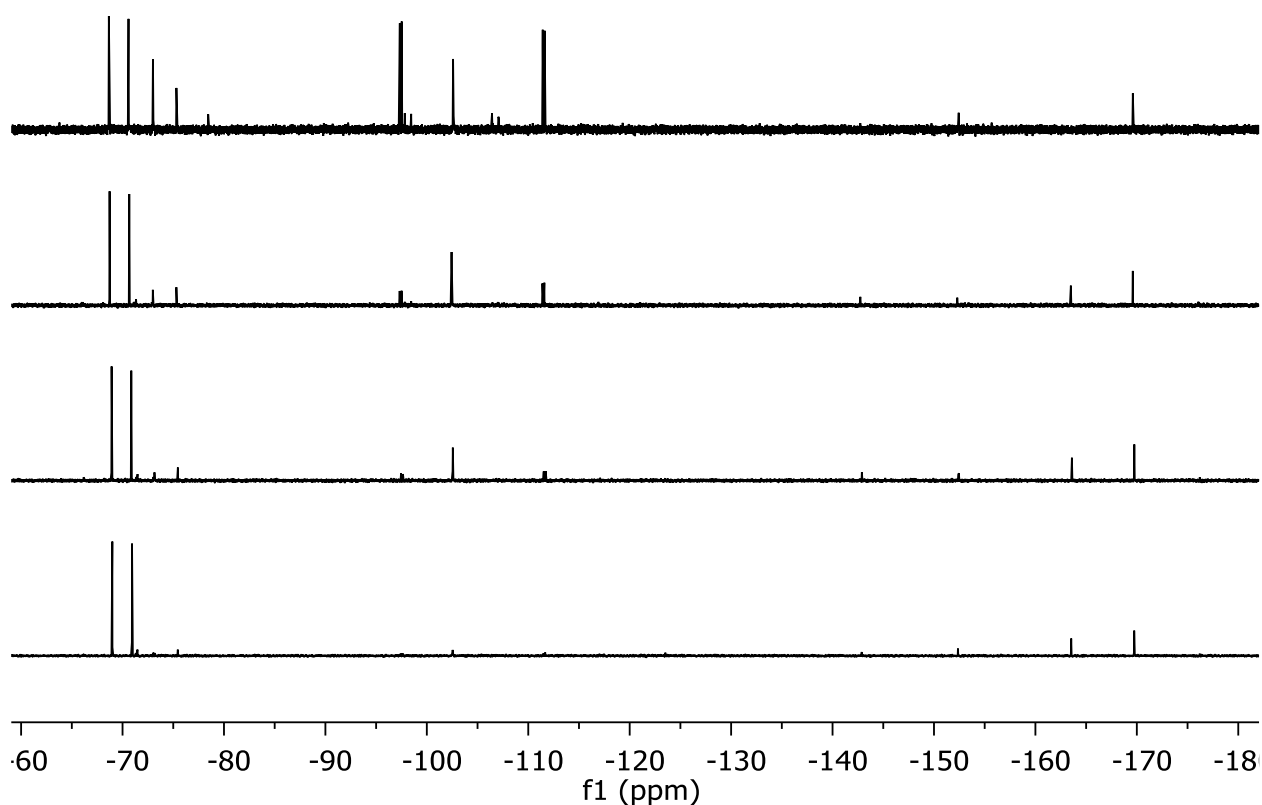
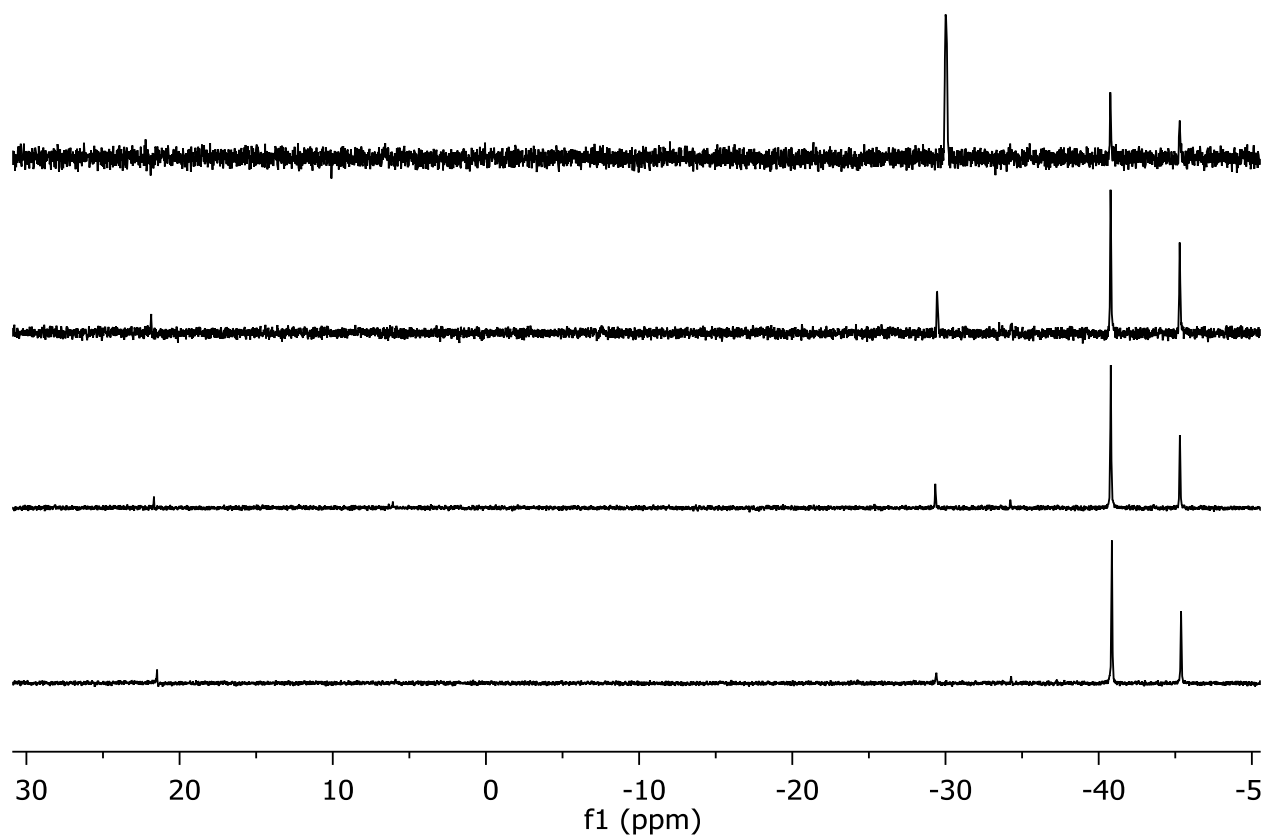
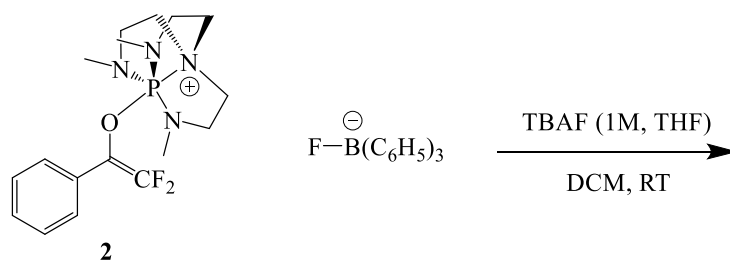


Figure S2: $^{19}\text{F}\{\text{H}\}$ NMR (377 MHz, CH_2Cl_2) stacked spectrum depicting half hour intervals starting from minute two after addition of 2,2,2-trifluoroacetophenone to **1** (top spectrum). CH_2FCl (triplet at -169 ppm, $^2J_{\text{F-H}} = 47$ ppm), CHF_2Cl (doublet at -163 ppm $^2J_{\text{F-F}} = 79$ Hz) suggest fluoride activation of DCM. HF_2^- (doublet at -152 ppm, $^2J_{\text{F-H}} = 121$ Hz) suggests fluoride release.

These chemical shifts and coupling constants were observed in Ramsden and coworkers paper on XeF₂ reactivity in different organic solvents.⁶⁶



*Figure S3: ³¹P NMR (162 MHz, CH₂Cl₂) stacked spectrum depicting half hour intervals starting from minute two after addition of 2,2,2-trifluoroacetophenone to **1** (top). Peak at -29 ppm suggests DFEP product (alongside presence of corresponding difluorovinyl peaks in ¹⁹F NMR). Fluoroazaphosphatrane evidently grows in as the reaction progresses (doublet at -43 ppm, 726 Hz).*

Addition of TBAF to DFEP[FB(C₆H₅)₃] in DCM:

To confirm in situ generated fluoride was responsible for the observed spectra above, a THF solution (1M) of TBAF was added to a DCM solution of DFEP[FB(C₆H₅)₃]. The spectra below show similar peaks present as compared to the above system where 2,2,2-trifluoroacetophenone was added to **1** in DCM.

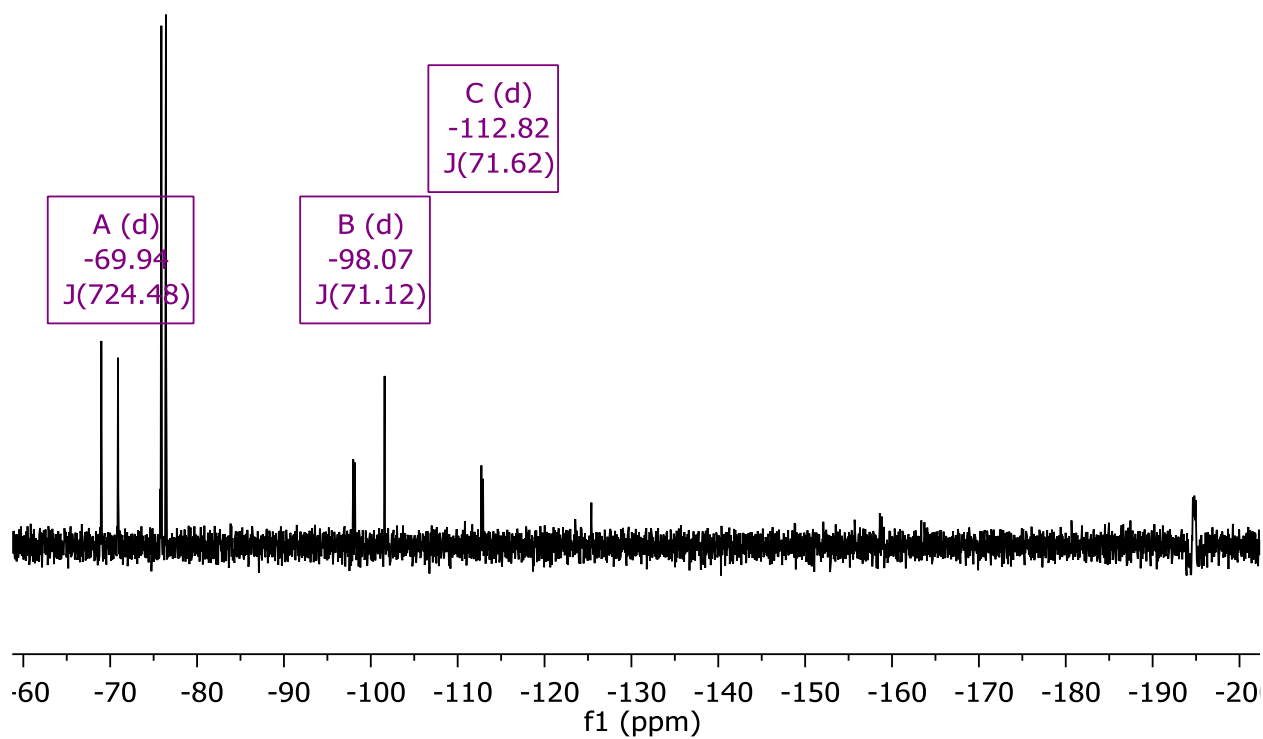


Figure S4 : ^{19}F NMR (377 MHz, CH_2Cl_2) spectrum of 1 M solution of TBAF added dropwise at -78°C to a stirring solution of DFEP[FB(C_6H_5) $_3$] in DCM. Peaks at -69, -98 and -112 ppm indicate fluoroazaphosphatrane, and unreactive DFEP, respectively. Intermediate observed at -101 ppm was generated but not isolated.

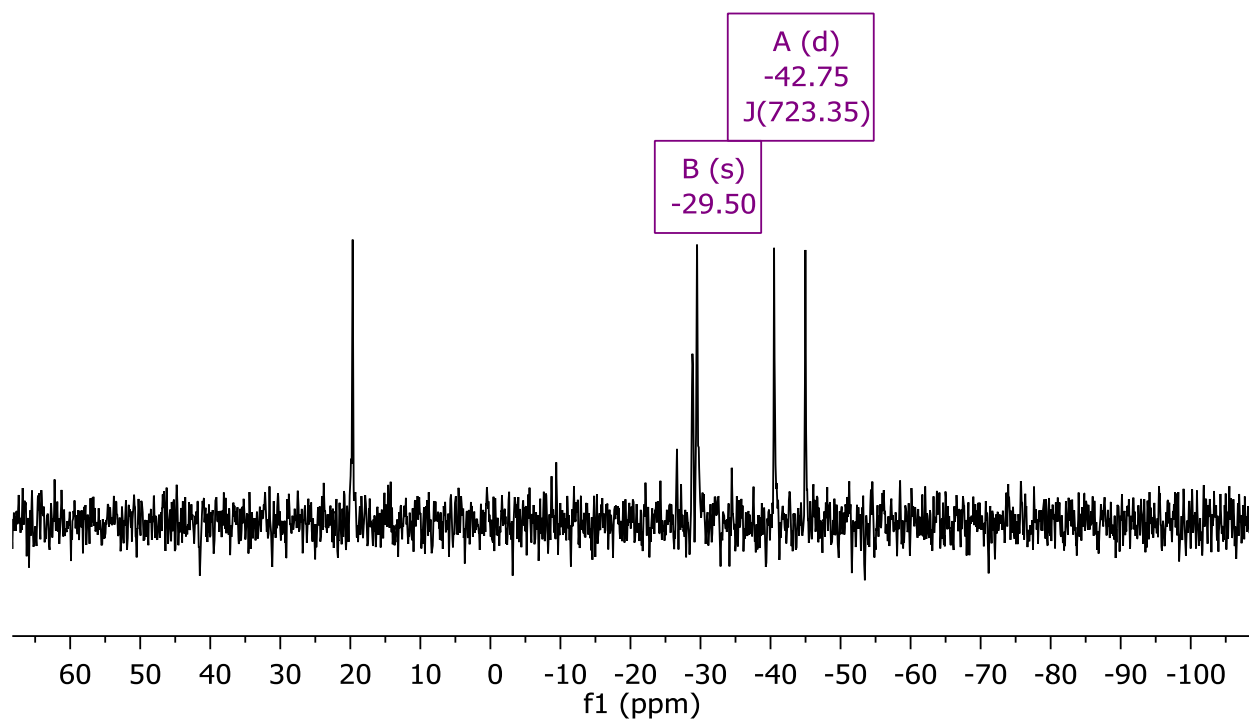
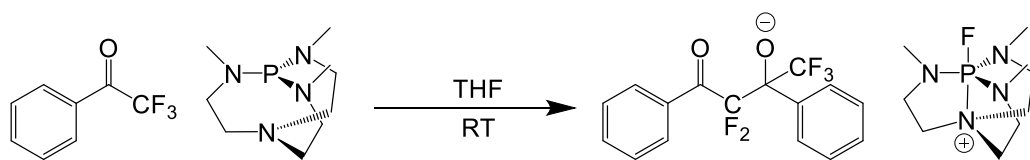


Figure S5: ^{31}P NMR (162 MHz, CH_2Cl_2) spectrum of 1 M solution of TBAF added dropwise at $-78\text{ }^\circ\text{C}$ to a stirring solution of DFEP[FB(C_6H_5) $_3$] in DCM. Fluoroazaphosphatrane is clearly present, with two peaks very similar to DFEP (-27 ppm), alongside phosphine oxide byproduct.

Equimolar mixture of 2,2,2-trifluoroacetophenone with me-VB in THF:



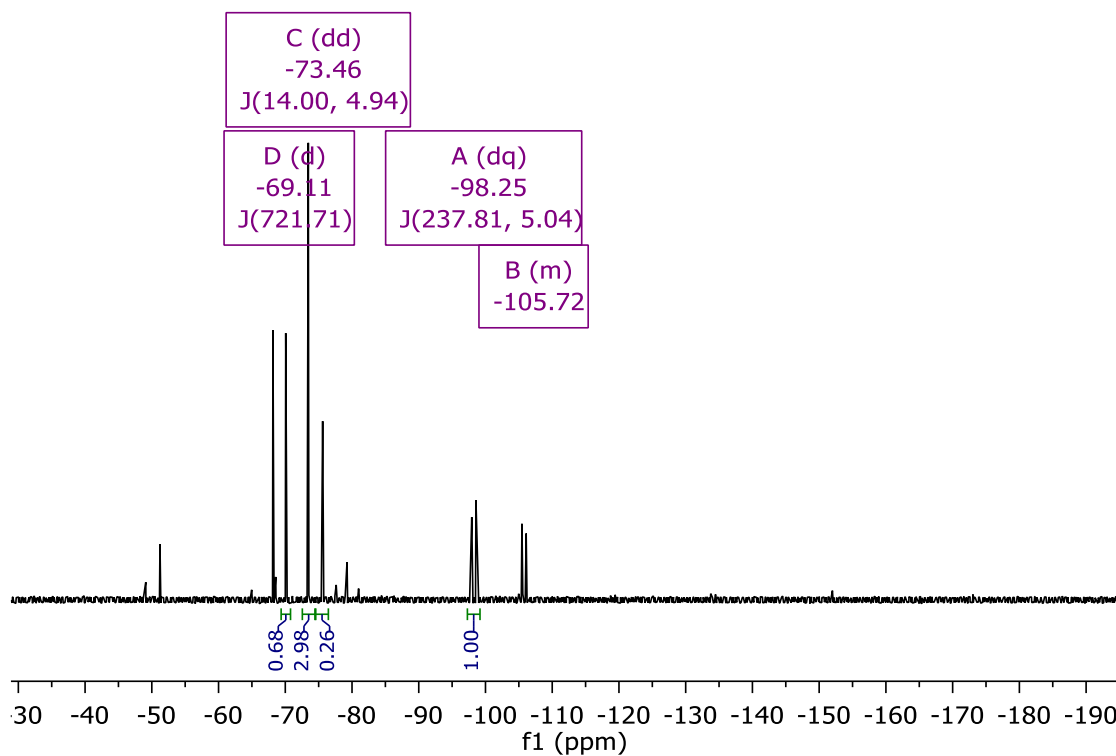


Figure S6: ^{19}F NMR (377 MHz, THF) spectra for equimolar mixture of 2,2,2-trifluoroacetophenone and **I** in THF (crude mixture). No observed DFEP after 5 minutes of addition. Set of doublets at -98 and -105 ppm same as in DCM condition. Coupling constant consistent with two geminal fluorides.⁶⁷

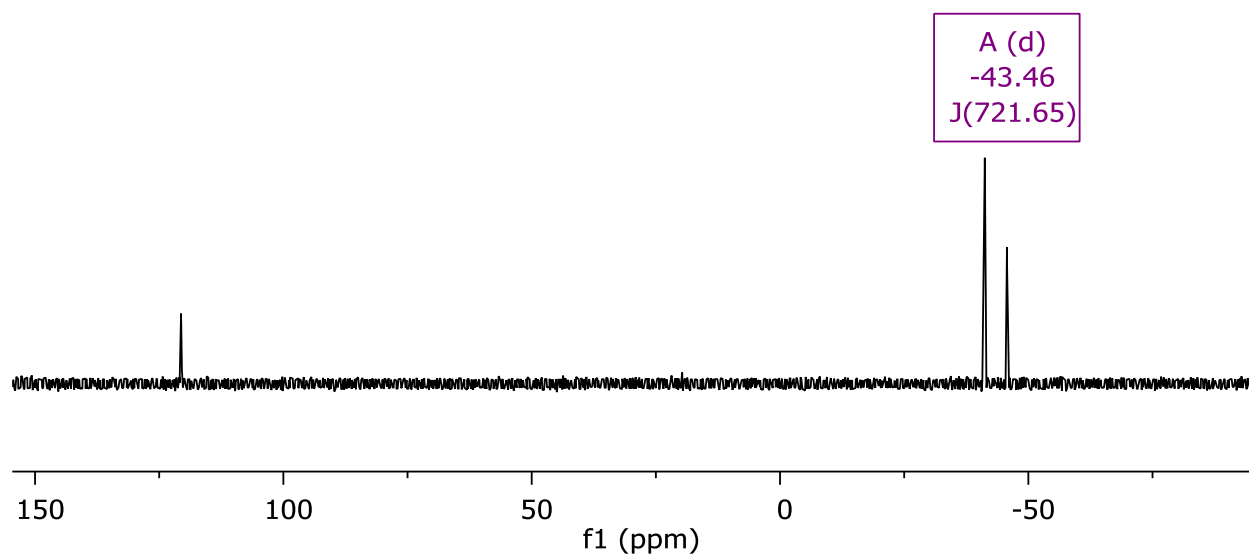


Figure S7: ^{31}P NMR (162 MHz, THF) spectra for equimolar mixture of 2,2,2-trifluoroacetophenone and **1** in THF. Excess **1** at 120.6 ppm and fluoroazaphosphorane doublet at -43 ppm (crude mixture).

Equimolar mixture of 2,2,2-trifluoroacetophenone with 1 in THF:

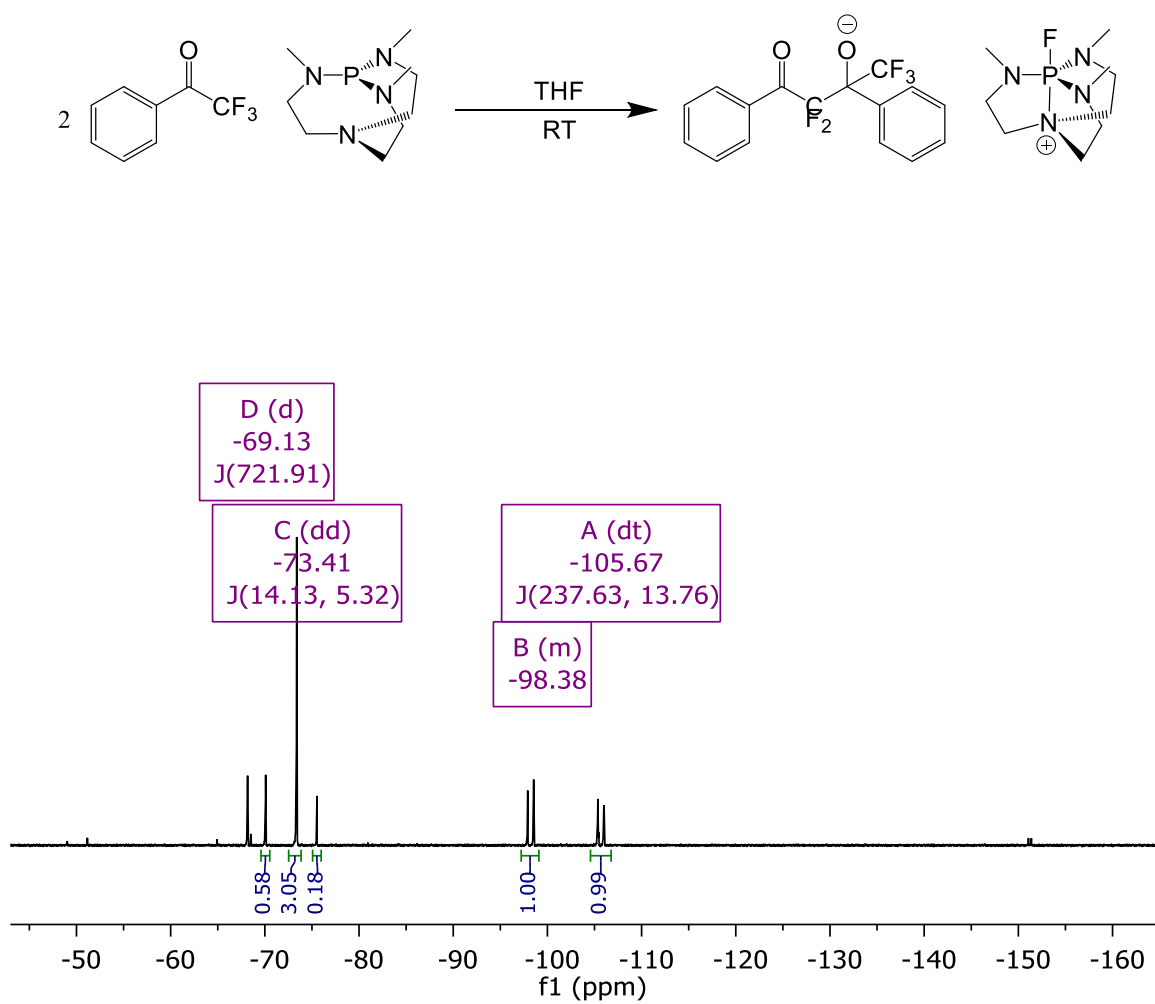


Figure S8: ^{19}F NMR (377 MHz, THF) spectra for solution of two equivalents of 2,2,2-trifluoroacetophenone to *me*-VB (crude mixture).

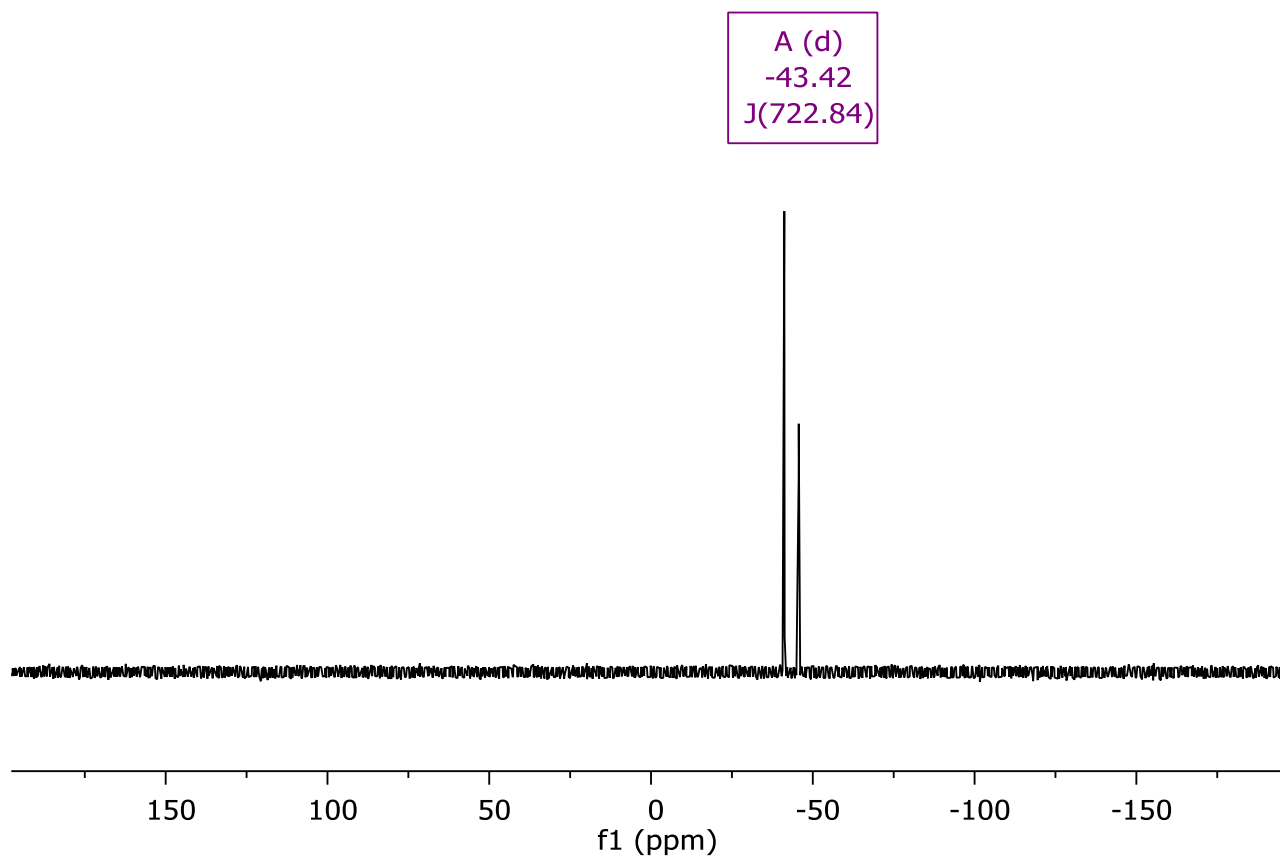
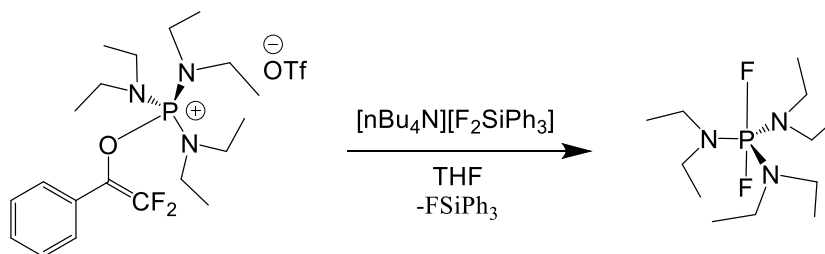


Figure S 9: ^{31}P NMR (162 MHz, THF) spectra for solution of two equivalents of 2,2,2-trifluoroacetophenone to *me*-VB

4.4 Nucleophilic reactions on [DFEPn3][OTf]

Addition of [nBu₄N][F₂SiPh₃] to DFEPn3[OTf] in THF



A THF solution (1.5 mL) of $[n\text{Bu}_4\text{N}][\text{F}_2\text{SiPh}_3]$ (0.025 mmol) was added dropwise to a THF (1 mL) solution of $[\text{DFEPn}_3][\text{OTf}]$ (0.025 mmol). The NMR spectral information was collected.

Isolation of the components was not investigated.

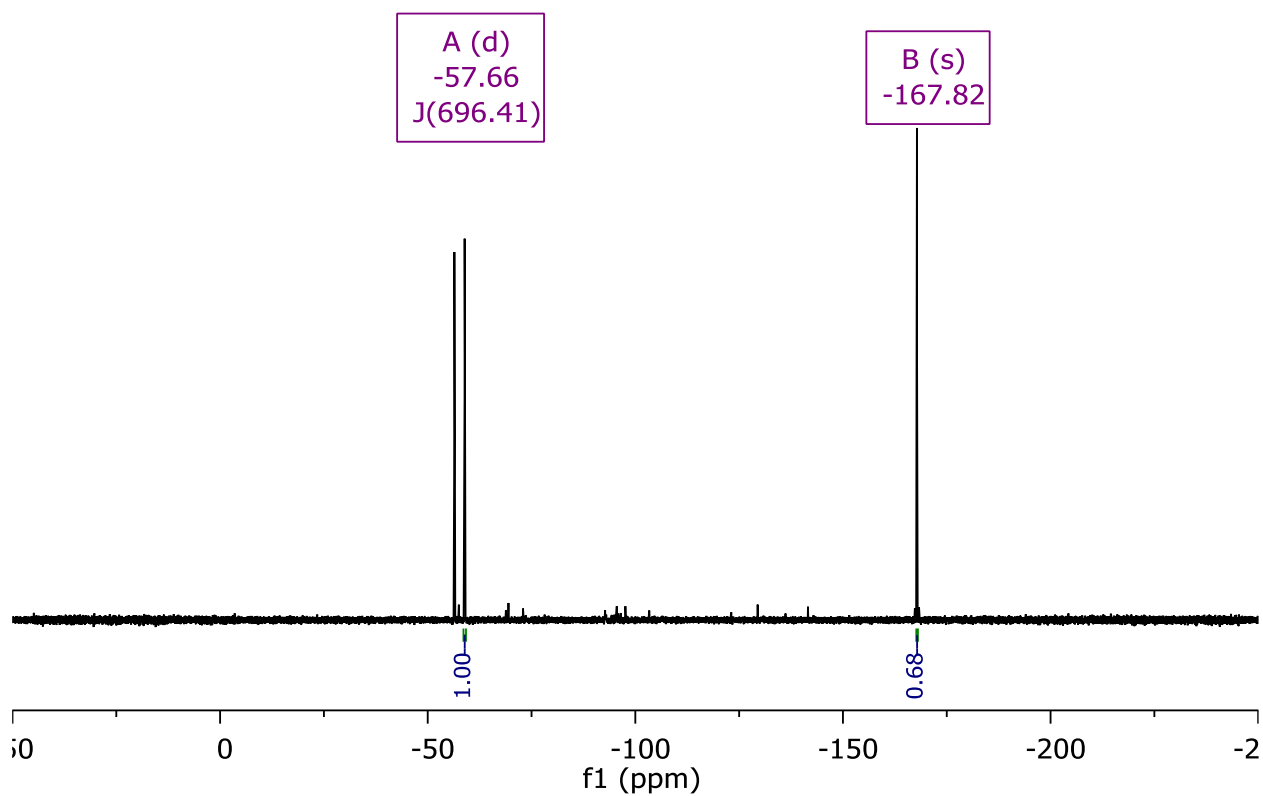


Figure S 10: ^{19}F NMR (377 MHz, THF) spectra for addition of $[n\text{Bu}_4][\text{F}_2\text{SiPh}_3]$ to $\text{DFEPn}_3[\text{OTf}]$. Doublet at -58 ppm represents $\text{F}_2\text{P}(\text{NEt}_2)_3$ and singlet at -168 ppm represents FSiPh_3 . Small product peaks observed not characterized

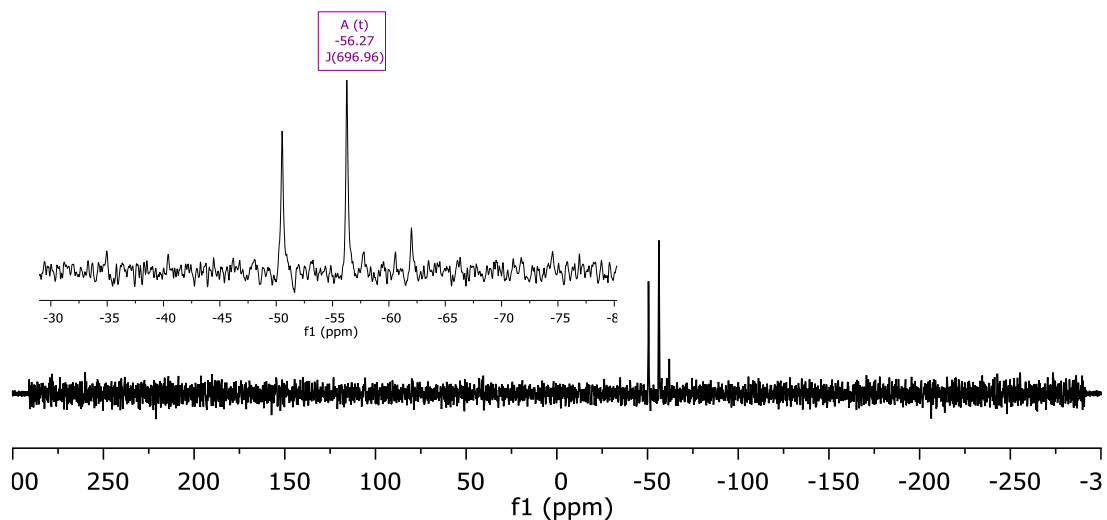
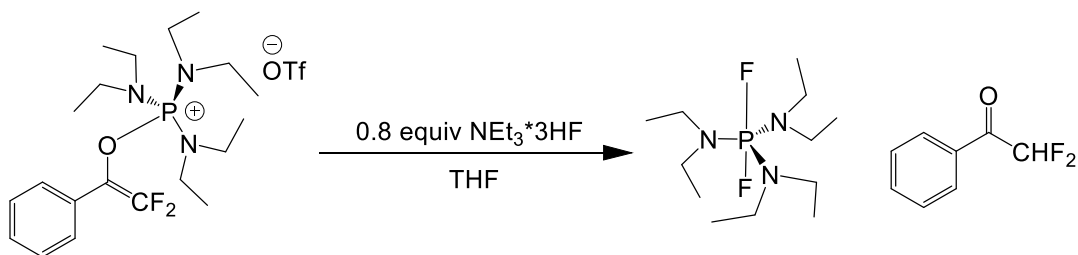


Figure S 11: ^{31}P NMR (162 MHz, THF) spectra for addition of $[\text{nBu}_4][\text{F}_2\text{SiPh}_3]$ to $\text{DFEPn}_3[\text{OTf}]$. Triplet at -56 ppm represents $\text{F}_2\text{P}(\text{NEt}_2)_3$

Addition of $\text{NEt}_3 \cdot 3\text{HF}$ to $\text{DFEPn}_3[\text{OTf}]$ in THF



A THF solution of $[\text{DFEP}][\text{OTf}]$ (0.025 mmol) was dropwise added to a THF solution (1 mL) of $\text{NEt}_3 \cdot 3\text{HF}$ (0.020 mmol). The NMR spectral data was collected.

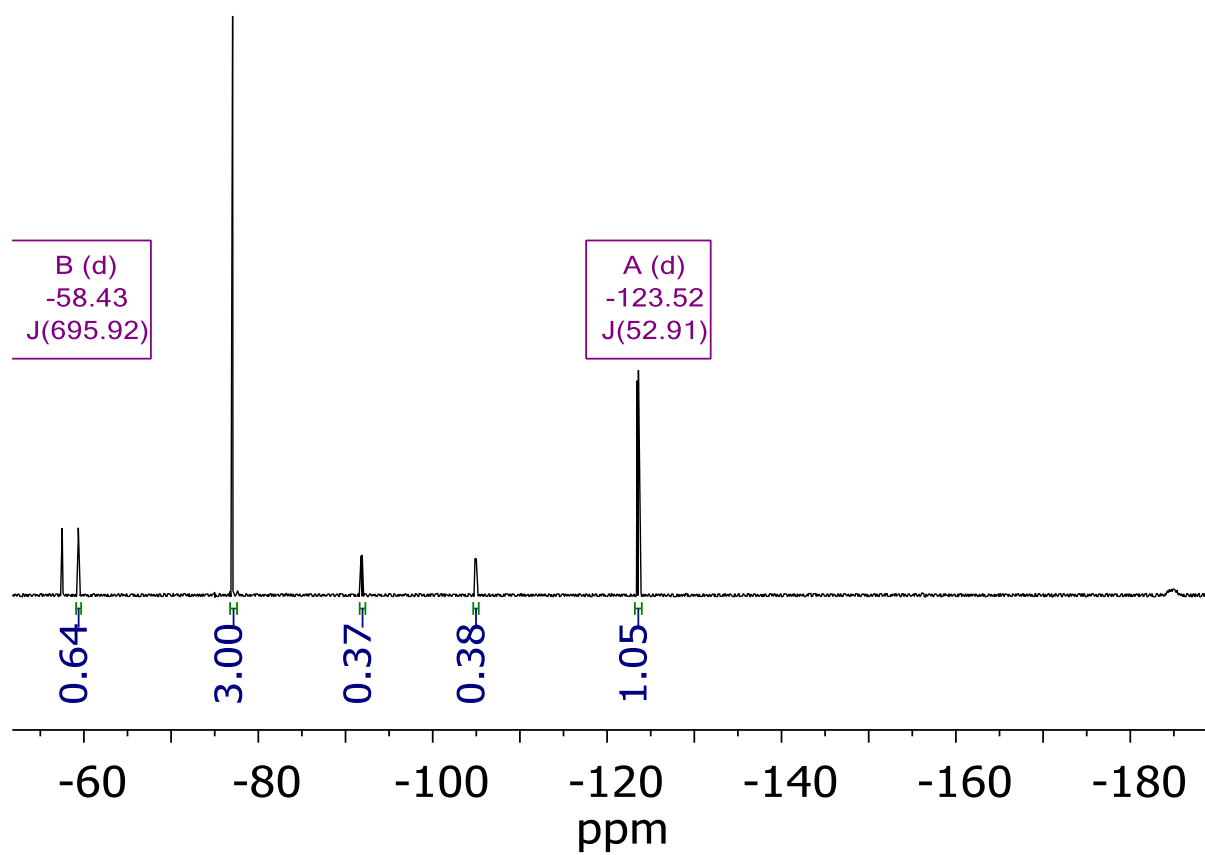


Figure S 12: ^{19}F NMR (377 MHz, THF) spectra for addition of 0.8 equivalent of $\text{NEt}_3 \cdot 3\text{HF}$ to a solution of $[\text{DFEPn3}][\text{OTf}]$.

Doublet at -58 ppm represents $\text{F}_2\text{P}(\text{NEt}_2)_3$ and doublet at -25 ppm represents 2,2-difluoroacetophenone. Small peaks at -92 ppm and -105 ppm represent unreacted DFEPn3.

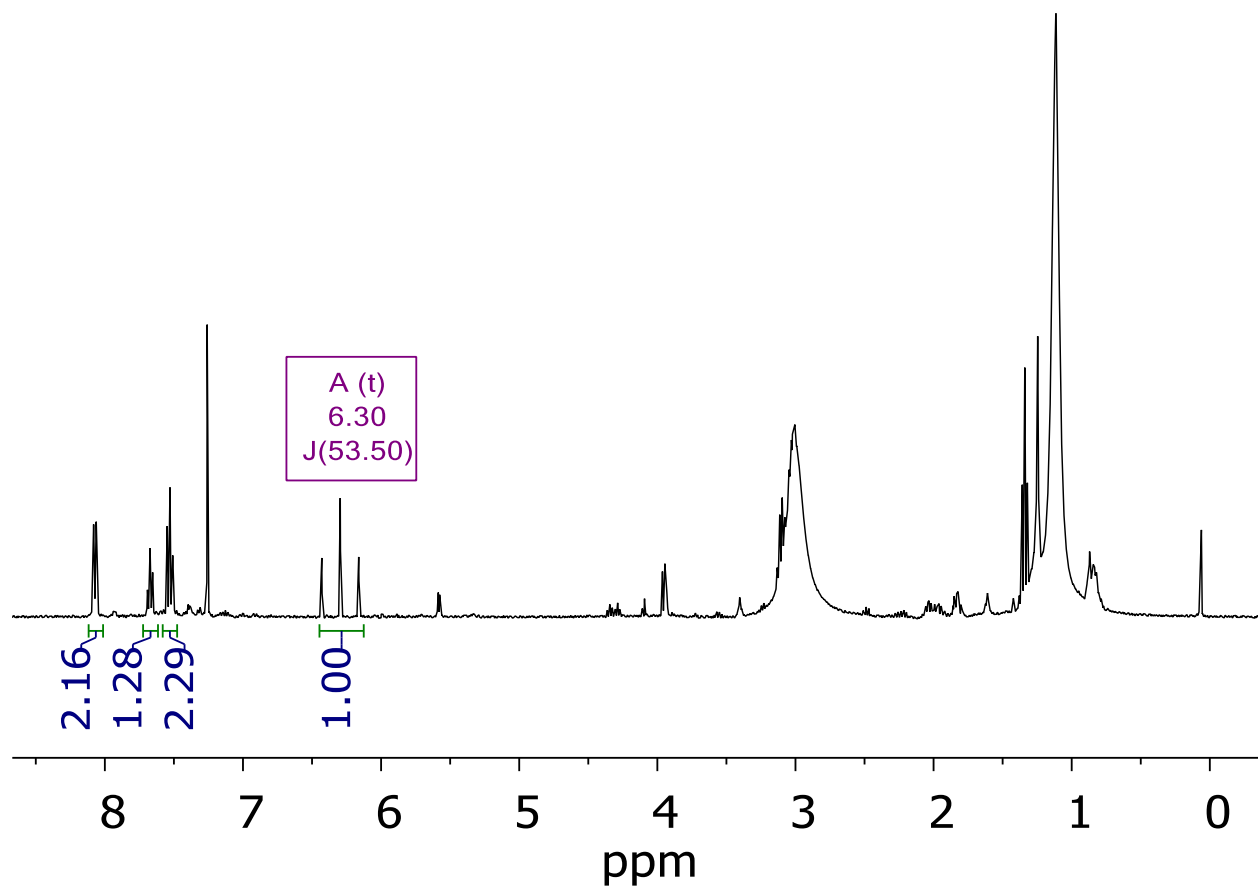


Figure S13: ^1H NMR (400 MHz, CDCl_3) spectra for addition of 0.8 equivalent of $[\text{NEt}_3][3\text{HF}]$. This spectrum is from a semi-purified sample where the crude mixture was dropped in pentane to remove starting material.

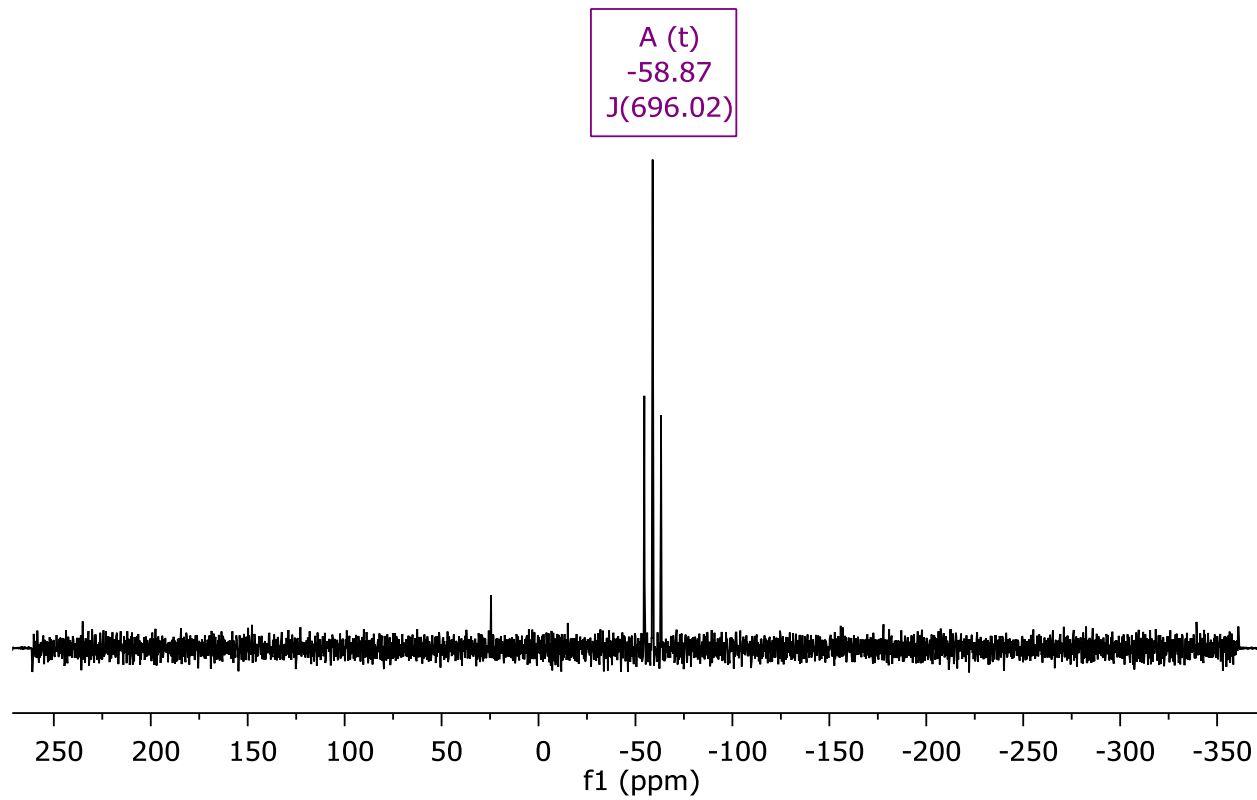
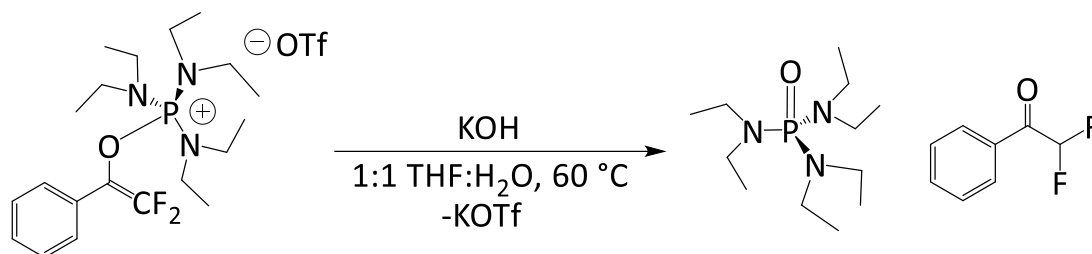


Figure S 14: ^{31}P NMR (162 MHz, THF) spectra for addition of 0.8 equivalent of $\text{NEt}_3 \cdot 3\text{HF}$ to a solution of $[\text{DFEPn3}][\text{OTf}]$.

Triplet represents $\text{F}_2\text{P}(\text{NEt}_2)_3$.

Reaction between [DFEPn3][OTf] and KOH in 1:1 THF and H₂O solution



A 1:1 THF and H₂O solution of [DFEPn3][OTf] (0.0254 mmol) was added to an equimolar solution of KOH in 1:1 THF and H₂O. The mixture was heated to 60 °C for 12 hours. NMR spectral data was collected.

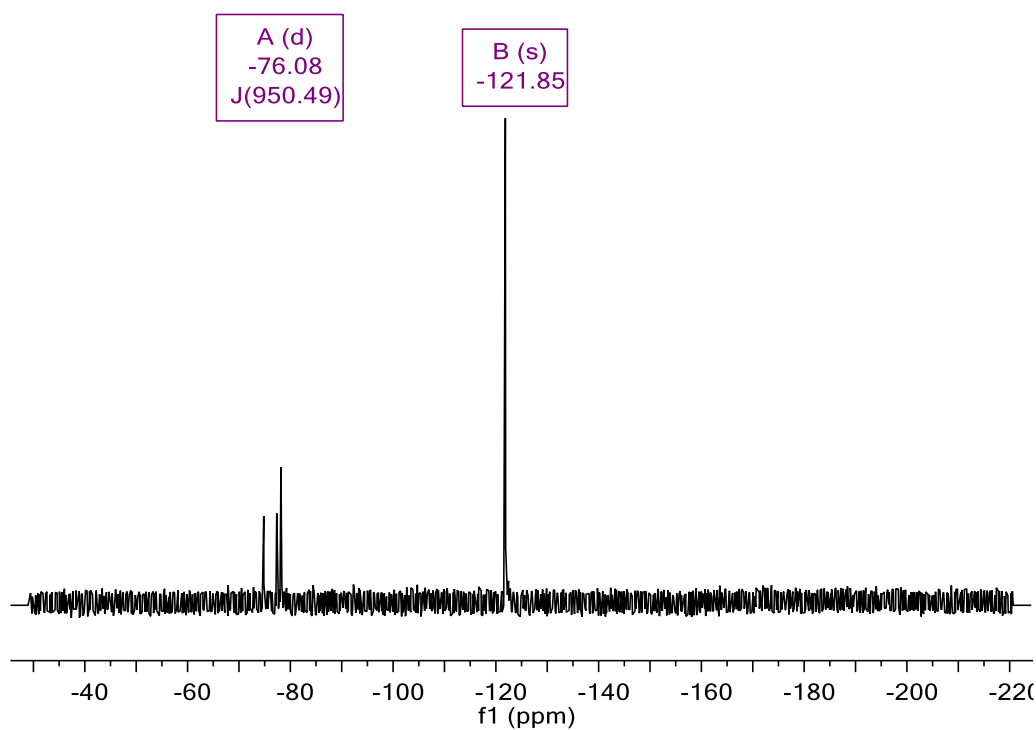


Figure S 15: ¹⁹F NMR (377 MHz, in CDCl₃) spectra for addition of 1 equivalent of KOH in 1:1 THF to H₂O. Doublet at -76 ppm suggests the formation of (Net)₂P(O)F

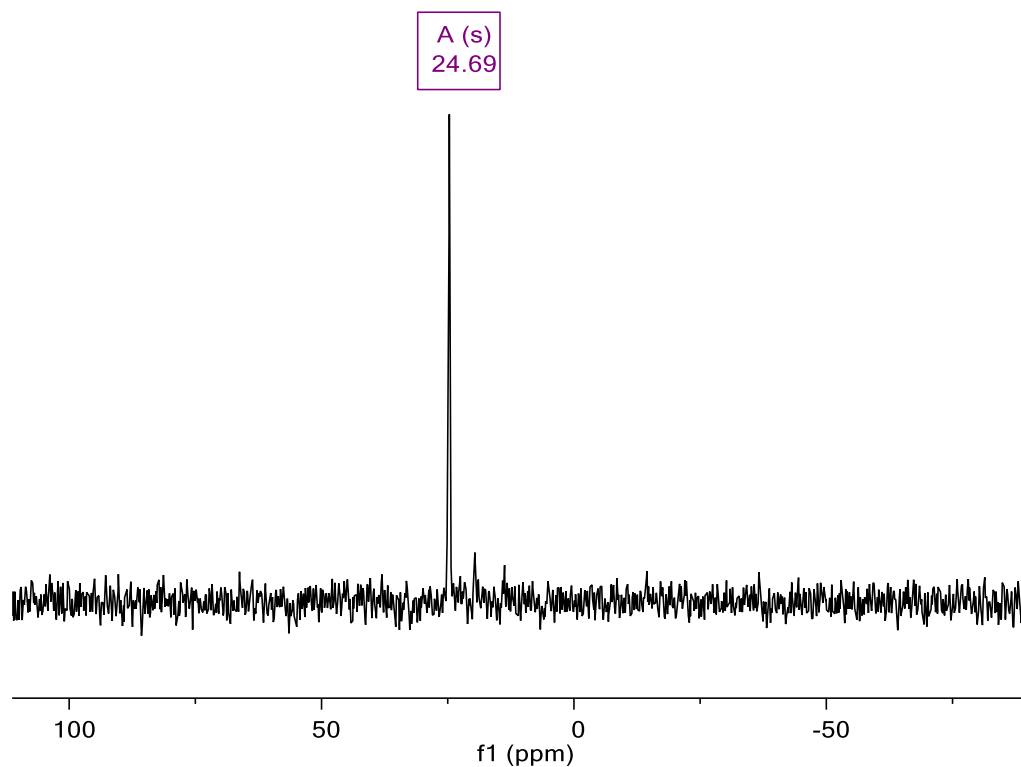
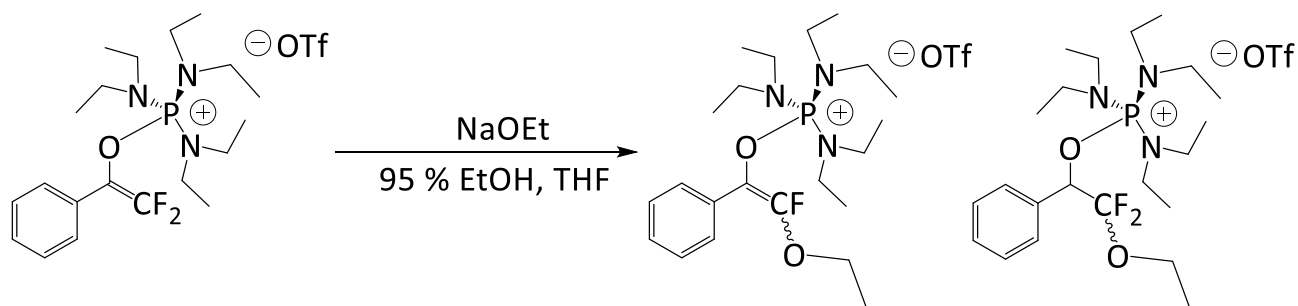


Figure S 16: ^{31}P NMR (162 MHz, in CDCl_3) spectra for addition of 1 equivalent of KOH in 1:1 THF to H_2O . Doublet at -76 ppm suggests the formation of $(\text{Net}_2)_2\text{P}(\text{O})\text{F}$

Addition of NaOEt to $[\text{DFEPn}_3][\text{OTf}]$ in THF



A 1:1 95 % EtOH: THF solution (1 mL) of $[\text{DFEPn}_3][\text{OTf}]$ (0.0254 mmol) was added dropwise to a 1:1 95 % EtOH: THF solution (1 mL) of NaOEt (0.0254 mmol). The NMR spectral data was collected.

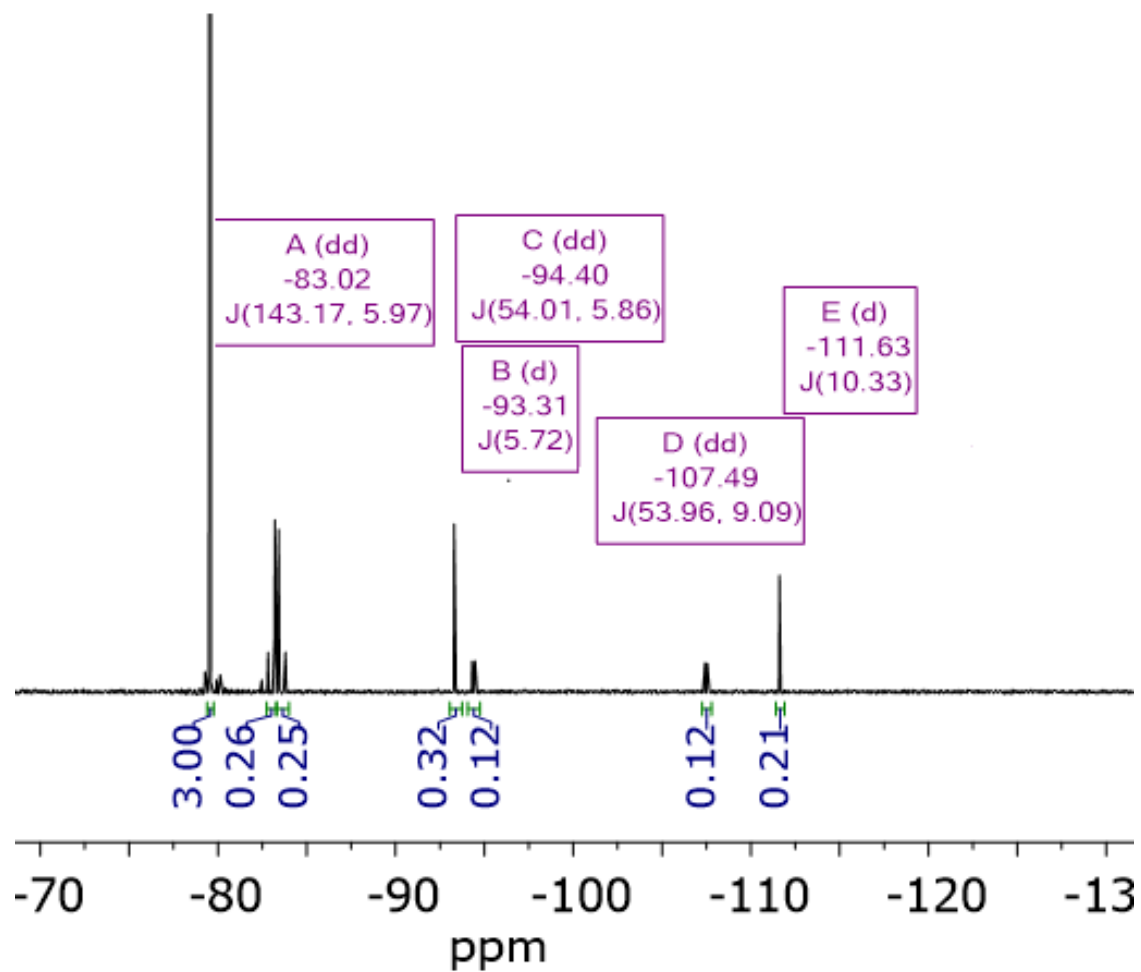


Figure S 17: ^{19}F NMR (377 MHz, in 1:1 95 % EtOH: THF) spectrum for the addition of [DFEPn3][OTf] to NaOEt in 1:1 95 % EtOH: THF mixture. Pair of doublet of doublets at -83.02 represents the ethanol addition product across DFEPn3 alkene. Doublet at -94 ppm and -111 ppm represent the E- and Z- addition-substitution products of ethoxide at the C-F bond. Residual DFEPn3 peaks at -94 ppm and -107 ppm.

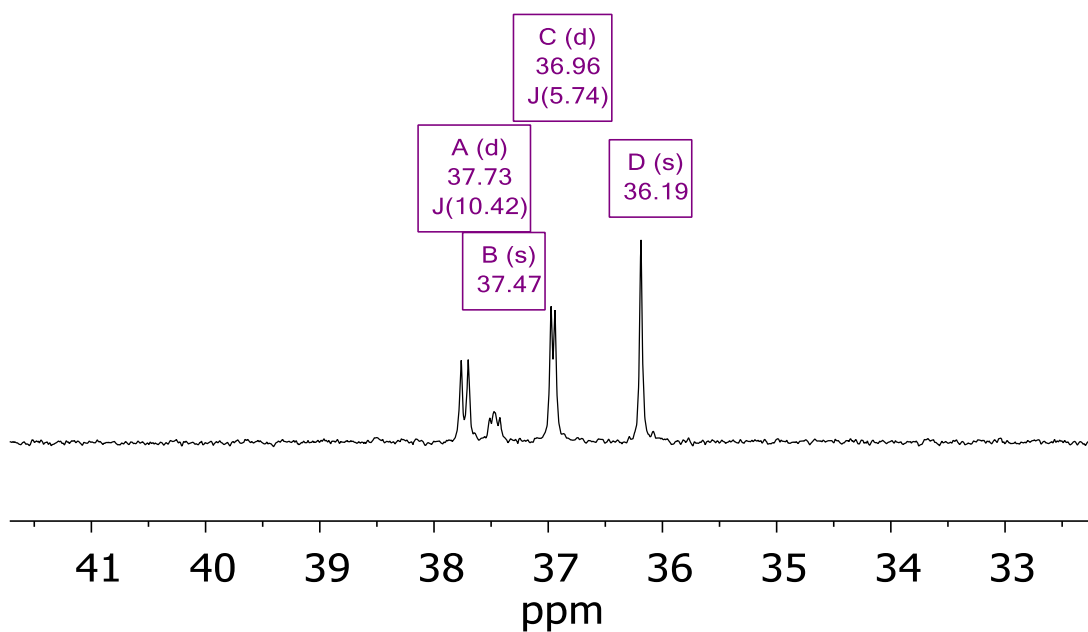


Figure S 18 ^{31}P NMR (162 MHz, in 1:1 95 % EtOH: THF) spectrum for the addition of [DFEPn3][OTf] to NaOEt in 1:1 95 % EtOH: THF mixture. Doublet at 38 ppm and 37 ppm represent the Z- and E- isomer. Doublet of doublets at 37 ppm represents residual DFEPn3. Singlet at 36 ppm represents the ethanol addition product.

4.5 NMR Spectra:

DFEP[FBPh₃]:

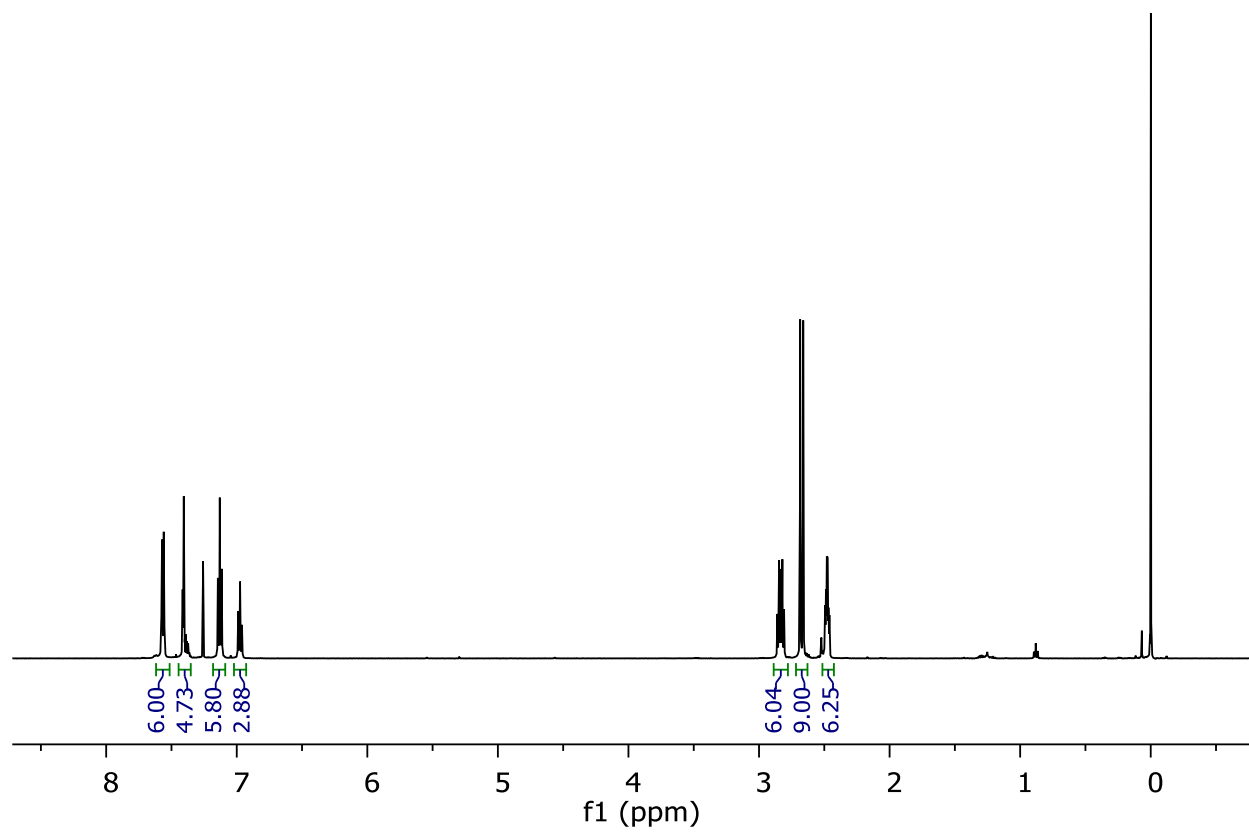


Figure S19: ^1H NMR (500 MHz, CDCl_3) spectrum of $\text{DFEP}[\text{FB}(\text{C}_6\text{H}_5)_3]$

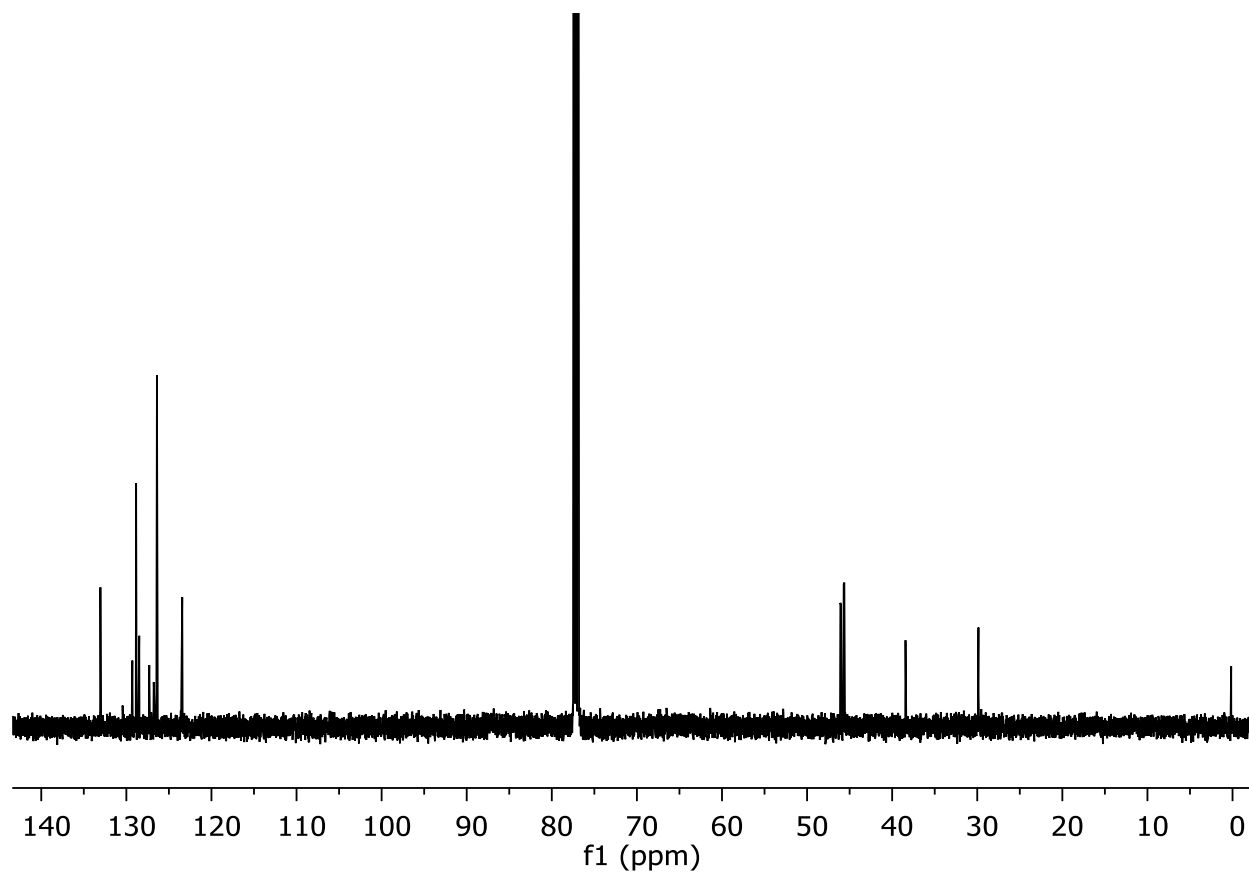


Figure S20 : ^{13}C NMR (100 MHz, CDCl_3) spectrum of DFEP[FB(C_6H_5) $_3$]

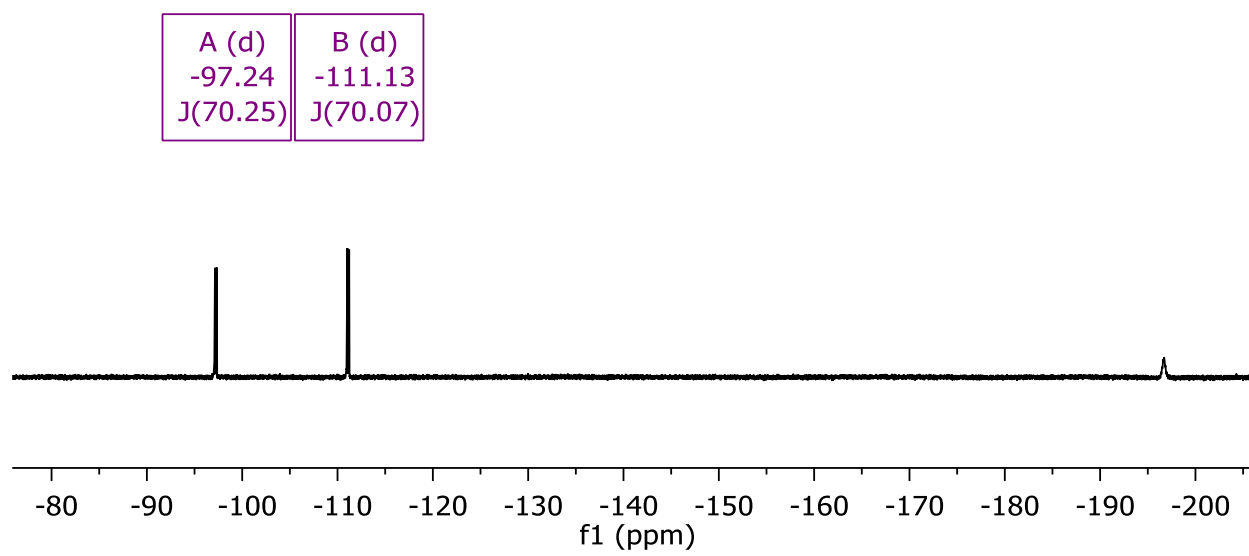


Figure S21: ^{19}F NMR (377 MHz, CDCl_3) spectrum of $\text{DFEP}[\text{FB}(\text{C}_6\text{H}_5)_3]$.

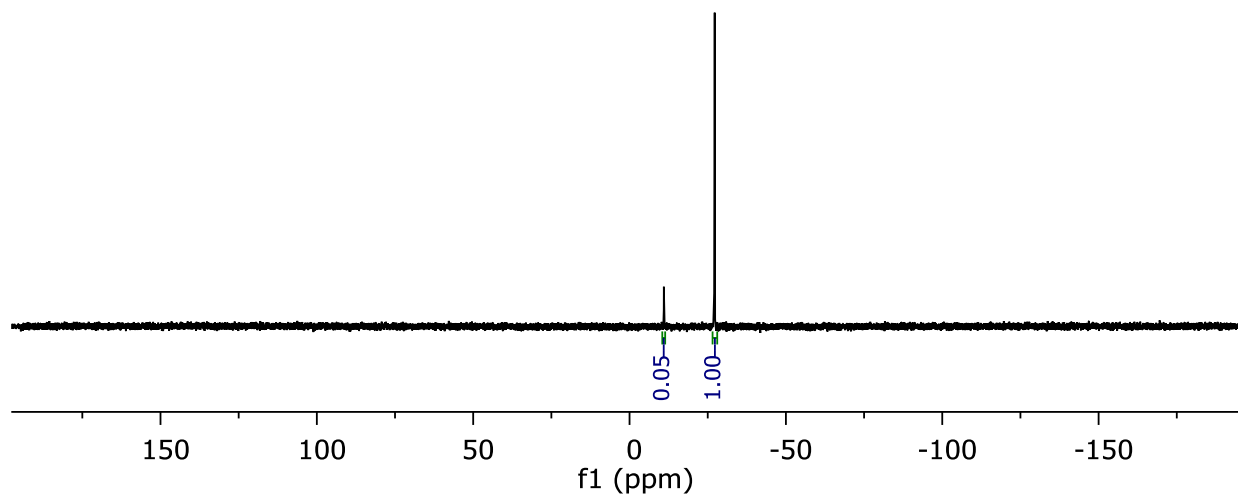


Figure S22: $^{31}\text{P}\{^1\text{H}\}$ NMR (162 MHz, CDCl_3) spectrum of $\text{DFEP}[\text{FB}(\text{C}_6\text{H}_5)_3]$. Peak at -10.9 ppm corresponds to $\text{HP}[(\text{MeNCH}_2\text{CH}_2)_3\text{N}]^+$,

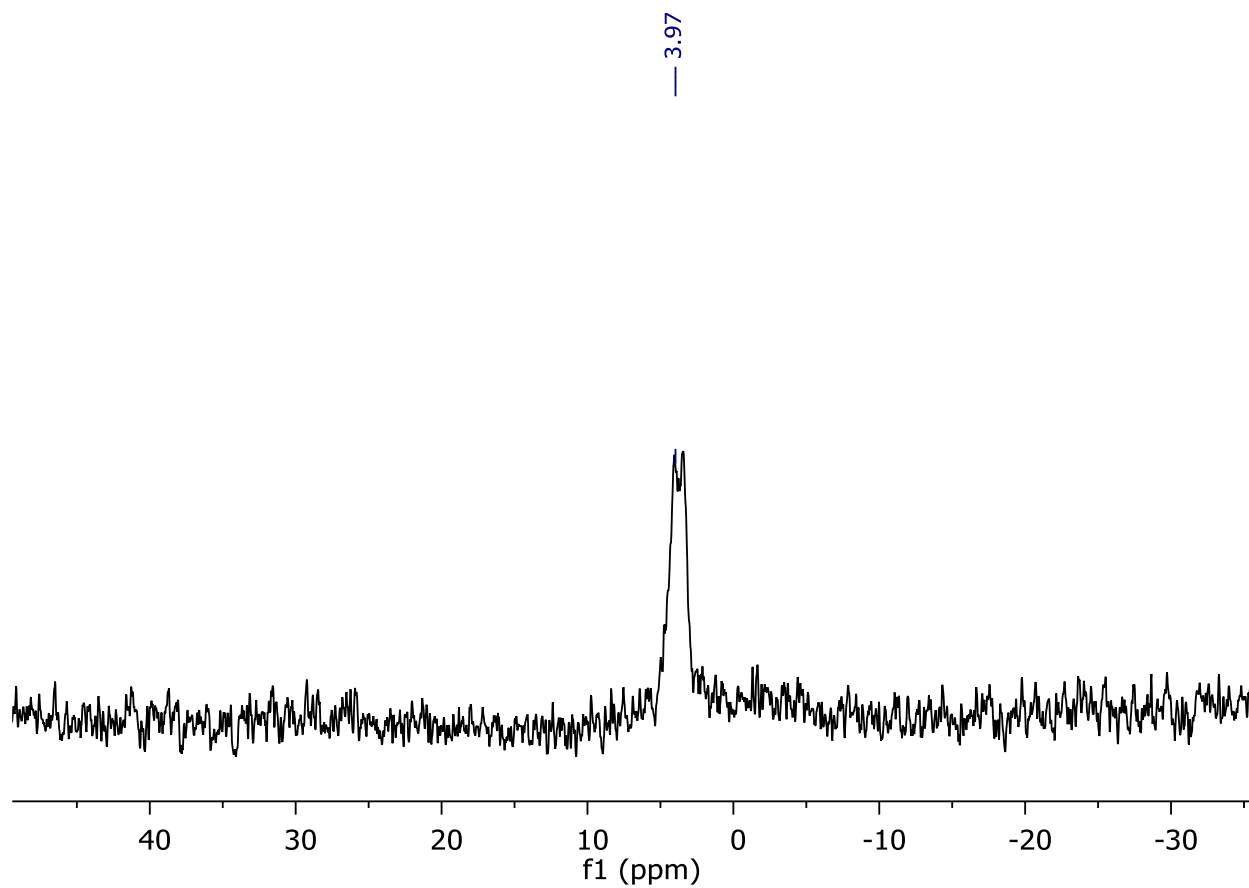


Figure S23: ^{11}B NMR (128 MHz, CDCl_3) spectrum of $\text{DFEP}[\text{FB}(\text{C}_6\text{H}_5)_3]$.

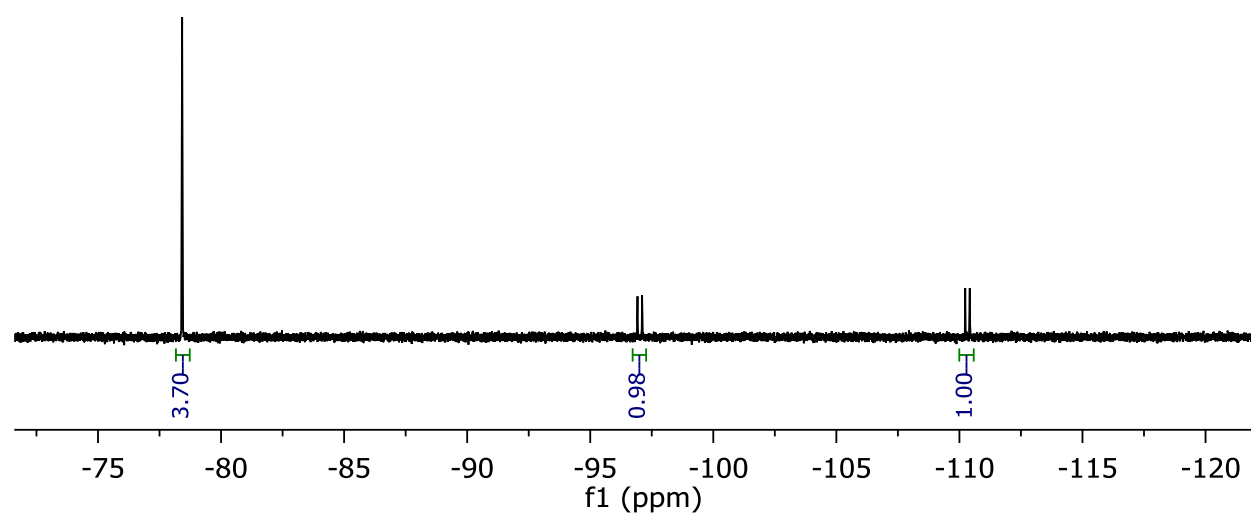
DFEP[OTf]:

Figure S24: ^{19}F NMR (377 MHz, CDCl_3) spectrum of DFEP[OTf].

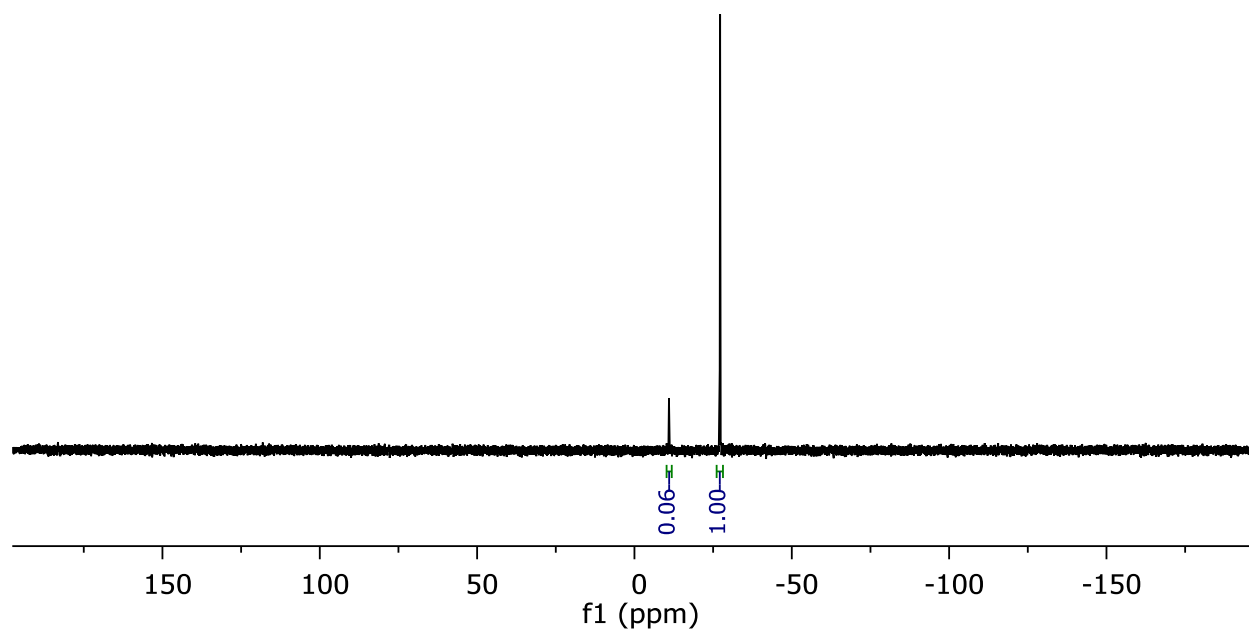


Figure S25: $^{31}\text{P}\{^1\text{H}\}$ NMR (162 MHz, CDCl_3) spectrum of DFEP[OTf].

FEP[OTf]:

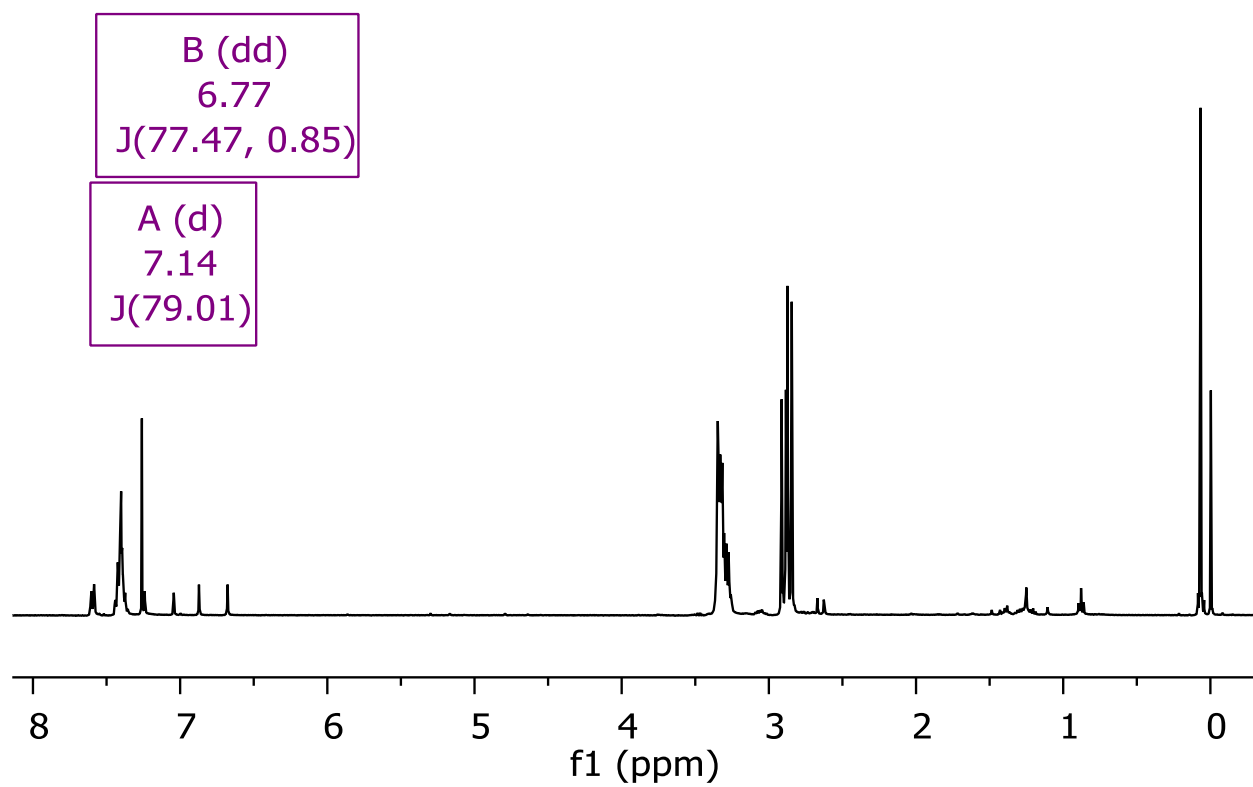


Figure S26: ^1H NMR (400 MHz, CDCl_3) spectrum of FEP[OTf].

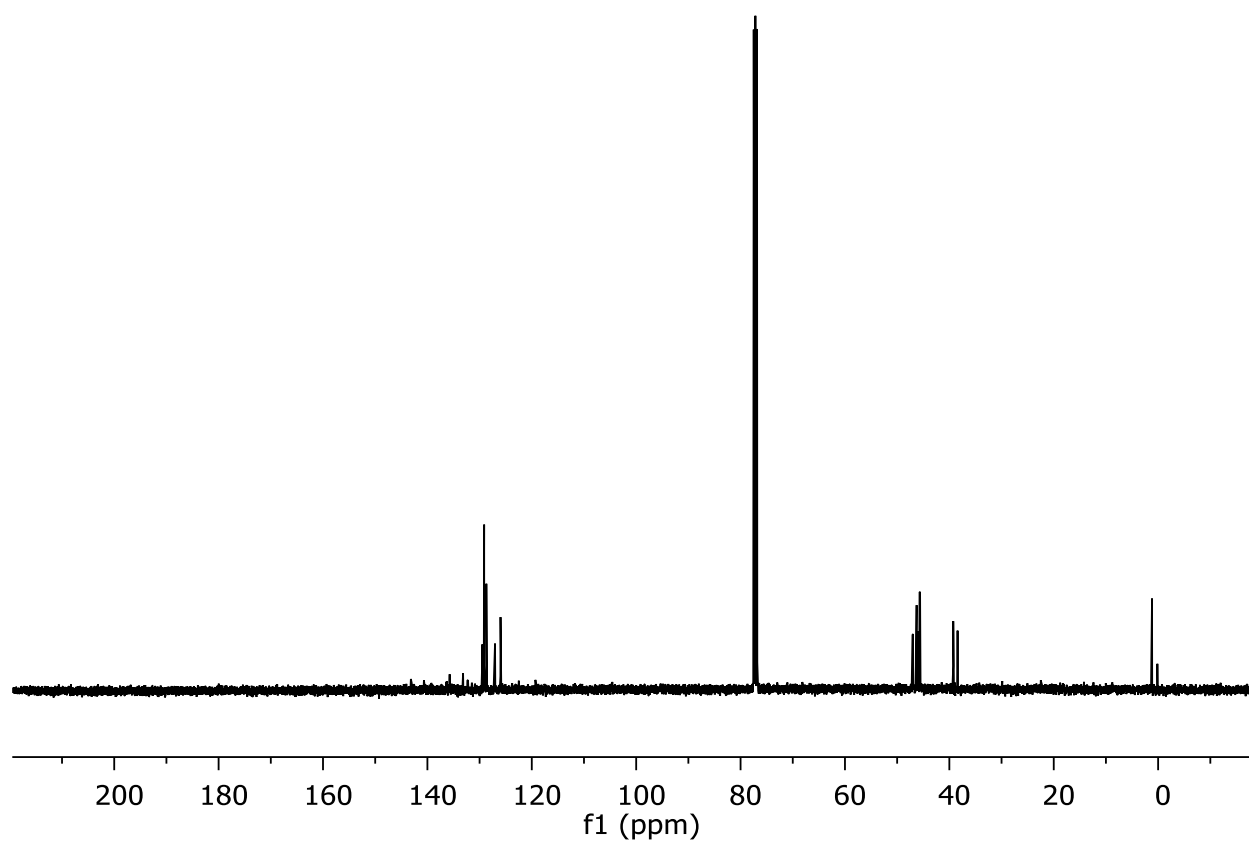


Figure S27: ^{13}C NMR (100 MHz, CDCl_3) spectrum of FEP[OTf].

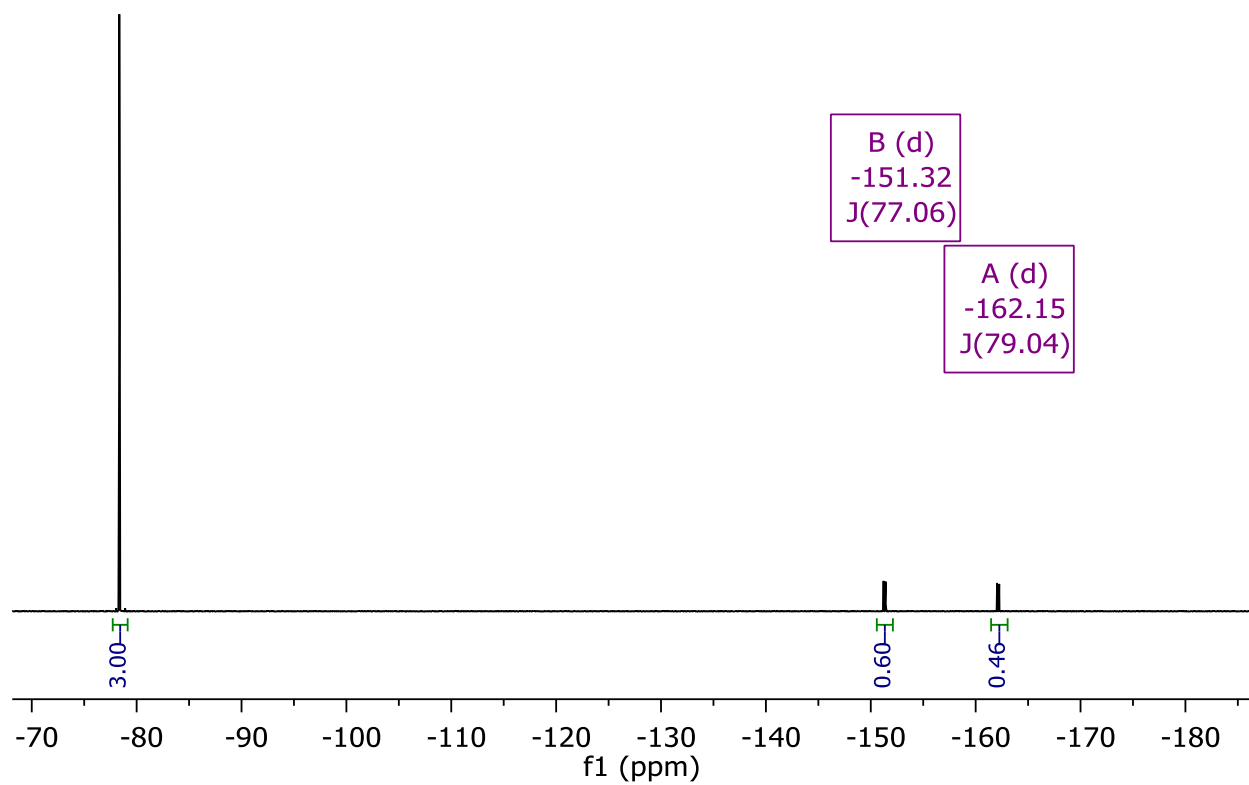


Figure S28: ^{19}F NMR (377 MHz, CDCl_3) spectrum of FEP[OTf].

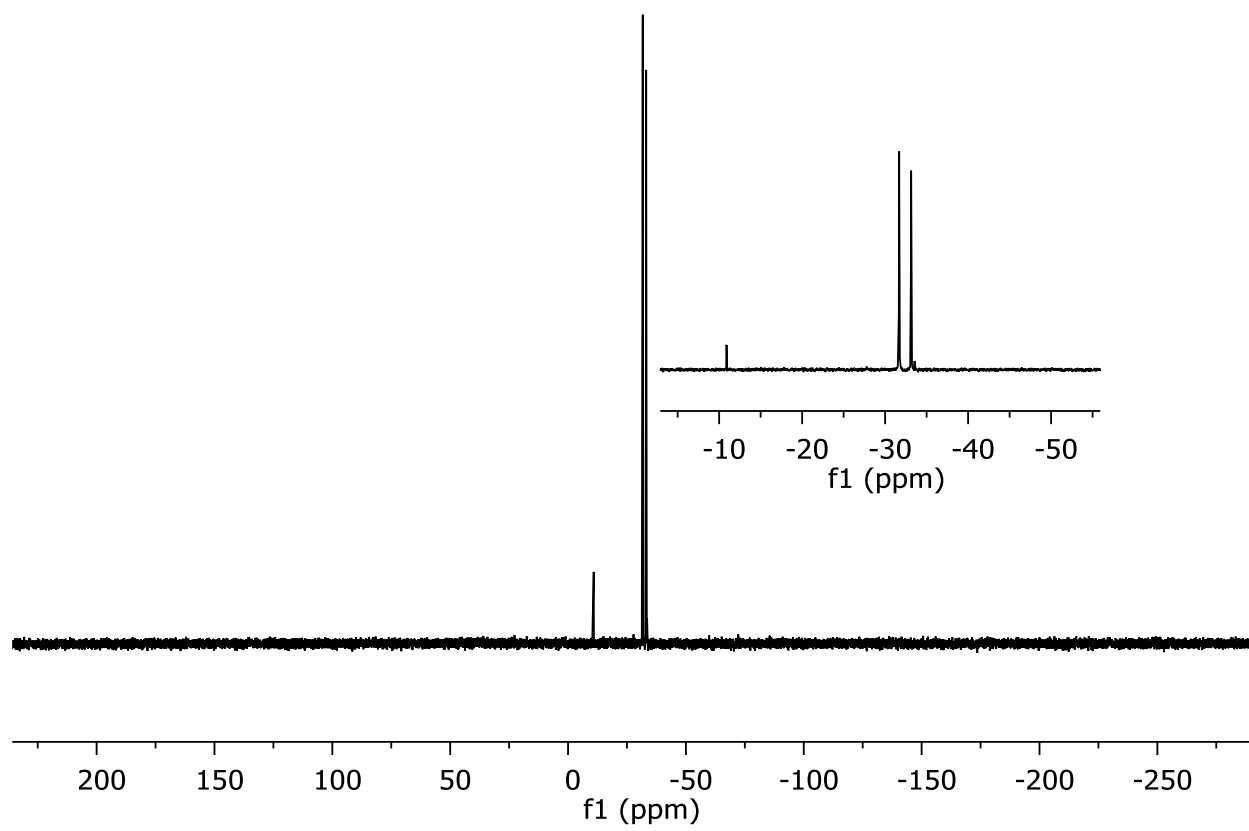


Figure S29: ^{31}P NMR (162 MHz, CDCl_3) spectrum of FEP[OTf].

EP[OTf]:

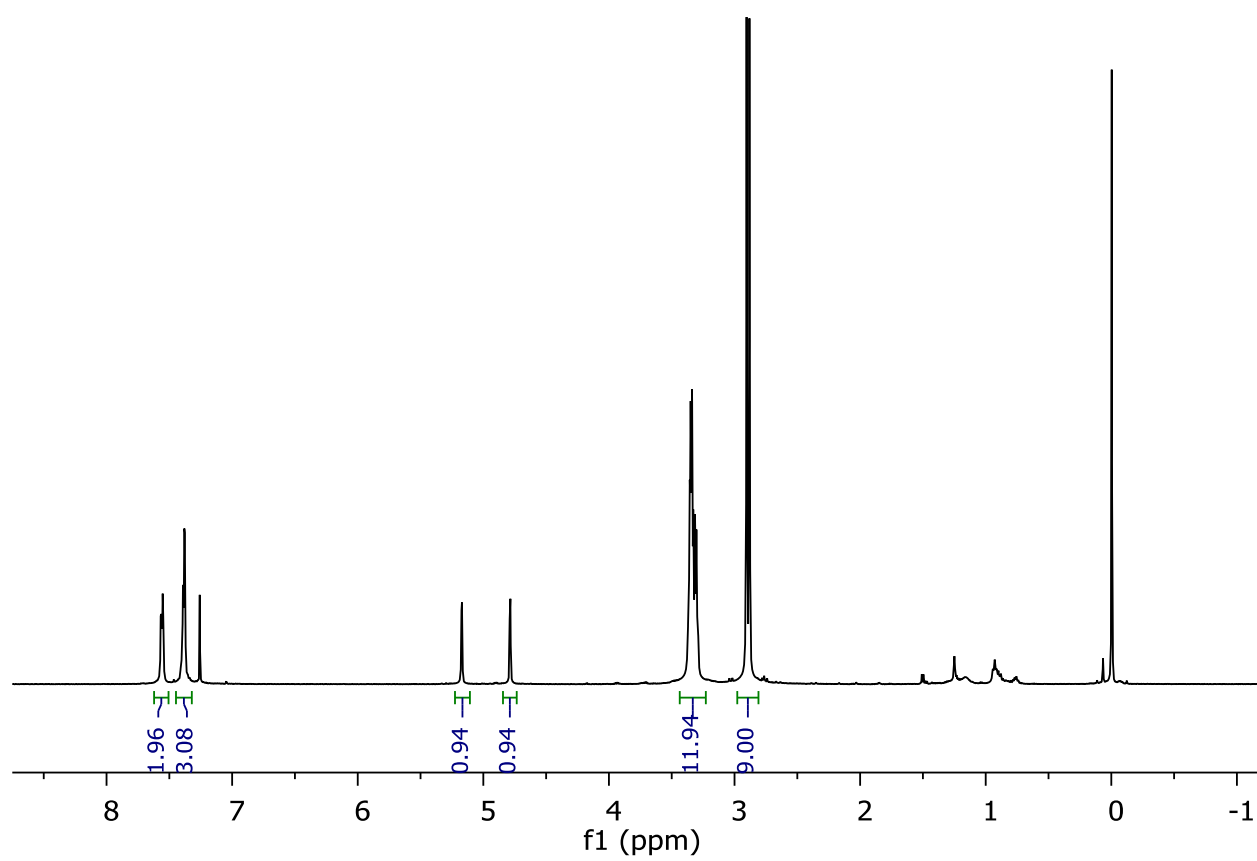


Figure S30: ^1H NMR (500 MHz, CDCl_3) spectrum of EP[OTf].

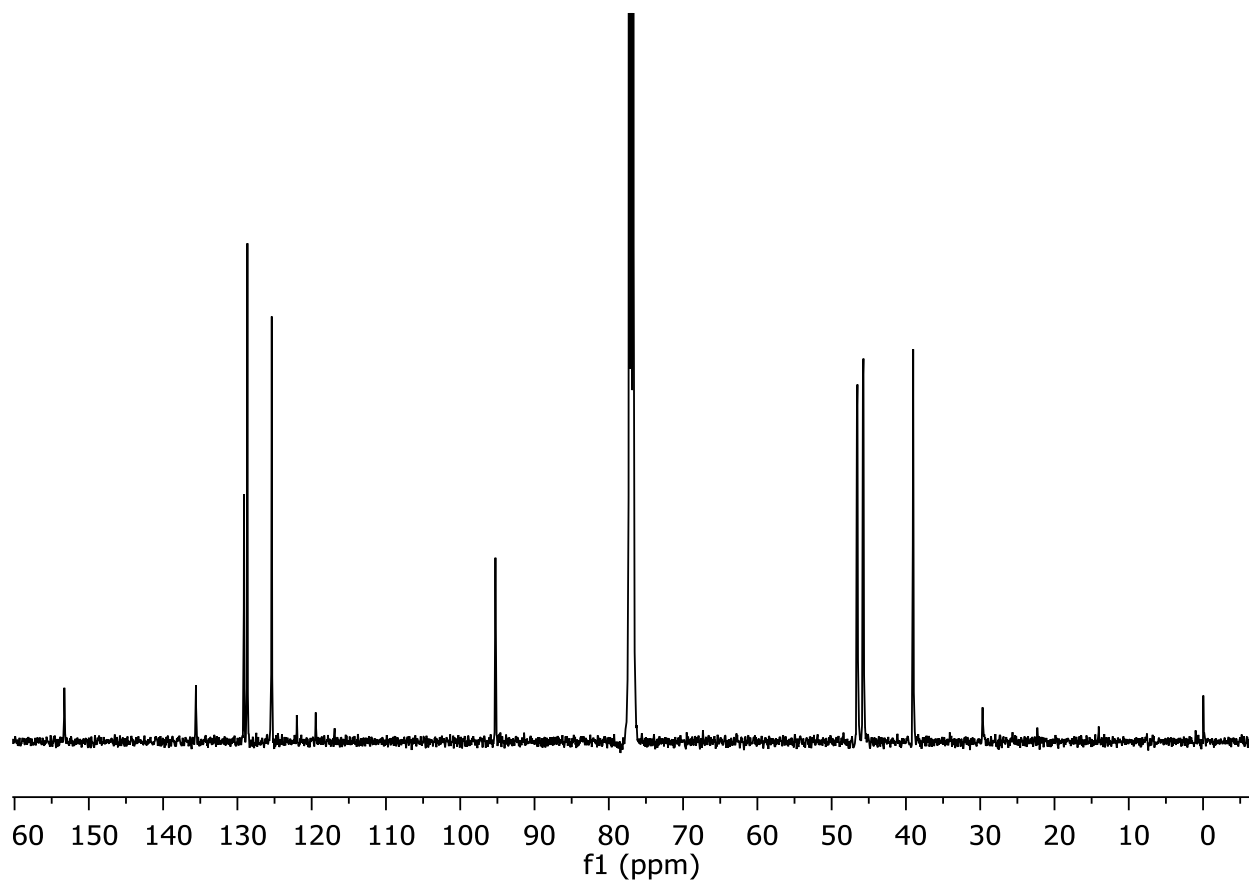


Figure S31: ^{13}C NMR (500 MHz, CDCl_3) spectrum of EP[OTf].

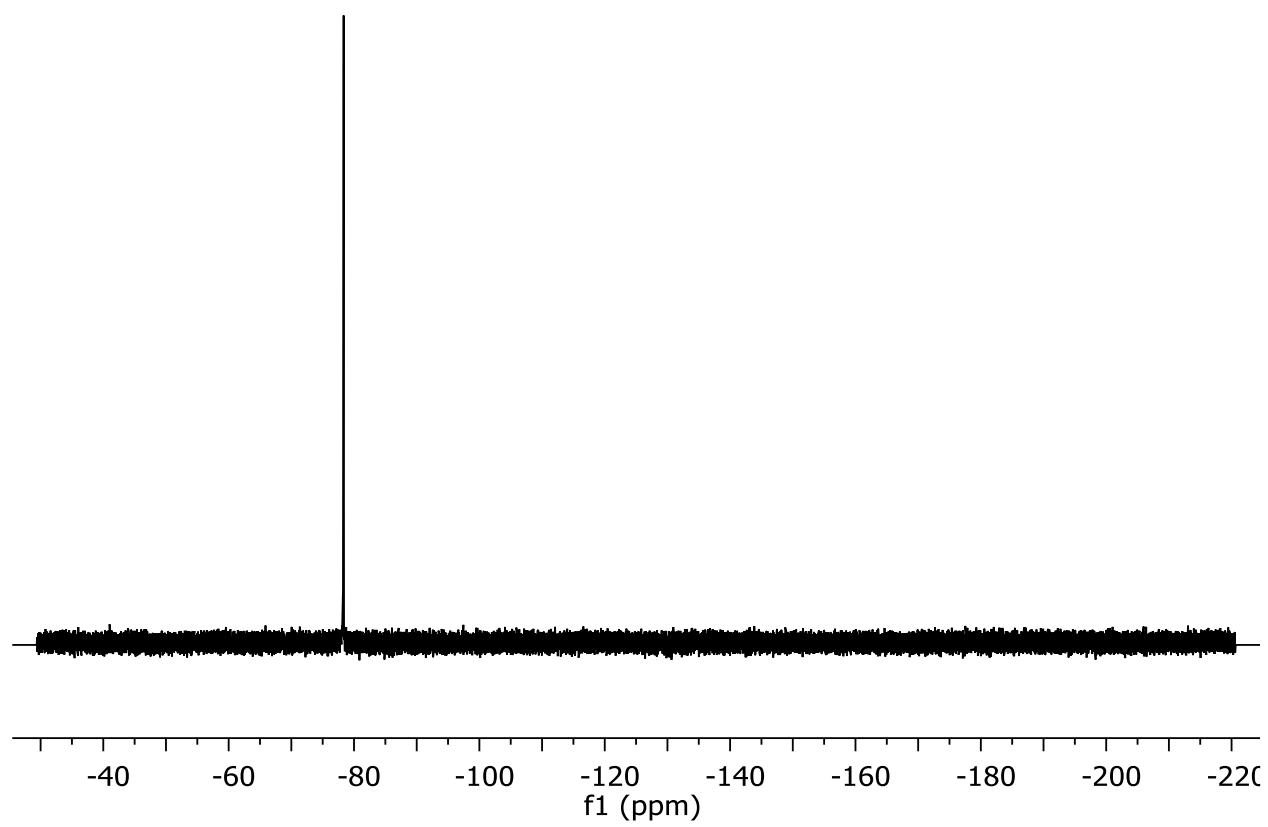


Figure S32: ^{19}F NMR (377 MHz, CDCl_3) spectrum of EP[OTf].

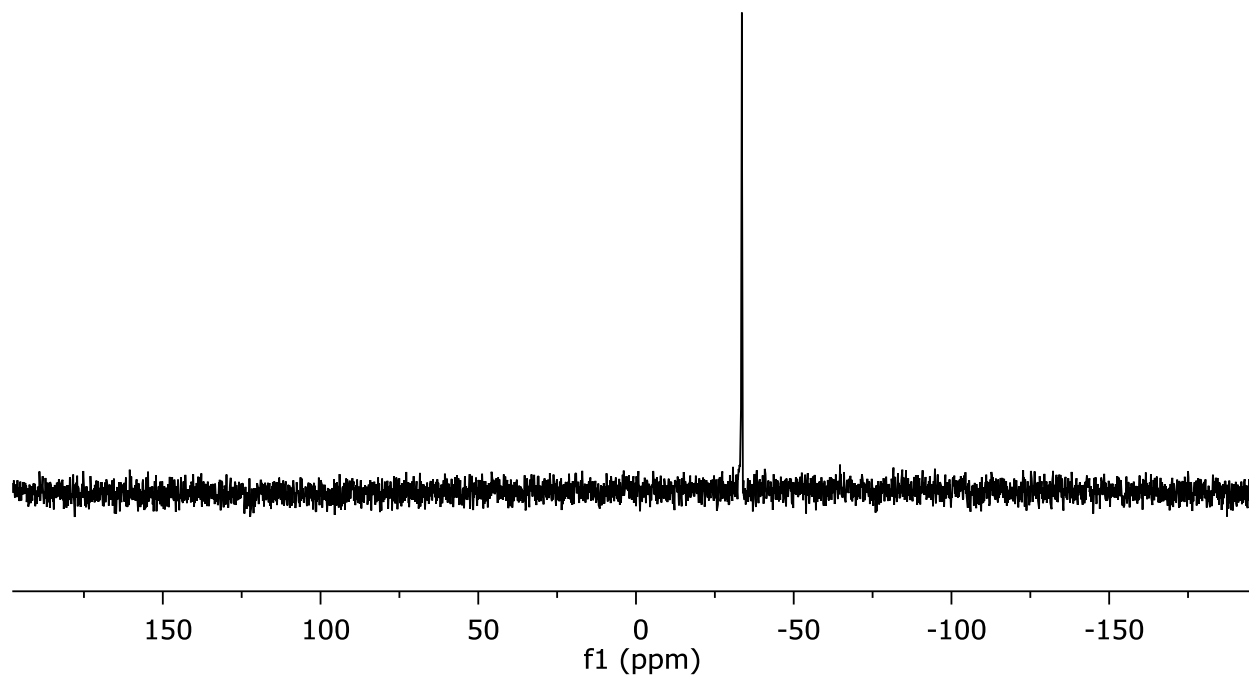


Figure S33: $^{31}\text{P}\{^1\text{H}\}$ NMR (162 MHz, CDCl_3) spectrum of EP[OTf].

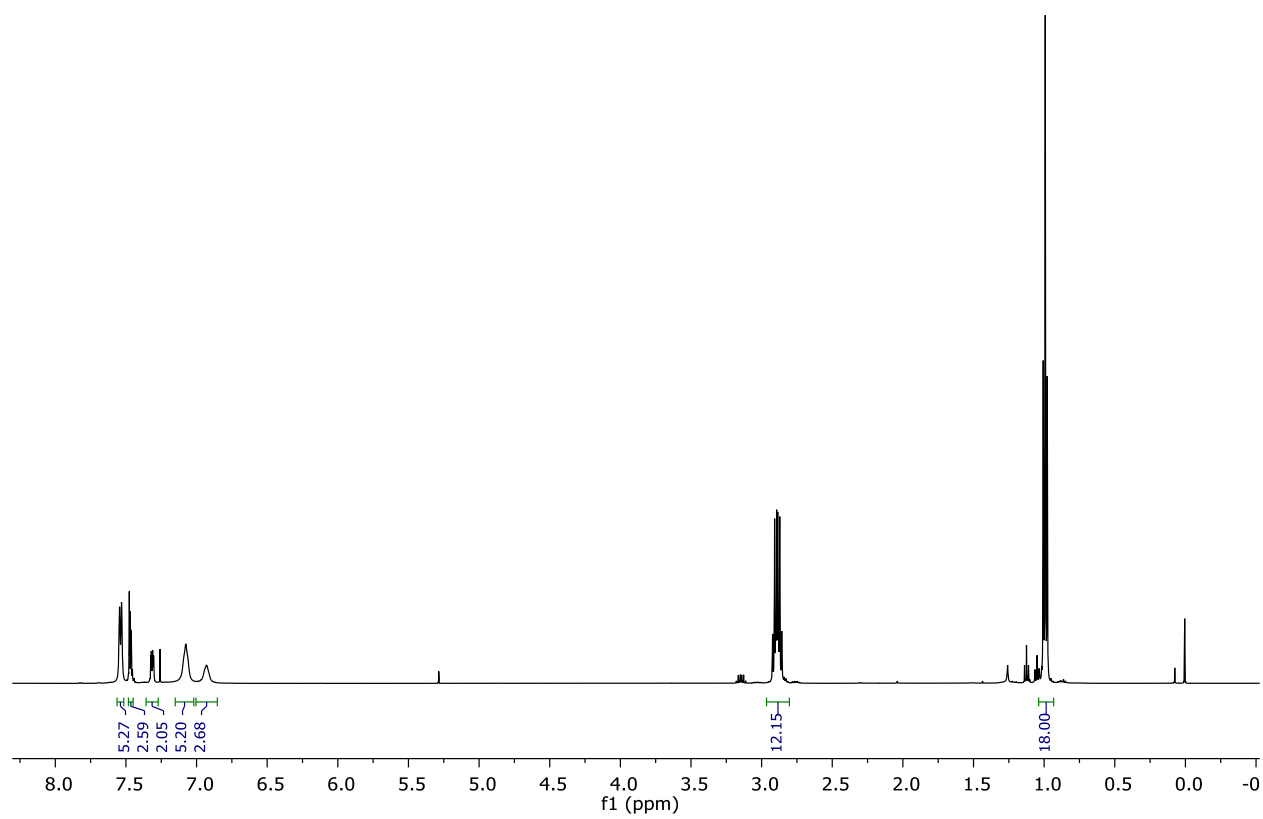
DFEPn3[FB(C₆H₅)₃]:

Figure S34: ¹H NMR (500 MHz, CDCl₃) of [DFEPn3][FB(C₆H₅)₃].

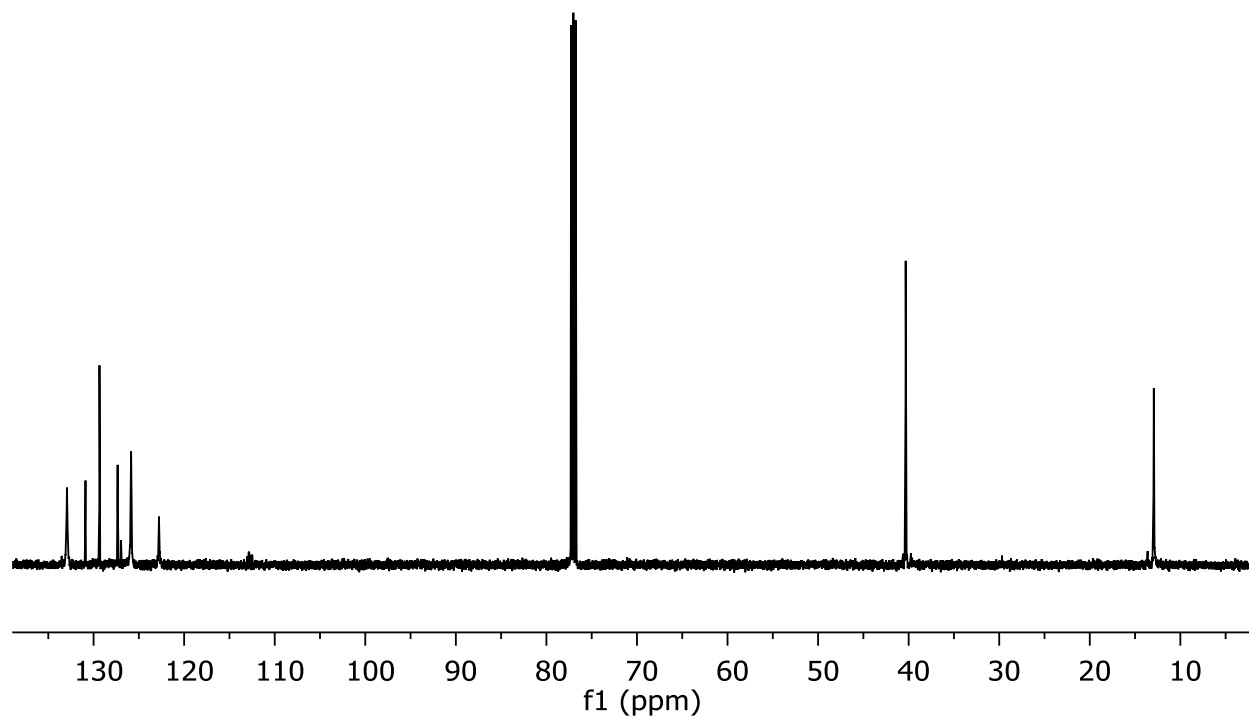


Figure S35: ^{13}C NMR (100 MHz, CDCl_3) spectrum of $\text{DFEPn}_3[\text{FB}(\text{C}_6\text{H}_5)_3]$.

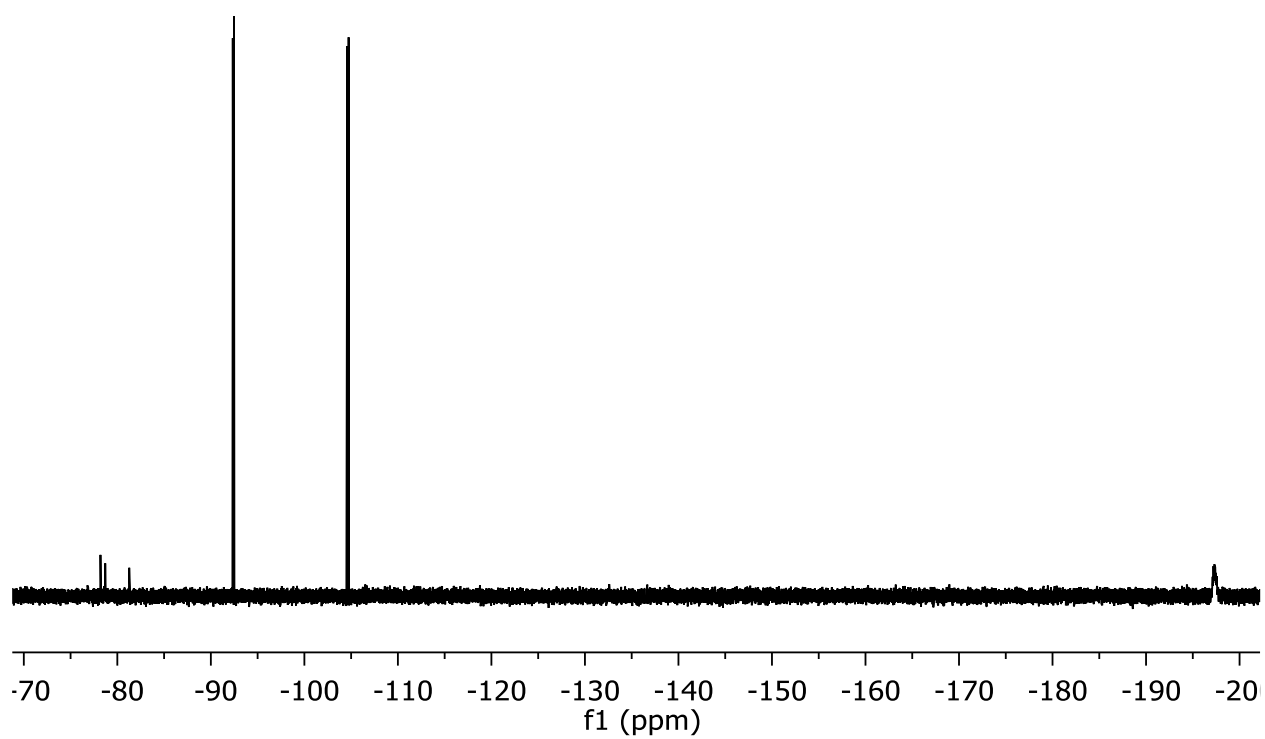


Figure S36: ^{19}F NMR (377 MHz, CDCl_3) spectrum of $\text{DFEPn}_3[\text{FB}(\text{C}_6\text{H}_5)_3]$.

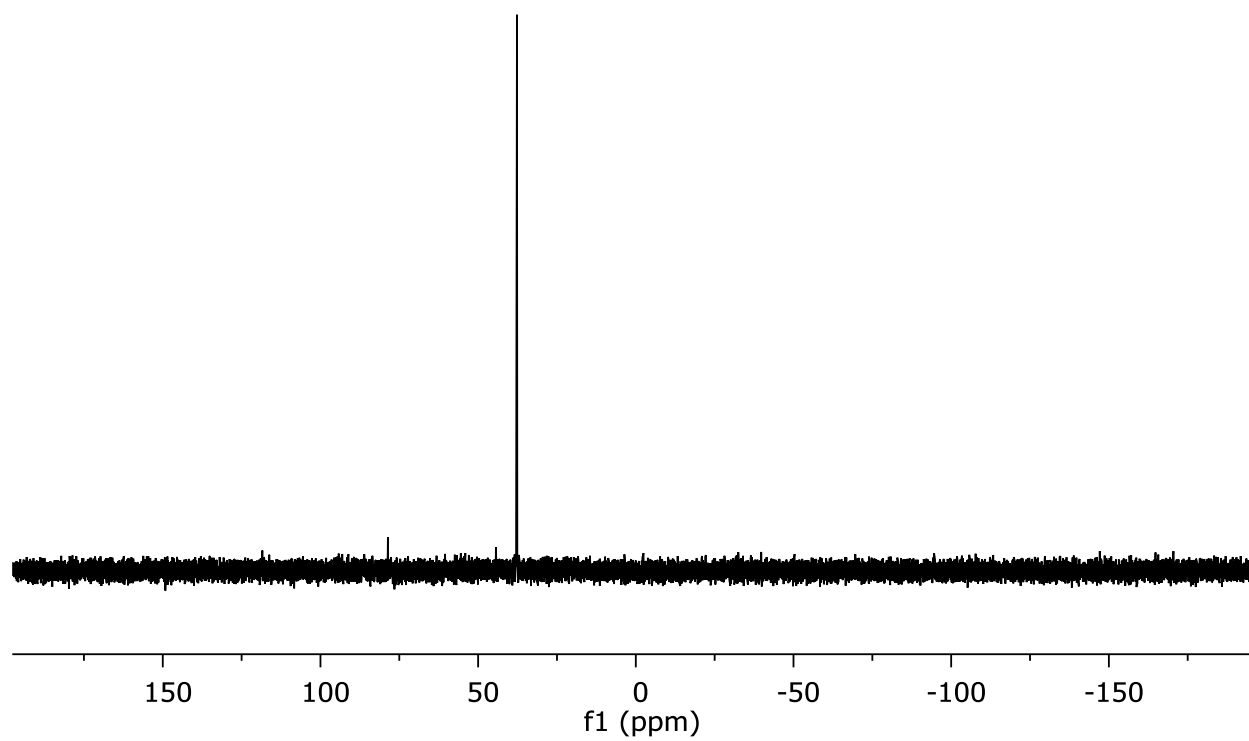


Figure S37: $^{31}\text{P}\{^1\text{H}\}$ NMR (162 MHz, CDCl_3) spectrum of $\text{DFEPn}_3[\text{FB}(\text{C}_6\text{H}_5)_3]$.

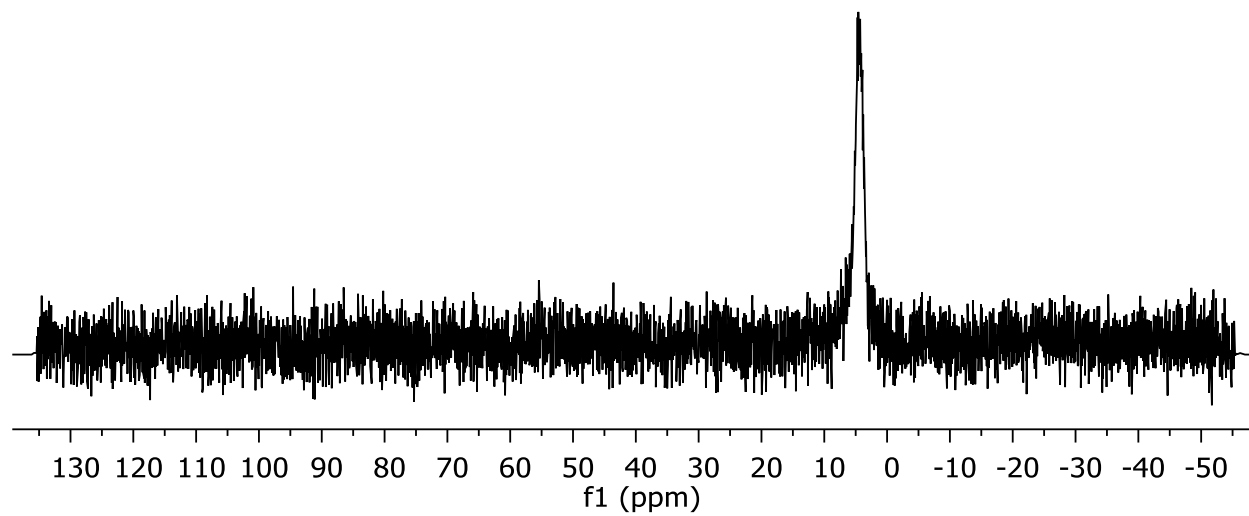


Figure S38: ^{11}B NMR (128 MHz, CDCl_3) spectrum of $\text{DFEPn}_3[\text{FB}(\text{C}_6\text{H}_5)_3]$.

[PhC(O-BPh₃)CH₂][HP(MeNCH₂CH₂)₃N]:

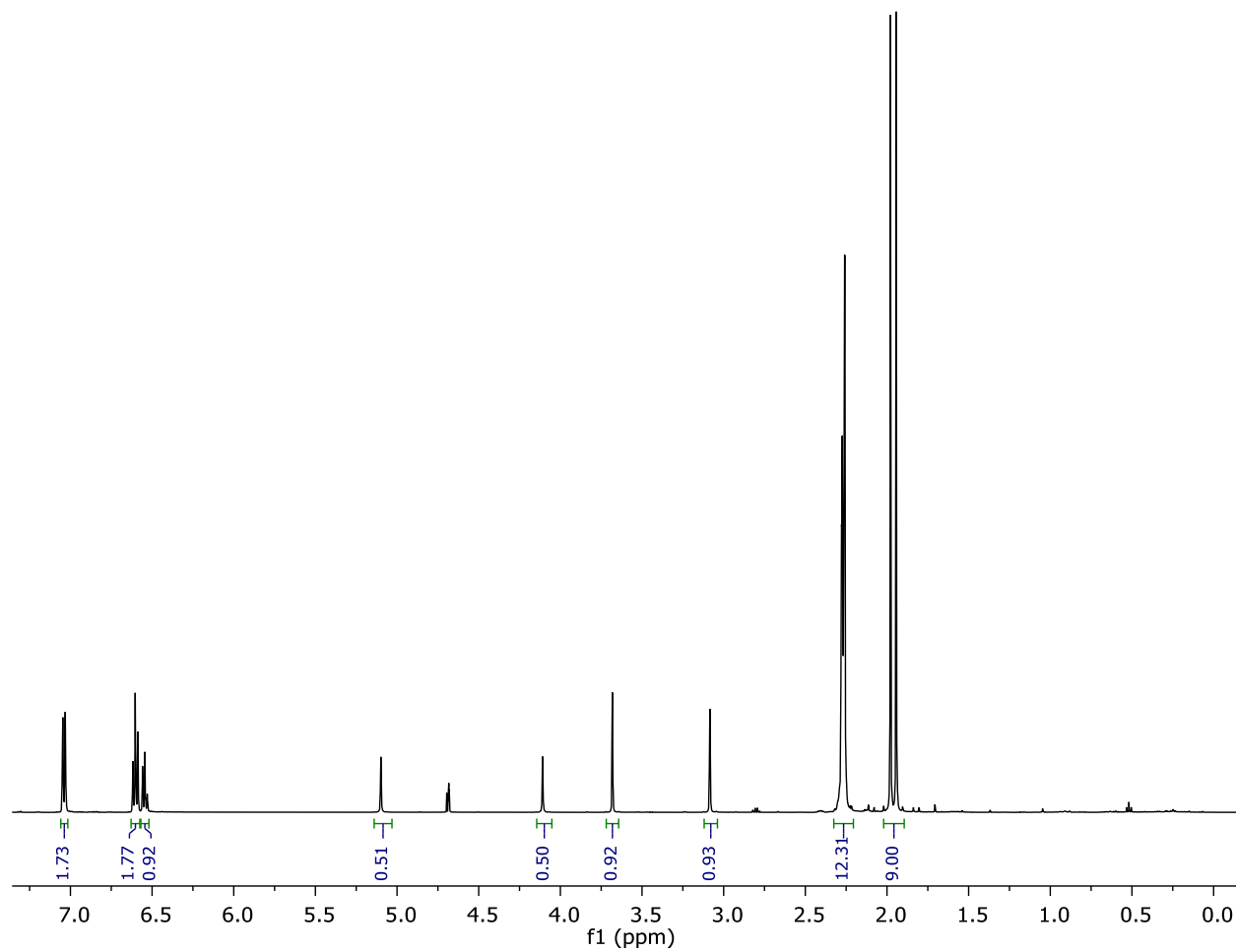


Figure S39: ¹H NMR (500 MHz, CD₂Cl₂) spectrum of [PhC(O-BPh₃)CH₂][HP(MeNCH₂CH₂)₃N].

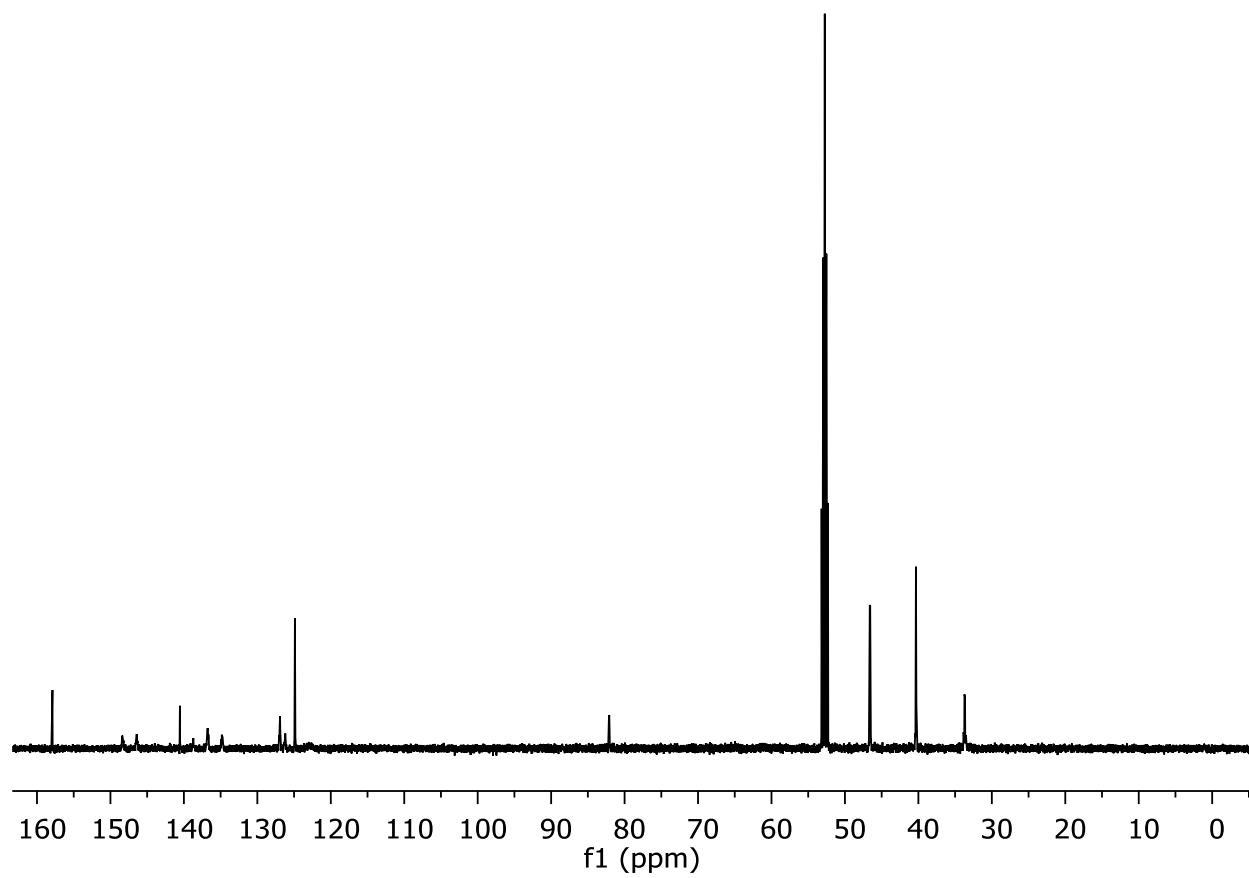


Figure S40: ^{13}C NMR (100 MHz, CD_2Cl_2) spectrum of $[\text{PhC}(\text{O}-\text{BPh}_3)\text{CH}_2][\text{HP}(\text{MeNCH}_2\text{CH}_2)_3\text{N}]$.

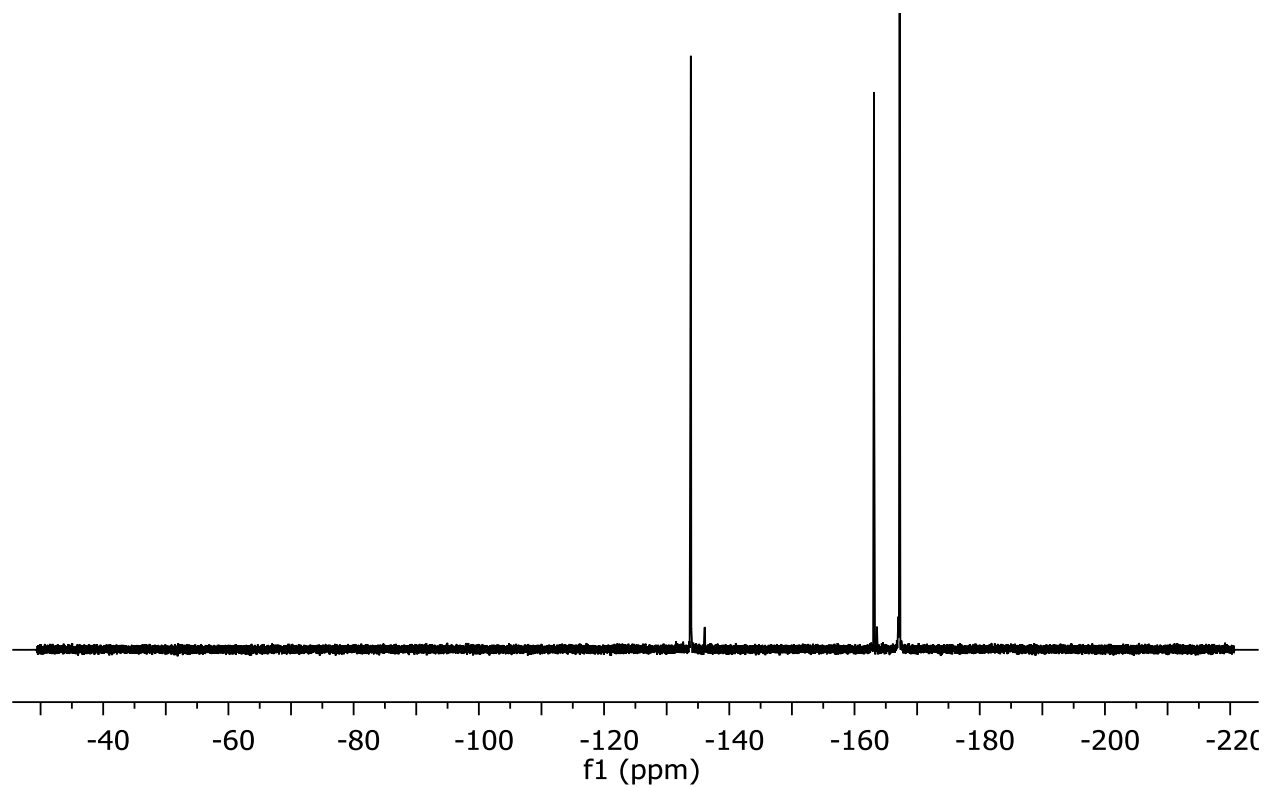


Figure S41: ^{19}F NMR (377 MHz, CD_2Cl_2) spectrum of $[\text{PhC}(\text{O}-\text{BPh}_3)\text{CH}_2][\text{HP}(\text{MeNCH}_2\text{CH}_2)_3\text{N}]$.

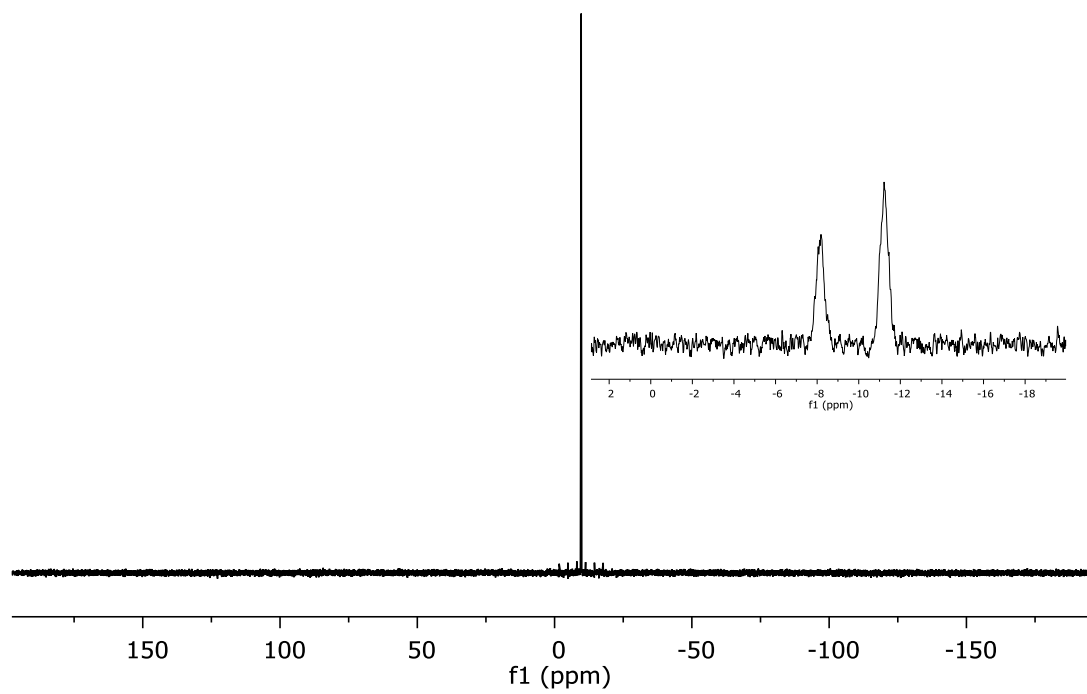


Figure S42: ^{31}P NMR (162 MHz, CDCl_3) spectrum of $[\text{PhC}(\text{O-BPh}_3)\text{CH}_2][\text{HP}(\text{MeNCH}_2\text{CH}_2)_3\text{N}]$.

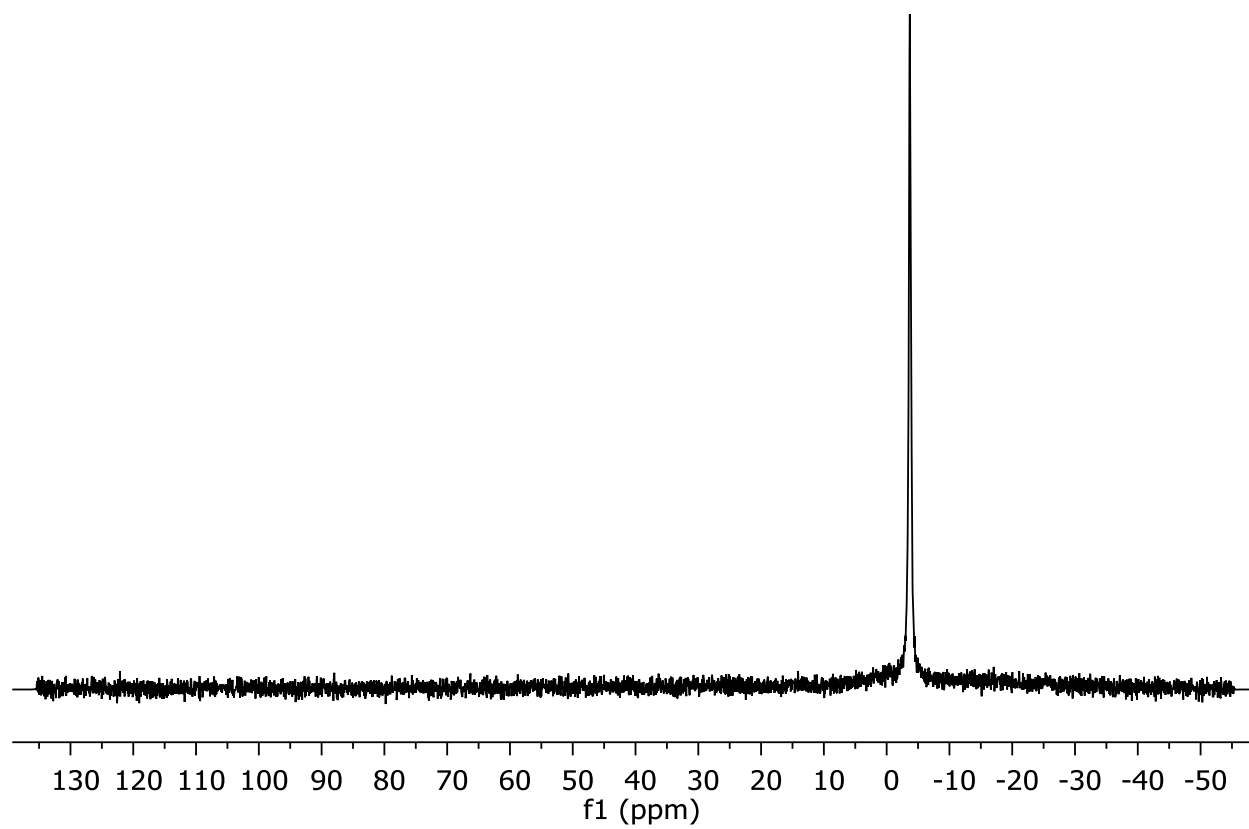


Figure S43: ^{11}B NMR (128 MHz, CD_2Cl_2) spectrum of $[\text{PhC}(\text{O}-\text{BPh}_3)\text{CH}_2][\text{HP}(\text{MeNCH}_2\text{CH}_2)_3\text{N}]$.

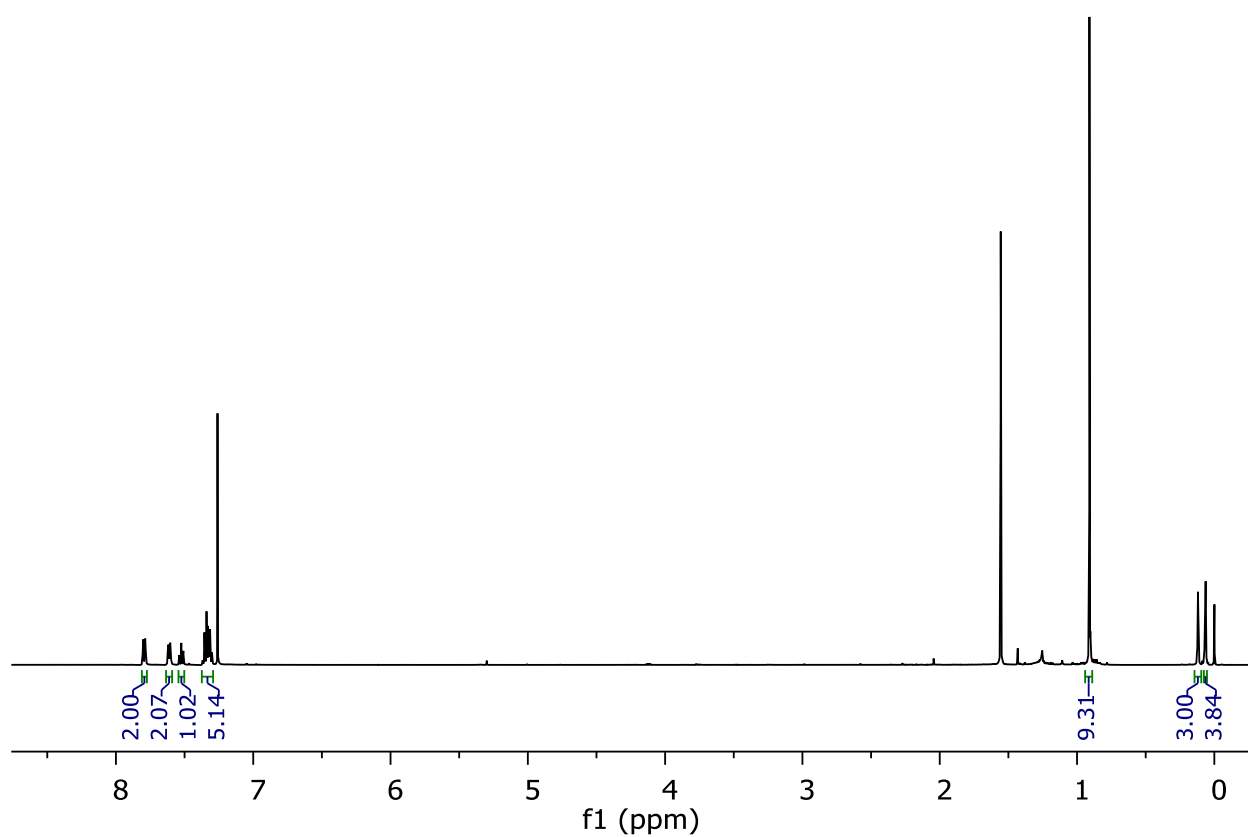
2,2,4,4,4-pentafluoro-3-silyl ether 1,3 diphenylbutan-1-one:

Figure S 44: ^1H NMR (500 MHz, CDCl_3) spectrum of 2,2,4,4,4-pentafluoro-3-silyl ether 1,3 diphenylbutan-1-one.

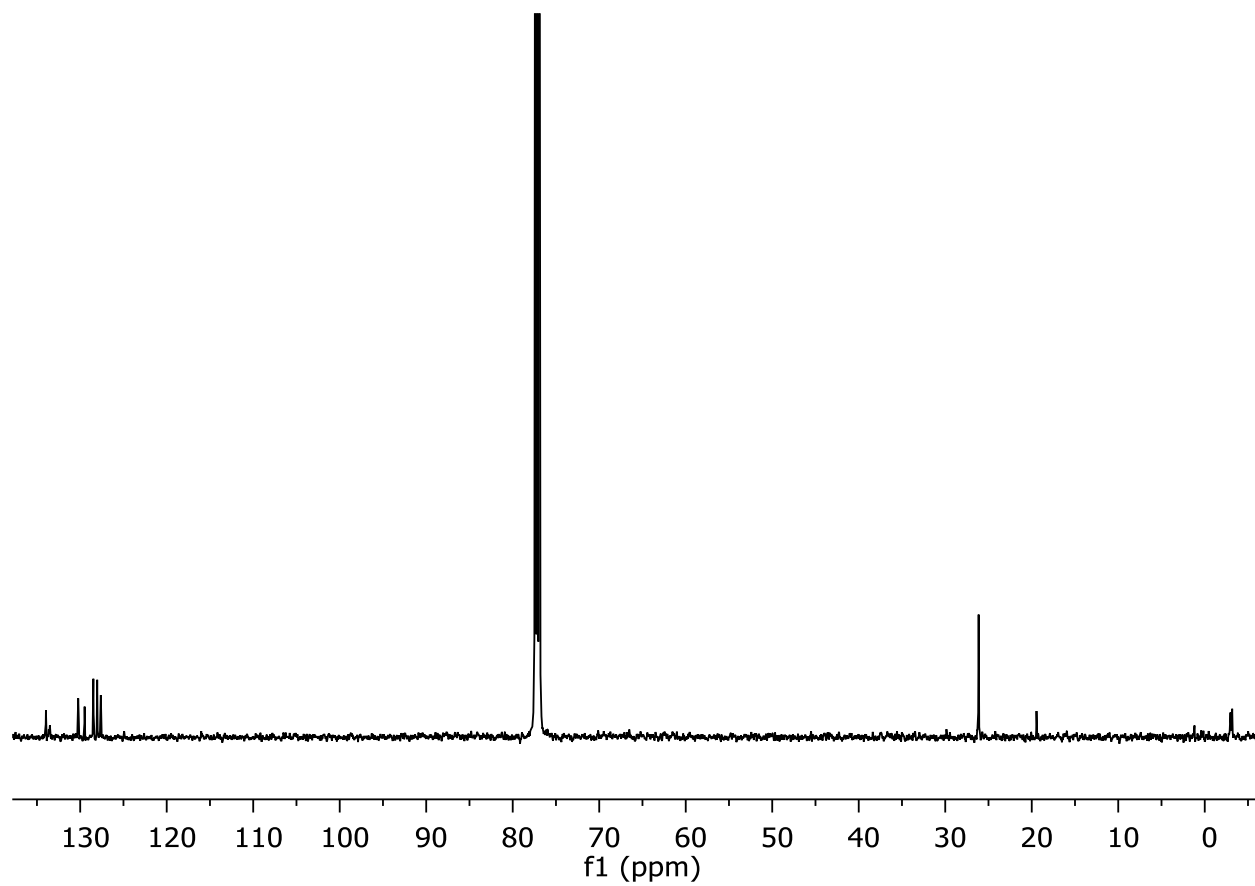


Figure S 45: ^{13}C NMR (100 MHz, CDCl_3) spectrum of 2,2,4,4-pentafluoro-3-silyl ether 1,3 diphenylbutan-1-one.

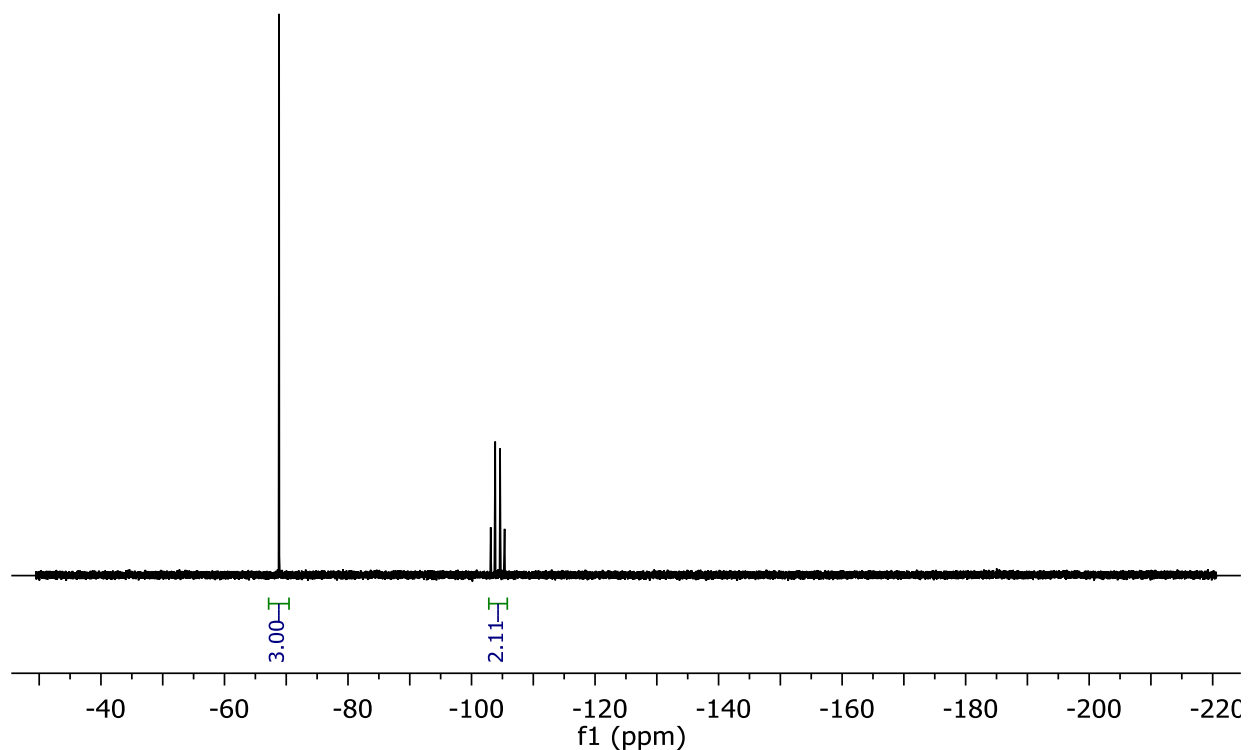


Figure S46: $^{19}\text{F}\{^1\text{H}\}$ NMR (377 MHz, CDCl_3) spectrum for 2,2,4,4,4-pentafluoro-3-silyl ether 1,3 diphenylbutan-1-one.

4.6 Computational Protocol

Calculations were carried out with the Gaussian 09 package,⁶⁸ All geometry optimizations were performed with the PBE1PBE functional. The optimizations also implemented Grimme's D3 empirical dispersion with Beck-Johnson damping (GD3BJ)⁵² alongside SMD solvent correction. Def2-SVPP basis set was used for all the atoms. Frequency calculations at the same level of theory, with the same corrections, were performed to identify the number of imaginary frequencies and provide the thermal corrections of Gibbs free energy. Intrinsic Reaction Coordinates (IRC) were performed for transition state structures to determine corresponding two minima.

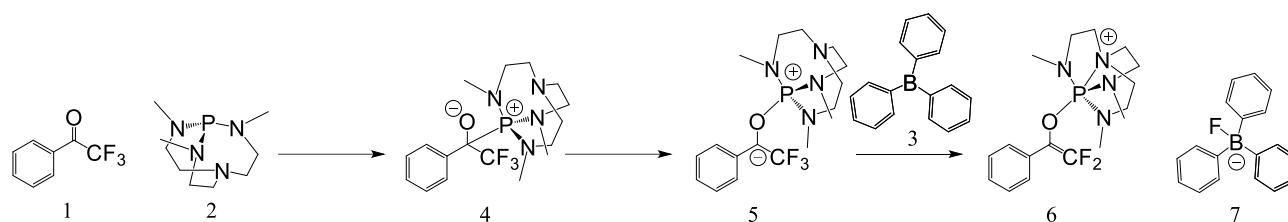
Single-point energy calculations were performed at the PBE1PBE/Def2-TZVPP level of theory alongside the SMD solvent correction and Grimme's GD3BJ. The Gibbs energy corrections from frequency calculations were added to the single-point energies to obtain the Gibbs free energies in solution. All the solution-phase free energies reported in the paper correspond to the reference state of 1 mol/L, 298K.

All geometry optimization and frequency calculations were performed using Gaussian 09. The PBE0 functional with def2-SVPP basis set was used. Stefan Grimme's D3 dispersion with added Becke-Johnson damping function for the empirical dispersion correction was implemented alongside the SMD model for solvent correction. The single-point energy calculations were performed with the same functional, empirical dispersion correction, and solvent corrections as the geometry and frequency calculations, but the basis set used was def2-TZVPP. Minimum stationary states were identified by the absence of imaginary frequencies, whilst the transition states resulted in a single imaginary frequency.

Compound	Single point energy (Hartree)	Thermal correction to Gibbs Free Energy (Hartree)	Sum of Electronic and Thermal Enthalpy (Hartree)
1	-682.194021429	0.079532	-682.1144894
2	-915.410104705	0.272955	-915.1371497
3	-719.260113261	0.235419	-719.0246943
TS1	-1597.61033494	0.380213	-1597.230122

4	-1597.61298337	0.381474	-1597.231509
5	-1597.62420599	0.379641	-1597.244565
TS2	-2316.88643402	0.635210	-2316.251224
6	-1497.69719234	0.382257	-1497.314935
7	-819.229559691	0.233689	-818.9958707

Table S 1: Thermodynamic intermediates and transition state calculation energies



Scheme S1: Proposed mechanism for $\text{DFEP}[\text{FB}(\text{C}_6\text{H}_5)_3]$

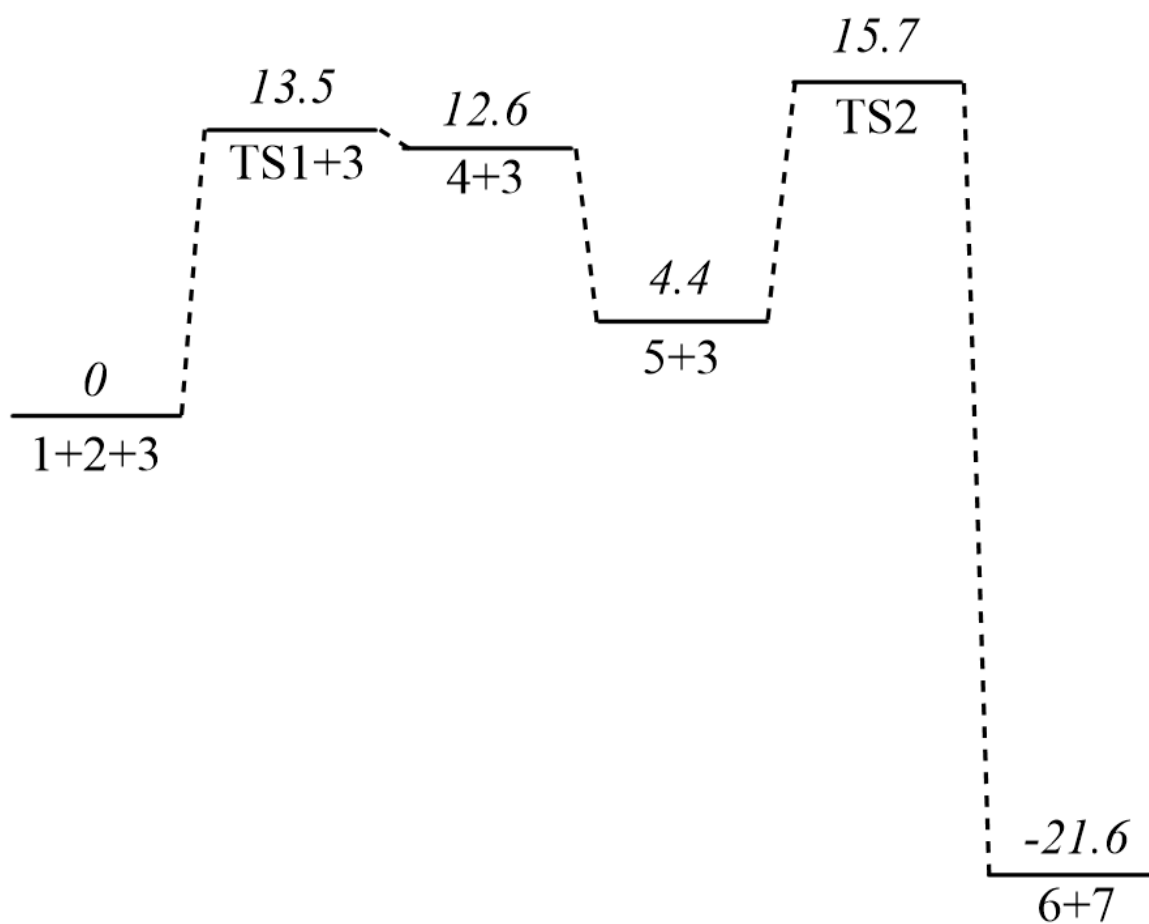
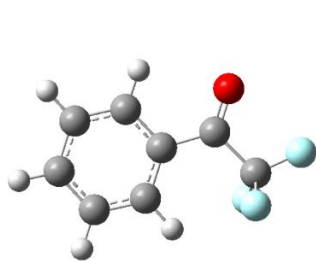
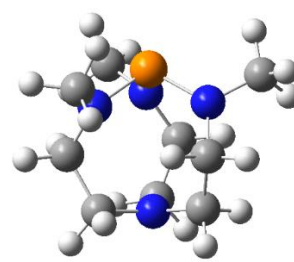


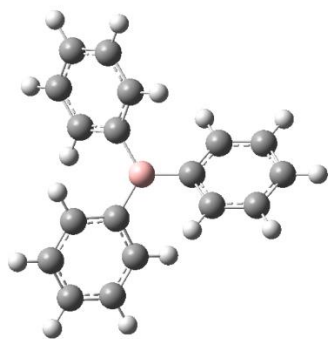
Figure S47: Thermodynamic and kinetic prediction using DFT for generation of DFEP[FBPh₃]. Energy's for stationary points, italicized, in kcal/mol.



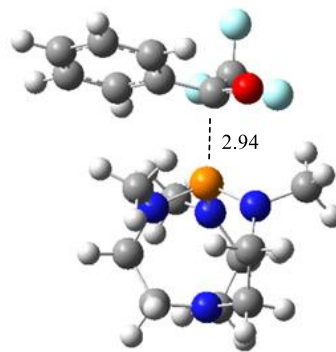
1



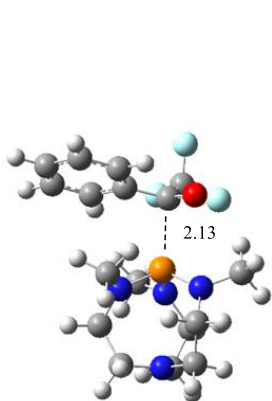
3



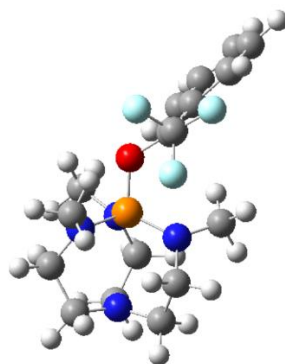
2



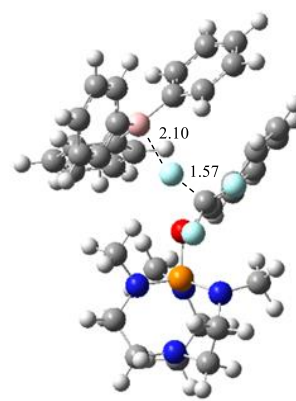
TS1



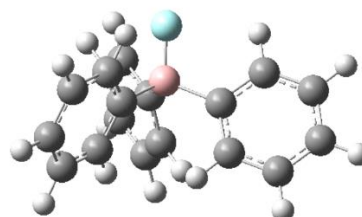
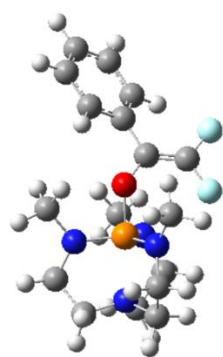
4



5



TS2



6

7

Figure S48: Approximated structures (SMD(DCM)/PBE0-GD3BJ/def2-TZVPP//SMD(DCM)/PBE0-GD3BJ/def2-SVPP) used for calculation thermodynamic profile for DFEP[FBPH₃] formation.

The computational approximations' coordinates for all the atoms are listed in the X, Y, Z Cartesian. The elemental symbols (i.e. P, N, O, C, B, F, H) are all for ground state electronic configurations. Therefore, the elemental symbols P, N, O, C, B, F, and H correspond to 15, 9, 8, 7, 6, 5, and 1 atomic numbers, respectively, in the singlet electronic configuration.

Optimized (SMD(DCM)/PBE0-GD3BJ/def2-TZVPP//SMD(DCM)/PBE0-GD3BJ/def2-svpp) Cartesian coordinates for **1**

C	-4.22270200	0.06235800	1.49168600	H	-4.66903700	3.44600900	1.50427300
C	-2.83106200	0.01396100	1.48988400	H	-5.97694700	1.32271000	1.49894300
C	-2.09001200	1.20702900	1.49262500	C	-0.61238200	1.25552400	1.49055100
C	-2.76325200	2.43981700	1.49717900	O	0.02904300	2.27755400	1.47940800
C	-4.15136900	2.48246500	1.49985000	C	0.17470700	-0.07883900	1.50552600
C	-4.88308600	1.29160700	1.49698700	F	1.47721500	0.15053700	1.51330700
H	-4.79613500	-0.86890500	1.48899300	F	-0.12579500	-0.80059200	2.58839100
H	-2.33859100	-0.96023200	1.48547800	F	-0.11019300	-0.81557500	0.42839800
H	-2.17303100	3.35977600	1.49922900				

Optimized (SMD(DCM)/PBE0-GD3BJ/def2-TZVPP//SMD(DCM)/PBE0-GD3BJ/def2-svpp) Cartesian coordinates for **2**

P	2.93932600	1.30957700	5.88622200	C	2.85058300	4.01051300	5.83081500
N	2.64177000	1.43144000	2.51661700	C	1.23477200	1.26680500	2.76040800
N	1.37344000	0.97237100	5.26380300	C	3.49568200	0.27552900	2.52242400
N	3.30830700	2.82309800	5.15959200	C	3.22642400	2.73909200	2.63666200
N	3.93670300	0.22014400	5.00716800	C	5.28939600	0.04232000	5.46397600
C	4.02982900	2.97557200	3.91805700	H	4.45415000	3.99706800	3.89157000
C	0.63156300	-0.09901100	5.87366200	H	4.89152400	2.28296900	3.91122600
C	3.51067000	-0.50966500	3.83640300	H	1.13568800	-0.40840800	6.80845800
C	0.76967100	1.67940300	4.15893700	H	-0.39734900	0.21894400	6.13829400

H	0.54844300	-1.00342000	5.23424000	H	0.64367500	1.86098600	2.02842500
H	2.49254400	-0.90517300	4.00593200	H	4.51980600	0.60540200	2.27316900
H	4.17026200	-1.39054900	3.72176600	H	3.19335400	-0.43261400	1.71915600
H	-0.32712100	1.55010700	4.22662000	H	2.41423500	3.48405200	2.56295500
H	0.96286200	2.76171100	4.27263800	H	3.90840200	2.93748700	1.78016500
H	2.48719100	3.74411600	6.84109400	H	5.40713300	0.51562800	6.45685000
H	2.01398700	4.52224500	5.30926000	H	5.54350600	-1.03163500	5.57344000
H	3.66890100	4.74883600	5.95406900	H	6.04852500	0.49931500	4.79432700
H	0.97674400	0.20854100	2.57830200				

Optimized (SMD(DCM)/PBE0-GD3BJ/def2-TZVPP//SMD(DCM)/PBE0-GD3BJ/def2-svpp) Cartesian coordinates for **3**

B	-0.49401600	0.22117600	0.00302600	C	-1.47043800	3.97853100	0.17201100
C	1.07302200	0.22096300	0.00080300	H	0.18748400	2.78671700	0.85034300
C	1.80642000	-0.67811300	0.80061300	C	-2.68905300	3.99194400	-0.50977300
C	1.80430100	1.11973100	-0.80128700	H	-4.16055900	2.81131100	-1.56781600
C	3.20033600	-0.67127600	0.81269300	H	-1.06254800	4.90702600	0.58405900
H	1.27128000	-1.38869900	1.43888300	H	-3.23584500	4.93173700	-0.63793800
C	3.19817200	1.11219800	-0.81783700	C	-1.27704500	-1.12343000	0.18778900
H	1.26745400	1.83056800	-1.43784200	C	-0.77159700	-2.33982600	-0.31308900
C	3.89936300	0.22027700	-0.00370100	C	-2.51419700	-1.16411500	0.86153700
H	3.74622000	-1.36872400	1.45604900	C	-1.47150200	-3.53601800	-0.16305200
H	3.74233400	1.80937600	-1.46294100	H	0.18501600	-2.34458100	-0.84544800
H	4.99418600	0.21999200	-0.00546500	C	-3.20635800	-2.36076100	1.04084400
C	-1.27720900	1.56596900	-0.17964800	H	-2.93536900	-0.23859400	1.26724700
C	-2.51589300	1.60697600	-0.85054600	C	-2.68855200	-3.54910800	0.52152600
C	-0.77037900	2.78219800	0.32023100	H	-1.06472400	-4.46464800	-0.57589300
C	-3.20824700	2.80377200	-1.02809800	H	-4.15743400	-2.36805000	1.58274000
H	-2.93815500	0.68159000	-1.25542400	H	-3.23521100	-4.48878500	0.65110300

Optimized (SMD(DCM)/PBE0-GD3BJ/def2-TZVPP//SMD(DCM)/PBE0-GD3BJ/def2-svpp) Cartesian coordinates for **TS1**

P	-0.13318700	-0.37481800	0.10527800	H	2.13290300	0.01646300	3.25140000
N	0.06959800	-0.05112600	3.30176800	H	1.37933800	1.52052900	3.80829900
N	1.31294700	0.34512200	0.58452600	H	-0.87584000	-1.85516900	3.65136900
N	-1.34929900	0.61004300	0.74599000	H	0.81071600	-1.81025400	4.19650600
N	-0.24920000	-1.84237200	0.94345300	H	-1.01443600	1.70454200	3.30570300
C	-2.02441500	0.30862200	1.99311100	H	-1.82323100	0.36095500	4.13063700
C	2.57617900	-0.10248300	0.03936400	H	-2.06389000	-2.31485900	-0.01348500
C	0.58961000	-2.15186400	2.08526800	H	-0.98695900	-3.71380900	0.26674300
C	1.38397500	1.30052400	1.67600100	H	-1.89573700	-2.97661300	1.62304200
C	-1.55304900	1.93082800	0.18976300	C	-3.79450600	0.39284600	-2.58061600
C	1.27743000	0.69120500	3.07486200	C	-2.58756700	-0.22631600	-2.25988500
C	0.12831200	-1.48338900	3.38200800	C	-1.36851600	0.37760400	-2.59445200
C	-1.19959000	0.61756300	3.24708600	C	-1.38901600	1.60621200	-3.26487600
C	-1.34217800	-2.75493300	0.69083600	C	-2.59384500	2.22636600	-3.58801900
H	-2.96875600	0.88238600	2.01543300	C	-3.80367500	1.62280800	-3.24175300
H	-2.31166800	-0.75525200	2.00894300	H	-4.73787200	-0.08879300	-2.30490600
H	2.40527700	-0.78040300	-0.80649600	H	-2.60770000	-1.18097000	-1.73210500
H	3.16108600	0.75579600	-0.33895400	H	-0.42965000	2.06674800	-3.51468100
H	3.18904900	-0.63362800	0.79529500	H	-2.58924400	3.18777800	-4.11152000
H	1.62764700	-1.84806400	1.87308200	H	-4.75339300	2.10840400	-3.48734200
H	0.60769700	-3.25003800	2.20904800	C	0.00829500	-0.17811900	-2.27683900
H	2.34162500	1.84276700	1.58089600	O	1.01085900	0.52861400	-2.47524000
H	0.59199900	2.05810900	1.56065700	C	0.19381300	-1.66638000	-2.64925500
H	-0.79929500	2.13765000	-0.58600300	F	1.35184100	-2.15312200	-2.19629500
H	-1.44588300	2.71033700	0.96825600	F	-0.76595500	-2.49720600	-2.22382700
H	-2.55520600	2.03599100	-0.26828600	F	0.22385900	-1.77145300	-3.98693700

Optimized (SMD(DCM)/PBE0-GD3BJ/def2-TZVPP//SMD(DCM)/PBE0-GD3BJ/def2-svpp) Cartesian coordinates for **4**

O 1				N	1.38952700	-0.17895400	-0.21114000
P	-0.14309500	-0.78338100	-0.48696100	N	-1.22263300	0.42126400	-0.04448300
N	0.22883800	0.06072100	2.52020400	N	-0.37180500	-2.08153600	0.55935100

C	-1.87770400	0.42804100	1.25096900	H	0.82803200	-1.56740200	3.72230200
C	2.58012200	-0.85252600	-0.68674400	H	-0.66281000	1.90400400	2.26736400
C	0.48920100	-2.26877700	1.71722400	H	-1.56158700	0.81769100	3.34105000
C	1.61157500	0.95709100	0.66876700	H	-2.30108600	-2.50387900	-0.18508200
C	-1.29233400	1.63747200	-0.83123500	H	-1.36220200	-3.93779600	0.31589700
C	1.49744600	0.62547300	2.15681200	H	-2.07743000	-2.84246100	1.54114400
C	0.15000800	-1.32787200	2.87501000	C	-3.93974500	-0.28358700	-3.09944500
C	-0.96384800	0.85091500	2.40511400	C	-2.77833900	-0.87268900	-2.59906600
C	-1.58048800	-2.88034800	0.55377800	C	-1.52084000	-0.48875200	-3.07793100
H	-2.74688700	1.10651500	1.18573900	C	-1.45621300	0.48433200	-4.07950400
H	-2.28471000	-0.57363800	1.46271000	C	-2.61313200	1.07221700	-4.58750300
H	2.31377300	-1.70955500	-1.31559200	C	-3.86247300	0.69362200	-4.09358300
H	3.19039100	-0.16862100	-1.30253900	H	-4.91407500	-0.59079300	-2.70614600
H	3.19907600	-1.21396400	0.15827600	H	-2.87150500	-1.63411900	-1.82281700
H	1.54047300	-2.12334200	1.42237300	H	-0.46172700	0.77067300	-4.43214700
H	0.39868500	-3.32173300	2.03852800	H	-2.54031100	1.83313900	-5.37156000
H	2.61727100	1.35495500	0.44695000	H	-4.77472700	1.15684900	-4.48289100
H	0.90349300	1.76518600	0.42660400	C	-0.16068700	-1.03609500	-2.60406000
H	-0.55324500	1.60286700	-1.64691300	O	0.87443100	-0.44034500	-3.03692500
H	-1.06280900	2.52325900	-0.20902400	C	-0.10493800	-2.56879100	-2.83459000
H	-2.29477900	1.77466600	-1.27730100	F	1.00492300	-3.11908200	-2.32348100
H	2.28597800	-0.09431700	2.43663700	F	-1.13628500	-3.26501300	-2.32879000
H	1.70439700	1.55473700	2.72987900	F	-0.08614000	-2.81628200	-4.15024400
H	-0.87502600	-1.53613500	3.22838600				

Optimized (SMD(DCM)/PBE0-GD3BJ/def2-TZVPP//SMD(DCM)/PBE0-GD3BJ/def2-svpp) Cartesian coordinates for **5**

P	0.03720300	0.00220800	-0.03754600	N	-0.63879800	-1.43473200	-0.49573500
O	0.06492300	0.01485600	1.57019400	C	-0.72309200	0.84540900	2.42092500
N	0.15830200	-0.02088300	-2.82171800	C	2.13975600	-0.66400500	-1.58167500
N	-0.85592000	1.28044300	-0.56668000	C	-1.83523600	0.24838100	3.06128300
N	1.64681600	0.03415600	-0.39910800	C	-2.25973100	1.42250800	-0.21354400

C	-1.43151700	-1.50794300	-1.71522500	H	2.20738200	1.14723600	1.29636200
C	-3.72417600	0.21928500	4.64521800	H	2.73940300	1.86474700	-0.25644100
C	-0.38433400	2.05786000	-1.70027400	H	3.54426700	0.40064600	0.39719900
C	2.57570700	0.91658000	0.28933600	H	-1.57052000	1.05767100	-3.20477000
C	-2.62217400	0.85691400	4.09152900	H	-0.09916700	1.82381600	-3.84415300
C	-2.27607100	-1.05092800	2.65748600	H	0.12977000	-2.07279600	-3.10146300
C	-4.13377500	-1.05430500	4.22914200	H	-1.24217500	-1.23591100	-3.85614900
C	-0.50478400	1.24490300	-2.99010700	H	1.97499800	0.96176600	-2.99382800
C	-0.58549700	-1.24476400	-2.96289100	H	1.96957900	-0.65243700	-3.73861500
C	1.59521900	-0.06652700	-2.87402400	H	0.48851700	-2.48016400	0.93965700
C	-0.16565200	-2.68253300	0.07789200	H	-1.01768000	-3.28886500	0.43253200
C	-3.38311100	-1.67190000	3.22466900	H	0.40481900	-3.27765000	-0.65993800
H	3.23999500	-0.62359200	-1.56077700	H	-2.35627300	1.84595100	4.46497900
H	1.86127000	-1.73061100	-1.52445200	H	-4.28207400	0.73841700	5.43371500
H	-2.58344000	0.60806400	0.45237100	H	-5.00467500	-1.54492400	4.67349700
H	-2.43126700	2.37831900	0.31082000	H	-3.66277000	-2.67084400	2.86883300
H	-2.88944600	1.39225400	-1.12290100	H	-1.71885000	-1.57471000	1.87971800
H	-2.25708000	-0.77881700	-1.66388600	C	0.00787200	2.04263000	2.78329500
H	-1.89685500	-2.50625200	-1.75624200	F	0.44054700	2.76922400	1.70531400
H	-0.97179100	2.98959400	-1.74641600	F	1.19023600	1.83550100	3.47486400
H	0.66627200	2.35146200	-1.53482000	F	-0.69336200	2.89486900	3.5444090

Optimized (SMD(DCM)/PBE0-GD3BJ/def2-TZVPP//SMD(DCM)/PBE0-GD3BJ/def2-svpp) Cartesian coordinates for **TS2**

P	2.47280500	1.80858200	5.77815200	C	0.83460400	1.62995900	7.94490400
O	2.00638300	2.07913100	7.30384100	C	3.60067300	3.72689800	4.22497400
N	3.22491800	1.51448000	3.39389500	C	1.03298100	0.73093800	9.04126600
N	1.27621800	0.86746000	5.12354700	C	0.98089400	-0.43810800	5.69264600
N	2.64660600	3.38315000	5.27311600	C	4.33247100	0.05378900	4.94938000
N	3.90101300	0.96954200	5.98983200	C	0.30614300	-0.48563700	11.04228400

C	0.90224200	1.07876800	3.73972800	H	-0.94061900	0.87263800	9.96281200
C	2.17460200	4.53065200	6.04029900	H	-0.48831400	-0.69421800	11.76731900
C	0.04395500	0.40687900	10.00982800	H	1.75078800	-1.80140200	11.99801600
C	2.29624800	0.09962900	9.20423900	H	3.53574600	-1.25184600	10.32236900
C	1.55459600	-1.10282000	11.17918800	H	3.09157700	0.32463700	8.49030900
C	2.10455200	0.77099500	2.85298600	C	-0.30221200	2.41976900	7.68530800
C	4.45759700	0.78756500	3.61705300	F	-1.47386900	1.92486200	8.07336800
C	3.33663800	2.89712300	2.98539800	F	-0.42728800	2.88357200	6.43149800
C	4.93565500	1.57020500	6.81597100	F	-0.35785700	3.81267600	8.40058700
C	2.54381900	-0.79236400	10.24381500	C	-0.41769000	3.93760000	11.18281100
H	3.48291000	4.79696600	3.99422300	C	1.73738500	4.99619000	9.87552600
H	4.64085700	3.58677800	4.57892400	C	-0.71348400	6.17057700	9.66759400
H	1.53979000	-0.59546000	6.62718100	B	0.17132500	4.92809200	10.09849300
H	-0.09489000	-0.52244200	5.92466600	C	-1.52299500	2.22921700	13.15179400
H	1.26073100	-1.24405500	4.98768700	C	-0.20708800	2.67532500	13.26793900
H	3.60901900	-0.77479200	4.85819200	C	0.33495500	3.51307500	12.29063200
H	5.29226200	-0.39371500	5.25252200	C	-1.74739500	3.48293900	11.09814300
H	0.03923400	0.43601900	3.50507000	C	-2.29389500	2.63457600	12.05875000
H	0.57686900	2.12392800	3.59811400	C	2.39067900	6.21807500	9.63306800
H	1.55834400	4.21892100	6.88744300	C	3.77653300	6.29309600	9.47797700
H	1.57945000	5.19657000	5.39013200	C	4.54969800	5.13414300	9.55894200
H	3.03431900	5.09916800	6.43926800	C	-2.35713100	7.89147200	10.23980300
H	2.33360100	-0.30593100	2.90378500	C	-2.24318000	8.44865000	8.96654400
H	1.90927900	1.02089500	1.79326700	C	-1.36878500	7.87434300	8.03961600
H	5.28847700	1.50946300	3.67231600	C	-0.61140300	6.75910900	8.39268300
H	4.68286300	0.08381300	2.79332100	C	-1.60705700	6.76213200	10.57674500
H	2.37701700	3.20906000	2.54366800	C	2.54314700	3.84498500	9.95535000
H	4.12497900	3.05319200	2.22410700	C	3.92641500	3.90687700	9.79854600
H	4.49385900	2.32601800	7.48216400	H	4.52205900	2.99099600	9.86734000
H	5.41109500	0.79933000	7.44746200	H	5.63701700	5.18677900	9.43939100
H	5.72015100	2.05958300	6.20704200	H	4.25557900	7.26112000	9.29729100

H	1.80148800	7.13890500	9.57459200	H	-1.27688600	8.30294100	7.03605300
H	2.07362700	2.87334300	10.13090400	H	1.37067000	3.85049000	12.39911500
H	-1.71563200	6.33258300	11.57831400	H	0.40487800	2.36362100	14.12066900
H	0.06820400	6.32161300	7.65419100	H	-1.94936000	1.56533200	13.91106600
H	-3.03872000	8.33406300	10.97376200	H	-3.32757000	2.28727900	11.95856800
H	-2.83498200	9.32872700	8.69412800	H	-2.36304300	3.79177800	10.24762300

Optimized (SMD(DCM)/PBE0-GD3BJ/def2-TZVPP//SMD(DCM)/PBE0-GD3BJ/def2-svpp) Cartesian coordinates for **6**

P	2.79629500	1.51008800	5.18447400	C	4.78463200	-0.23174900	5.99461500
F	0.93787900	3.49377800	6.74113100	C	3.63184200	-0.47778000	10.44518100
O	2.97386100	1.53294800	6.85482200	H	3.58014000	4.62211600	3.54117300
F	0.21743300	2.91780300	8.69132500	H	4.72891300	3.26557200	3.44042400
N	2.59070300	1.47973700	3.07953100	H	1.56501900	-0.49642300	6.56453400
N	1.16808100	1.06583800	5.19317700	H	-0.15610100	-0.08776400	6.35694300
N	3.24439500	3.10890600	4.94397100	H	0.71505200	-1.01167800	5.08600700
N	3.93162000	0.29858700	4.94527400	H	3.09120500	-1.20846800	3.69489300
C	2.03461200	1.71100600	7.82797000	H	4.84270900	-0.94542500	3.53225300
C	3.66646800	3.52656900	3.61962400	H	-0.56676500	0.90450100	4.03602500
C	2.17564500	0.81611400	8.99352700	H	0.21772900	2.49651500	3.97945800
C	0.80643100	-0.19488500	5.82752000	H	3.48339400	3.65935000	6.98579300
C	3.88203100	-0.43246100	3.69395600	H	3.37192100	5.00463900	5.82274300
C	1.24892100	-0.49845800	10.81181400	H	4.87179200	4.02928100	5.93247600
C	0.40983500	1.40977800	4.01019900	H	1.28022600	-0.13740300	2.79023100
C	3.76680400	3.98611400	5.98097000	H	0.86727800	1.32867700	1.84927900
C	1.07031900	0.35839200	9.72784800	H	4.57231500	1.18820600	2.47151700
C	1.10265800	2.67292700	7.75206000	H	3.38287600	0.14140100	1.63426000
C	3.45810800	0.38091300	9.36225100	H	1.76434000	3.35422600	2.65211300
C	2.52848700	-0.91892900	11.17690200	H	3.13262300	2.89789700	1.59290400
C	1.23731800	0.96223900	2.82038300	H	5.14142000	0.57186800	6.65217800
C	3.65888900	0.58891100	2.60312700	H	4.27957400	-0.99668200	6.61329200
C	2.74954000	2.86694100	2.62537100	H	5.66489700	-0.69534100	5.51937200

H	0.05950700	0.65941800	9.44378200	H	4.63989800	-0.80170300	10.72172600
H	0.37547300	-0.84866200	11.37031100	H	4.32542400	0.72736900	8.79630100
H	2.66468900	-1.59411500	12.02709200				

Optimized (SMD(DCM)/PBE0-GD3BJ/def2-TZVPP//SMD(DCM)/PBE0-GD3BJ/def2-svpp) Cartesian coordinates for **7**

F	-1.61222600	-6.74007800	13.13567000	H	-1.33640500	-5.18847200	17.00562100
C	-3.06782100	-6.37161400	15.13794200	H	0.62793100	-5.70056000	13.21162000
C	-1.10417800	-8.21295000	15.09602500	H	0.38540500	-3.55394200	17.68396800
C	-0.48752900	-5.59501800	15.05705100	H	2.24459400	-2.96076900	16.12347900
B	-1.56941700	-6.72942300	14.59043400	H	2.34712500	-4.04605900	13.87460700
C	-5.66460400	-5.64003900	16.04588100	H	-2.86645900	-7.27054300	17.09619400
C	-4.79351000	-6.34179000	16.88170900	H	-5.11036200	-6.61795300	17.89383200
C	-3.52241300	-6.70168800	16.42628700	H	-6.66386400	-5.35913300	16.39541700
C	-3.96931200	-5.66964400	14.31853300	H	-5.91993800	-4.76226400	14.08567500
C	-5.24543800	-5.30745200	14.75592700	H	-3.65910800	-5.40305900	13.30201500
C	-0.52294600	-8.45561900	16.35260100				
C	-0.17519900	-9.74100700	16.77631100				
C	-0.39206700	-10.83701400	15.93877800				
C	0.44694600	-4.02800900	16.69778100				
C	1.48599700	-3.69322100	15.82736700				
C	1.54046700	-4.30169500	14.57125700				
C	0.56904900	-5.23491200	14.20198700				
C	-0.52044300	-4.95903700	16.31001100				
C	-1.30562600	-9.33550800	14.27392600				
C	-0.95796900	-10.62629000	14.67946700				
H	-1.12890400	-11.47593000	14.00841100				
H	-0.11758200	-11.84662000	16.26276000				
H	0.27589900	-9.88814400	17.76420600				
H	-0.32239200	-7.61014200	17.02150700				
H	-1.74680300	-9.18997700	13.28142100				

4.7 X-Ray Crystallography:

X-Ray Data Collection was collected by coating crystals in Paratone-N oil in a dry-box atmosphere (N₂ filled), mounted on a MiTegen Micromount and placed on a N₂ stream. The spectrometer used for data collection was Bruker Kappa Apex II diffractometer using a graphite monochromator with Mo K α radiation ($\lambda = 0.71073 \text{ \AA}$). Bruker SAINT software package was used to integrate the frames with a narrow-frame algorithm. Absorption effects were corrected using empirical multi-scan method (SADABS)

Structures were solved by direct methods using XS and subjected to full-matrix least-squares refinement on F² using XL as implemented in the SHELXTL. Non-hydrogen atoms were refined with anisotropic thermal parameters. Appropriate riding models and coupled isotropic thermal parameters were used for placement of carbon-bound hydrogens.



Empirical formula	C ₃₅ H ₄₁ BF ₃ N ₄ OP
formula weight	632.519
crystal system	triclinic
space group	P -1
<i>a</i> (Å)	10.5556(6)
<i>b</i> (Å)	10.6686(5)
<i>c</i> (Å)	18.9054(10)
α (°)	98.024(3)
β (°)	90.220(3)
γ (°)	119.185(2)
<i>V</i> (Å ³)	1834.15(17)
<i>Z</i>	2
<i>D</i> _{calc} (g·cm ⁻³)	1.276
μ (mm ⁻¹)	0.128
reflections measured	23912
unique reflections, <i>R</i> _{int}	6441, 0.0329
No. of parameters	556
<i>R</i> ₁ , <i>wR</i> ₂	0.0550, 0.1631
GOF on <i>F</i> ²	1.030



Empirical formula	C35H42BF2N4OP
formula weight	614.529
crystal system	triclinic
space group	P -1
a (Å)	11.039(5)
b (Å)	11.174(5)
c (Å)	16.167(8)
α (°)	77.082(17)
β (°)	83.487(17)
γ (°)	61.238(18)
V (Å ³)	1703.9(14)
Z	1
D_{calc} (g·cm ⁻³)	0.992
μ (mm ⁻¹)	0.175
reflections measured	13921
unique reflections, R_{int}	7014, 0.0682
No. of parameters	400
R_1, wR_2	0.1369, 0.3785
GOF on F^2	1.821

[EP][OTf]

Empirical formula	C18H28F3N4O4PS
formula weight	484.475
crystal system	triclinic
space group	P -1
a (Å)	9.0748(8)
b (Å)	14.7556(14)
c (Å)	17.4680(17)
α (°)	71.896(5)
β (°)	89.899(5)
γ (°)	89.942(6)

V (Å ³)	2223.2(4)
Z	4
D _{calc} (g·cm ⁻³)	1.4473
μ (mm ⁻¹)	0.275
reflections measured	34926
unique reflections, R _{int}	10143, 0.1461
No. of parameters	581
R ₁ , wR ₂	0.0488, 0.0806
GOF on F ²	0.7597
